AD/A-006 039

THE CHARACTERISTICS OF SELF-SUSTAINED PARTICULATE BORON COMBUSTION IN AIR AT AMBIENT PRESSURE

Lowell Wesner Ormand

Air Force Institute of Technology
Wright-Patterson Air Force Base, Ohio

September 1974

AD/A006 039

REPORT DOCUMENTATION PAGE	READ INSTRUCTIONS BEFORE COMPLETING FORM

1. REPORT NUMBER	2. GOVT ACCESSION NO.	3. RECIPIENT'S CATALOG NUMBER
DS/ME/74-2		

4. TITLE (and Subtitle)	5. TYPE OF REPORT & PERIOD COVERED
THE CHARACTERISTICS OF SELF-SUSTAINED PARTICULATE BORON COMBUSTION IN AIR AT AMBIENT PRESSURE	DISSERTATION
	6. PERFORMING ORG. REPORT NUMBER

7. AUTHOR(s)	8. CONTRACT OR GRANT NUMBER(s)
Lowell Wesner Ormand Lt. Col., USAF	

9. PERFORMING ORGANIZATION NAME AND ADDRESS	10. PROGRAM ELEMENT, PROJECT, TASK AREA & WORK UNIT NUMBERS
Air Force Institute of Technology (AFIT-EN) Wright-Patterson AFB, Ohio 45433	

11. CONTROLLING OFFICE NAME AND ADDRESS	12. REPORT DATE
AF Aero Propulsion Laboratory (AFAPL-RJT) Wright-Patterson AFB, Ohio 45433	Sept., 1974
	13. NUMBER OF PAGES 163 164

14. MONITORING AGENCY NAME & ADDRESS(if different from Controlling Office)	15. SECURITY CLASS. (of this report)
	Unclassified
	15a. DECLASSIFICATION/DOWNGRADING SCHEDULE

16. DISTRIBUTION STATEMENT (of this Report)

Approved for public release; distribution unlimited

17. DISTRIBUTION STATEMENT (of the abstract entered in Block 20 if different from Report)

18. SUPPLEMENTARY NOTES

Approved for public release; IAW AFR 190-17

JERRY C. HIX, Captain, USAF
Director of Information

19. KEY WORDS (Continue on reverse side if necessary and identify by block number)

Combustion
Boron Combustion
Solid Particle Combustion
Ramjet Combustion

PRICES SUBJECT TO CHANGE

20. ABSTRACT (Continue on reverse side if necessary and identify by block number)

A one-dimensional analytical model for the steady state combustion of a multiparticle cloud of boron in air was established. This model stressed the importance of radiant heat transfer from the luminous flame and heat of combustion from burning particles adhering to the combustor walls to heat the suspended particles to ignition temperature. A steady state, self-sustained flame of elemental boron in air was investigated to verify the model. Trona amorphous boron powder, with nominal particle size of one

(164)

20.

micron, was used as the fuel. Combustion in 1.9 and 2.54 cm ID and 22.8 to 76 cm long combustors constructed of zirconia plaster was investigated for fuel-to-air equivalence ratios ranging from one to two at air mass fluxes up to 6.5 gm/cm^2-sec.

Complete oxygen depletion and flame temperatures near the adiabatic flame temperatures were recorded for combustor lengths in excess of 61 cm and combustor residence times greater than five milliseconds. Experimental combustion characteristics calculated from the analysis yielded an Arrhenius activation energy near 40 Kcal/mole, an Arrhenius pre-exponential factor of 9.04 x 10^{-3} moles of air/cm-sec and a d^{2}law evaporization constant of 949 μ^2/sec. Although the analysis assumed a d^{2}law or diffusion controlled reaction, the findings correlated best with a chemical controlled reaction.

ia

THE CHARACTERISTICS OF

SELF-SUSTAINED PARTICULATE BORON COMBUSTION

IN AIR AT AMBIENT PRESSURE

by

Lowell Wesner Ormand, M. S.
Lt. Col.   USAF

Approved:

_____ 25 Sept 1974
                              Chairman

_____ 25 Sept 1974

_____ 25 Sept 1974

_____ 25 Sept 1974

Accepted.

_____
Dean, School of Engineering

DS/ME/74-2

THE CHARACTERISTICS OF
SELF-SUSTAINED PARTICULATE BORON COMBUSTION
IN AIR AT AMBIENT PRESSURE

DISSERTATION

Presented to the Faculty of the School of Engineering

of the Air Force Institute of Technology

Air University

in Partial Fulfillment of the

Requirements for the Degree of

Doctor of Philosophy

by

Lowell Wesner Ormand, M. S.
Lt. Col.   USAF

September 1974

ACKNOWLEDGMENT

This research was conducted at the Aero Propulsion Laboratory (AFAPL), Wright-Patterson AFB, Ohio. I would like to express my appreciation to my faculty advisor, Dr. Harold E. Wright, for his suggestions, support, encouragement and patience; to Dr. Paul J. Ortwerth, my adviser at AFAPL, for his introduction into the peculiarities of boron combustion, his support, and encouragement; to my many compatriots at AFAPL especially Messrs. Bob Schlentz and Dan Cincerilli who aided me in constructing the experimental apparatus and the men in the instrumentation shops for their aid in developing the necessary instrumentation; and to the Chemistry Laboratory of the Aerospace Research Laboratories for their help in obtaining the particle size distributions of the boron powder, also for providing the gas sampling containers and the mass spectrographic data from my exhaust gas samples.

I would like to dedicate this effort to the late Mr. James Gray, master machinist at AFAPL, for his aid, suggestions and interest in helping me design and fabricate the boron press mold and the particle mill.

Last, but certainly not least, I would like to acknowledge my family for their patience, trust, faith in my abilities and solace only they could give and to my wife in particular for bearing with me during the long hours of study and for her great effort in typing these manuscripts.

CONTENTS

CONTENTS

LIST OF FIGURES

LIST OF FIGURES

NOMENCLATURE

English letter symbols:

A	Arrhenius pre-exponential constant, moles/cm-sec
A'	Constant defined by Eq 28, sec^{-1}
a_i, a_{ij}	Molar coefficients
B/A	Boron/air ratio, dimensionless
$(B/O_2)_s$	Stoichiometric boron/oxygen mass ratio
C	Concentration of gaseous species in air
c_p	Specific heat at constant pressure, cal/gm-K
D	Combustor diameter, cm
d	Mean fuel particle diameter, cm
E_a	Arrhenius activation energy, cal/mole
e	Internal energy, cal/gm
F	Physical quantity per unit mass
F/A	Fuel/air ratio, dimensionless
g	Constant of proportionality, $sec^{-1}-K^{-1}$
Δh_f^o	Heat of formation of B_2O_3/gm of boron, cal/gm
I	Radiant intensity or power
J	Volumetric extinction coefficient, cm^{-1}
K(T)	Proportionality coefficient, moles/cm-sec
k	Volumetric absorption coefficient, cm^{-1}
L	Combustor length, cm
ℓ	Liquid phase
M	Molecular weight, gm
M_N	Mach number
m	Mass in a unit volume
N	Number of moles
n	Number density, particles/cc

O_2/A	Mass ratio of oxygen in air
P	Pressure, atm
P_V	Vapor partial pressure, dimensionless
P_λ	Monochromatic spectral constant, dimensionless
$\dot{Q}$	Volumetric energy addition, cal/cc-sec
q	Heat flux, cal/cm^2-sec
R	Universal gas constant, 1.987 cal/mole-K
$\underline{R}$	Gas constant for air, cal/mole-K
r	Mean radius of the fuel particles, cm
S	Surface enclosing a volume, cm^2
S_λ	Monochromatic brightness temperature, K
s	Volumetric scattering coefficient, cm^{-1}
T	Temperature, K
t	Time, sec
u	Axial velocity, cm/sec
V	Volume, cc
$\vec{v}$	Velocity vector, cm/sec
X_o	Nitrogen/oxygen molar ratio
x	Longitudinal distance, cm
Z	Absorption coefficient proportionality factor, dimensionless

Greek Letter symbols:

α	Absorptivity
β_{diff}	Rate constant for diffusion limited reaction, μ^2/sec
β_{chem}	Rate constant for chemical limited reaction, μ/sec
γ	Ratio of specific heats
Γ	Coefficient of conductance, cal/cm-sec-K
δ_B	Solid density of boron, 2.34 gm/cc

Symbol	Description
ϵ	Emissivity
ς	Spherical dimension, radians
η	Combustion efficiency
η'	$\eta/(1+\Lambda)$
$\circledcirc$	Dimensionless ratio of specific heats
Θ	Spherical dimension, radians
χ	Mass absorption coefficient, cm^2/gm
Λ	Ratio of fuel impurities to mass of boron
λ	Monochromatic wave length, μ
μ	Length, $10^{-4}cm$
ν	Volumetric emission coefficient, cm^{-1}
ξ	Combustor residence time parameter, sec
ρ	Density, gm/cc
σ	Stefan-Boltzman constant, $cal/cm^2\text{-}sec\text{-}K^4$
τ	Optical distance, dimensionless
ϕ	Fuel/air equivalence ratio, $(B/A)/(B/A)_s$
ϕ'	$(1+\Lambda)\phi$
ψ	Oxygen depletion parameter
ω	Solid angle, steradians

Subscripts:

Symbol	Description
air	Air as a chemical species
B	Boron chemical species
B_2O_3	Boron trioxide chemical species
chem	Chemical reaction
cloud	Condition within the gas-particle mixture
diff	Diffusion limited reaction
E	Combustor exit condition
F	Flame

f	Fuel
g	Product
i	Ignition
j	Phase state
k	Reference value
m	Mixture species
N_2	Nitrogen chemical species
O_2	Oxygen chemical species
o	Initial condition
p	Particle
r	Radiation
s	Stoichiometric
T	Total value
v	Specific volume
w	Condition at the combustor wall surface
λ	Monochromatic value

DS/ME/74-2

ABSTRACT

A simplified one-dimensional analytical model for the
steady state combustion of a multiparticle cloud of boron in
air was established. This model stressed the importance of
the radiant heat exchange between the luminous flame and the
burning particles adhering to the combustor walls with the
cold gas-particle mixture. The model assumed no thermal or
dynamic slippage between the fuel particles and the carrier
gas. Further assumptions included spherical, uniformly
distributed, one-micron diameter particles and an optically
thin cloud during heat up to ignition temperature. The
particle reaction model, based on a single particle reacting
in air, was formulated to consider the finite environment of
oxygen and the temperature dependence of the reaction.

A steady state, self-sustained flame of elemental boron
in air at atmospheric pressure was investigated to evaluate
the theoretical analysis. A particulate cloud of boron was
ignited using a hydrogen flame; once the flame was establish-
ed, the hydrogen supply was removed. The flame was then
allowed to stabilize as a self-sustained, steady state flame.
Combustion gas sampling and absorption-emission measurements
were taken to evaluate the combustion efficiency and tempera-
ture. These data were taken at the combustor exit plane for
combustors 1.9 to 7.62 centimeters in diameter and up to 76
centimeters in length. Particulate concentrations providing
fuel-to-air equivalence ratios ranging from one to two at
air mass fluxes up to 6.35 gm/cm^2-sec were investigated.

Trona amorphous boron powder, with a nominal particle size of one micron, was used as the fuel. A fuel feed system was devised that permitted measurement of the boron powder flow rate and provided a steady flow of fuel particles. A portion of the boron adhered to and burned on the combustor walls providing a refractory surface that, coupled with the energy radiated from the flame, produced sufficient energy to heat the oncoming particle cloud to ignition temperature when the chamber residence times were in excess of two milliseconds.

Complete oxygen depletion and flame temperatures near the adiabatic flame temperatures were recorded for combustor lengths in excess of 61 centimeters and combustor residence times greater than five milliseconds. Experimental combustion characteristics calculated from the analysis yielded an Arrhenius activation energy near 40 Kcal/mole, an Arrhenius pre-exponential factor of 9.04×10^{-3} moles of air/cm-sec and a d^2-law evaporation rate constant of $949 \, \mu^2$/sec. Although a d^2-law or diffusion controlled reaction analysis was assumed, these findings correlated best with previous results using a d-law or chemical controlled reaction. However, the d^2-law analysis was used to be consistent with previous investigators.

I. INTRODUCTION

There has been a continuous interest in the combustion of metals for the past few decades. This interest has been due to the high volumetric heating values and high combustion temperatures possible with these systems. In spite of this interest, our present understanding of metal combustion lags far behind that of conventional gaseous, liquid and solid fuels. The reasons for this lag in understanding lie not only in the lack of research efforts on metals as an energy source but on the very aspects of metal combustion that make it attractive as a high energy fuel. The large exothermic heat of formation of the combustion products implies that they are condensed phase products which are highly stable. Thus, the fuel and the products of combustion are present in the combustion zone in the liquid or solid state at normal combustion temperatures (Ref 1).

Boron, like some other metals, has been shown special interest because of its high theoretical energy content. Of the basic elements, listed in Table I of Appendix J, only hydrogen and beryllium have greater energy content per unit weight than boron; but due to their lesser densities, boron has the highest heating value per unit volume. However, boron as a propellant additive has been very disappointing because it exhibits serious combustion inefficiencies. Boron has been burned as a liquid slurry in a ramjet (Ref 2) and as a solid propellant additive in a ducted rocket (Ref 3). The primary problems encountered in these instances were the difficulty of igniting the boron and the slow reaction rates

resulting in unreacted boron in the exhaust plume. Many theories have been postulated as to the causes for this poor performance. Primary among these are: (a) the formation of an inhibiting oxide layer on the metal particles, (b) the agglomeration of the particles, and (c) the formation of unstable products of combustion that inhibit the reaction and thus reduce the heat of combustion (Ref 5).

Boron has other interesting characteristics as well. Technically, boron is not a metal; it is the only element not classed as a metal that has less than four electrons in its outer shell. From the standpoint of safety, boron differs from the other metals in that it presents no problem from bulk fire hazards, spontaneous dust explosions, or toxic combustion products (Ref 4). From thermodynamic considerations at ambient conditions, boron is the only metal whose adiabatic flame temperature in air can exceed the vaporization temperature of its oxide. As shown in Table II of Appendix J, it is one of the few metals that evaporate at a temperature higher than that of its primary oxide and also well above its adiabatic flame temperature, approximately $3000^{\circ}K$. These characteristics indicate that while B_2O_3 is liquid or solid, it forms a protective coating on the boron surface. This coating inhibits low temperature combustion; thus, only when the protective coating has evaporated will the reaction rate of boron be fast enough to be a satisfactory propellant additive.

Background

The rates of the ignition and combustion processes of metals have been found to be directly proportional to the subdivision of the metal fuel; therefore, most studies of metal combustion have investigated fuel particles with diameters less than 100 μ (Ref 1). Most fundamental studies have been carried out on single particles; although, the qualitative effects of concentration of dust clouds have been investigated (Refs 5 through 14). The investigations with particulate boron have shed light primarily on its ignition characteristics. The best evaluation of the combustion characteristics was accomplished by Talley (Ref 15) using bulk boron.

Talley studied the combustion of boron in oxygen using a boron rod approximately one mm in diameter heated electrically through an embedded tungsten wire. He observed very slow reaction below 723°K, the melting point of B_2O_3. The reaction rate increased gradually until vigorous reaction started near 1600-1800°K where the B_2O_3 vaporization rate became significant. He investigated the region where the evaporation of the surface oxides were rate limiting and found the combustion rates to be inversely proportional to pressure and to obey a temperature dependent Arrhenius law with an activation energy of 77 Kcal/mole. The activation energy corresponded to the heat of vaporization of B_2O_3. By adding water vapor to the oxidant, he observed an increase in the reaction rate and calculated a change in the activation energy to 56 Kcal/mole. The pressure law was the same

indicating the reaction was still controlled by an evaporating species. This indicated that if the surface oxide could be removed, the ignition and combustion characteristics could be greatly improved. This would be true in the region where the surface oxide vaporization was the rate controlling factor.

Above the boiling point of B_2O_3, the oxide deposit disappeared leaving a clean reacting surface. In this region, the reaction rate was independent of pressure. Here boron would exhibit the ideal heterogeneous surface reaction with the reaction rate limited either by the surface chemical reaction or the diffusion of oxygen to the reacting surface.

Most studies of particulate boron used particles or particle agglomerates from 30 to 50 μ average diameter. Cassel (Refs 6 and 7), Gordon (Ref 8) and Maček (Ref 9) used a hydrocarbon flame as the ignition source. Kelley (Ref 10) and McLain (Ref 11) ignited the particle by laser energy. Cassel and Gordon reported on the gross characteristics while Maček recorded the burning times. Maček used photographic film to record the residence time of the particle in the flame before "first light" and computing the heat rise of the particle, he calculated an ignition temperature of near 1900°K. Kelley and McLain studied nontreated boron and LiF coated particles to determine whether the surface treatment would influence the chemical kinetics. They reported no observable difference. McLain did report a factor of two improvement on burning time for particles irradiated by cobalt-60 gamma radiation. No explanation is given for

this phenomenon. The latter three investigators, Maček, Kelley and McLain, all report diffusion limited reaction processes or the so called "d^2 burning law". They also assumed an unlimited oxygen environment and a constant combustion temperature.

Uda and Jones (Refs 13 and 14) investigated dense cloud ignition in a shock tube. They found that ignition and burning times of multiple particle boron systems agreed with the trends of the single particle investigations. They reported a particle size dependence on ignition temperature with 0.015μ particles (this particle size was later reported to be 0.06μ, Ref 16) igniting near $1200^\circ K$ and $30-40\mu$ agglomerates igniting near $1900^\circ K$ at one atmosphere. Gordon noted the particle interactive effects of multiple particles on ignition temperature. He reported that although single particles ignited with difficulty and burned slowly in a Bunsen burner type flame, denser concentrations ignited readily and burned rapidly. Bryant (Ref 12) reported an increase in the time required to burn 35μ particles in a dense cloud over that reported by Maček. However, by taking the influence of oxidizer depletion into account, the effective single particle burning time was in agreement with Maček's. The data by Maček, Bryant and McLain are in agreement on the d^2 law for boron particle burning rates with approximately 40 ms for a 60μ particle and 15 ms for a 35μ one. This indicates diffusion controlled reaction rates with no effects due to surface coatings or combustion environments.

All of the aforementioned studies used an external means to ignite and sustain the combustion of boron. Bryant attempted to establish a steady state, self-sustained flame but was unsuccessful. He attributed his lack of success to the large size particles and to particle flow fluctuations. A steady state, self-sustained boron/air flame was successfully established by Ortwerth and Wilkinson (Ref 17). They supplied a flow of Trona amorphous boron particles in air to a 1.9-centimeter steel combustion tube and ignited the boron/air mixture with an acetylene torch. Once a layer of glowing oxides and boron was deposited on the tube walls and the boron flame was well established, the pilot flame could be removed. They attributed the ability to sustain a boron flame without the aid of a pilot flame to the radiative energy transfer from the wall deposits and the luminous flame to the particles entering the combustion chamber. Their system did not have a uniform powder flow nor was there any attempt to measure the particle flow, the boron/air concentration or other combustion characteristics.

The theory of steady state, self-sustained combustion of solid particles is not new. The analysis for a plane flame propagating through a dust cloud sustained by the radiant heat transfer from the flame zone was postulated by Nusselt (Ref 18). This theory was extended to include the effects of the heat conduction from the fuel particles to the air and the concentration density of fuel particles in the carrier air by Essenhigh (Ref 19). These theories considered only an effective flame temperature heating the particles to an

6

ignition temperature and contained no information on the
fuel particle temperature history after ignition. Because
boron particles react vigorously at their self-sustained
combustion temperatures and provide a highly luminous flame,
the steady state combustion of a dense particle cloud
ignited by radiant energy from the reacting particles should
be possible. However, at present, there is no theoretical
analysis for the temperature history from the beginning of
the heat up zone through completion of the reaction.

Purpose and Scope

The purpose of the present investigation is to estab-
lish a one-dimensional model for the ignition and combus-
tion of a dense concentration of boron particles in air and
to validate it experimentally. The theoretical analysis of
the model is derived by dividing it into two zones. The
first zone considers the energy sources and heat transfer
mechanisms to heat the oncoming gas-particle mixture to
ignition temperature. The second zone is the combustion
region; here the diffusion controlled or d^2law chemical
kinetic model for the single fuel particle, reported by
previous investigators, was modified to include the effects
of temperature and the finite oxygen environment.

A steady state, self-sustained boron/air flame was
investigated to evaluate the characteristic parameters
derived in the analysis. Combustion of both fuel rich and
fuel lean mixtures were investigated to evaluate the depend-
ence of particle loading on the combustion characteristics.
Different combustor tube lengths and air mass flow rates

were used to evaluate combustor residence time and flow characteristics on the combustion. The different combustor lengths were assumed to simulate the conditions at different cross sections of a complete combustor. Trona amorphous boron was used as the fuel. Trona boron is reported (and was verified) to have an average particle size of one micron; thus, this average diameter was used for the analysis.

Data on oxygen content of exhaust gases and flame emissivity taken at the combustor exit plane were used to deduce the combustion efficiency, emissivity and temperature of the flame. Finally, these data were compared to the combustion and chemical kinetic models to provide quantitative values for the characteristic parameters of the model.

In the following sections, a one-dimensional analytical model will be derived and the parameters to be experimentally evaluated will be identified. A description of the experimental combustion system, apparatus and instrumentation will then be presented. The discussion of the results will present the degree of success of this combustion system in obtaining high combustion efficiency and theoretical flame temperatures. These results will then be compared to the predictions obtained from the theoretical model and the findings of previous investigators.

II. THEORETICAL CONSIDERATIONS

There are many analyses for radiant heat transfer to solid particles suspended in a transparent gas. Simple radiant heat transfer applies to a single particle or a sparse particle mixture; but as the number of particles is increased, the reflections and shielding from the surrounding particles must be taken into account. Nusselt treated these phenomena statistically to obtain an analysis for a gas-particle mixture being heated by radiant heat transfer. The same result can be derived by assuming an optically thin particle cloud. This method can be used to model the heat up to ignition of a particle cloud but no analysis has been accomplished to characterize the radiant heat transfer from a chemically reacting luminous flame. Nor has the energy addition due to radiant wall deposits caused by wall reactions been treated analytically.

Combustion Model

The combustion model for this investigation was developed for an idealized system of solid fuel particles transported in suspension by a carrier gas. This model represented a steady state gas-particle mixture flowing through an insulated chamber as depicted in Fig 1. The flow entered the chamber at room temperature at approximately atmospheric pressure. The suspended fuel particles were heated to ignition temperature by radiant heat transfer from the luminous flame and heat generated by the reaction of fuel particles that adhered to the chamber walls. During the heat up phase, that is prior to vigorous combustion of the
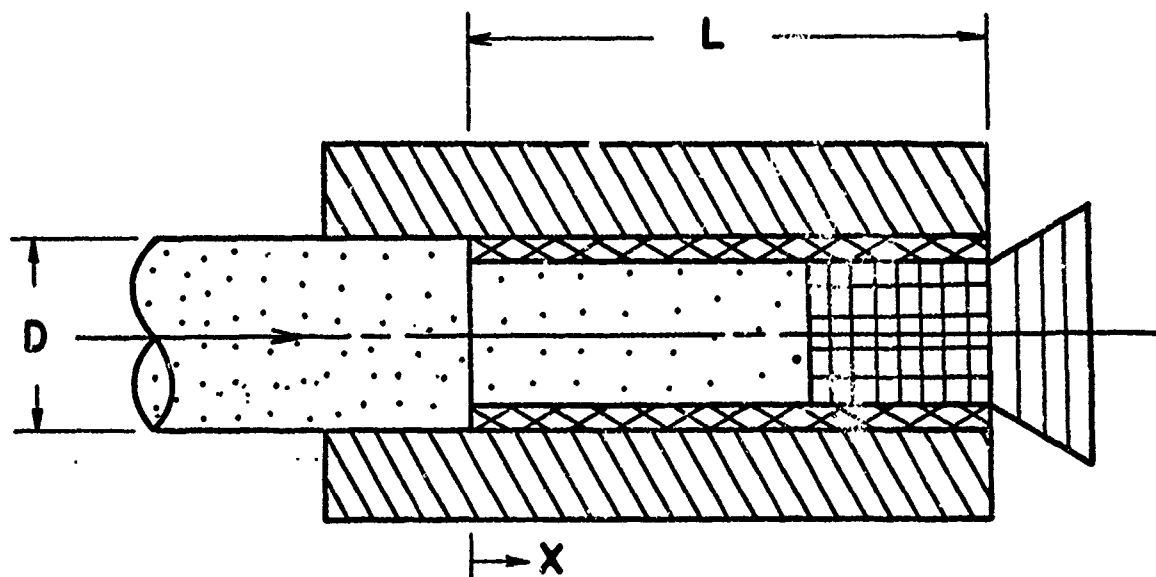
D Combustor Diameter

L Combustor Length

x Distance from Beginning
   of Heat up Zone

Gas-particle Mixture

Insulated Combustor

Boron and Boron Oxide
Deposit

Flame Zone

Exhaust Plume

Figure 1. Model of Combustion System

particles in suspension, the carrier gas was assumed to be transparent to the thermal radiation. The carrier gas was heated by convection from the suspended particles and the wall deposits. For very small particles, on the order of one micron, the temperature difference between the particles and the gas has been found to be very small (Ref 19); so, for this model, it was neglected.

Once the suspended particles were ignited to vigorous combustion, the heat of reaction on the surface of the particles provided the energy source to heat the gas-particle mixture. The carrier gas could no longer be considered transparent to radiation and radiant energy from the fuel particles and luminous products was transferred from the flame to the cold particles entering the chamber. This provided the radiant energy source to heat the oncoming gas-particle mixture. Thus, the combustion system can be described by two major zones, as depicted in Fig 2.

In Zone I, the heat up zone, energy was transferred to the gas-particle mixture from the flame zone and the combustor walls; the fuel particles in suspension were essentially nonreacting and the carrier gas was transparent to thermal radiation. Zone II, the flame zone, was assumed to be reached when vigorous combustion was initiated and the gas-particle mixture had become luminous. In the flame zone, the particles in suspension had ignited and the energy release from this reaction was the dominant source of heat for the gas-particle mixture. Here the radiant energy from the luminous fuel particles and solid and/or gaseous
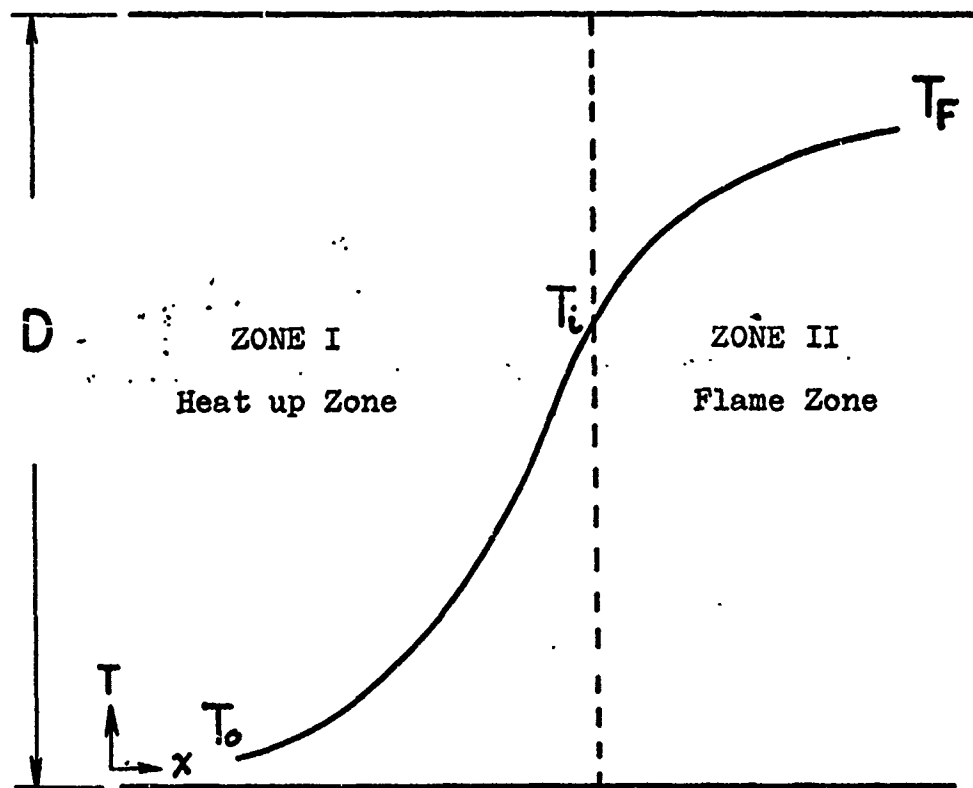
Figure 2. Depiction of Temperature Dependent
Zones in the Gas-Particle System

products was transferred to the oncoming cold particle cloud.

Assumptions

The assumptions for this model were largely standard simplifications for particle flows and contain those stated by Essenhigh and Csaba (Ref 19). They were as follows:

(a) The combustor geometry considered was a constant area tube and hence had no recirculating zones to support the flame; therefore, neglecting turbulent or wall mixing, the gas-particle mixture was one-dimensional and the flow properties were constant across any given cross section.

(b) The boron particles were spherical of uniform size with the number of particles n in a given gas volume a constant.

(c) The gas and particle temperatures and velocities were identical.

(d) The volume occupied by the solid particles was negligible compared to the gas volume; thus, the system velocity was considered to be that of the gas without particles.

(e) The gas properties did not vary significantly from those of air.

(f) The viscous drag on the combustor wall was neglected.

(g) The thermal conductivities and specific heats of the gases and particles were constant over the temperature ranges concerned.

13

(h) In Zone I, the solid particles within the mixture received energy from the flame. The flame was assumed to be at an effective temperature T_F.

(i) The combustor tubes were constructed of high thermal resistant materials; thus, the inner wall of the combustor was considered to be surrounded by an adiabatic jacket and all the energy generated by the heat of reaction on the combustor walls during heat up to ignition temperature was returned to the flow system.

(j) The mass of fuel and air that burned on the chamber walls was returned to the flow as products.

(k) Before reaction of the suspended boron particles became an important source of energy, the air surrounding the particles was transparent to thermal radiation. It received its energy by convection from the particles.

(l) The gas-particle mixture behaved like an optically thin absorbing-emitting gray gas in Zone I.

(m) In the boron/air reaction, only boron and oxygen took part in the reaction with B_2O_3 as the primary product.

Definitions

Elemental boron is difficult to obtain in a completely pure state and the boron used in this experimental investigation, Trona amorphous boron, has approximately 10% inert impurities by weight, Table III of Appendix J. There are times when the value for the mass of boron will be used in the analysis instead of that of the fuel. The subscript f for fuel will be used when the impurities in the fuel must be considered to account for the total mass of the fuel;

14

when only the mass of boron is to be considered, the sub-
script B will be used. For a fuel that has a fuel-to-boron
mass ratio $m_f/m_B = 1 + \Lambda$, the fuel is said to have
$\Lambda/(1 + \Lambda) \times 100\%$ impurities. Examples of where this will
arise are in the definition of combustion efficiency η and
fuel-to-air mass ratios. From Appendix A, the definition of
the combustion efficiency η is

$$\eta \equiv \left[(m_B)_o - m_B\right]/(m_B)_o = \frac{\Delta m_B}{(m_B)_o} \tag{A-6}$$

But $\Delta m_B = \Delta m_f$ since boron is the only active element in
the fuel, therefore

$$\eta = \frac{\Delta m_f}{(m_B)_o} = \frac{(m_f)_o}{(m_B)_o} \frac{\Delta m_f}{(m_f)_o} = (1+\Lambda)\frac{\Delta m_f}{(m_f)_o} \tag{A-6a}$$

Fuel-to-air ratios are defined as

$$F/A = \frac{(m_f)_o}{(m_{air})_o} = (1+\Lambda)\frac{(m_B)_o}{(m_{air})_o} = (1+\Lambda)(B/A) \tag{1}$$

For the stoichiometric condition

$$(F/A)_s = (1+\Lambda)(B/A)_s \tag{2}$$

The F/A and B/A ratios are interchangeable in the definition
of the equivalence ratio ϕ.

$$\phi = \frac{(B/A)}{(B/A)_s} = \frac{(1+\Lambda)}{(1+\Lambda)} \frac{(B/A)}{(B/A)_s} = \frac{(F/A)}{(F/A)_s} \tag{3}$$

The completeness of the boron/oxygen reaction can be measured by the depletion of the oxygen as well as the boron. For fuel lean combustion ($\phi < 1$), the boron would be completely consumed when the reaction was completed and the combustion efficiency would range from zero to one. For fuel rich combustion, the oxygen would be depleted when the reaction was complete but unconsumed fuel would remain. Thus, the combustion efficiency would always be less than unity, $\eta_{max} = 1/\phi$. However, in this case, the oxygen depletion parameter ψ defined in Appendix A as

$$\psi = \left[(m_{O_2})_o - m_{O_2}\right]\big/(m_{O_2})_o = \frac{\Delta m_{O_2}}{(m_{O_2})_o} \qquad \text{(A-8)}$$

would range from zero to one. Equation A-8 defined the oxygen depletion parameter and indicated the relation between the combustion efficiency and the oxygen depletion parameter to be

$$\psi = \phi\eta \qquad \text{(A-8)}$$

It is seen from Eqs 1, 2 and 3 that the equivalence ratio ϕ is defined from the initial conditions of the gas-particle mixture and is therefore a constant. However, the combustion efficiency and oxygen depletion parameters define the completeness of the combustion process and are functions of time or combustor station for a steady process.

Control Volume

The elemental control volume of the combustor model,
Fig 3, was used to apply the conservation equations of the
flow and to determine the range of the variables encountered
in this combustion system. The initial conditions of the
flow included the temperature to be at room temperature and
the velocity in the low subsonic range, while the temperature
condition at the combustor exit was at or greater than the
ignition temperature. The ignition temperature was reported
by all investigators to be near $1900^{\circ}K$. For complete
combustion however, the exit temperature was expected to be
near the adiabatic flame temperatures shown on Fig 18.

Conservation Equations

The conservation equations for a gas-particle mixture
were developed in Appendix C. The assumptions for these
equations included one-dimensional flow, no viscous forces,
constant area duct and identical velocity and temperature
for all phase states. Since the velocity of all phase
states was the same, the mass within an elementary control
volume at distance x from the combustor entrance was propor-
tional to the mass in an identical volume at the combustor
entrance. Therefore, even when combustion takes place and
the chemical species or phase states change, the mass of the
elementary (atomic) species remains constant within any
given volume.
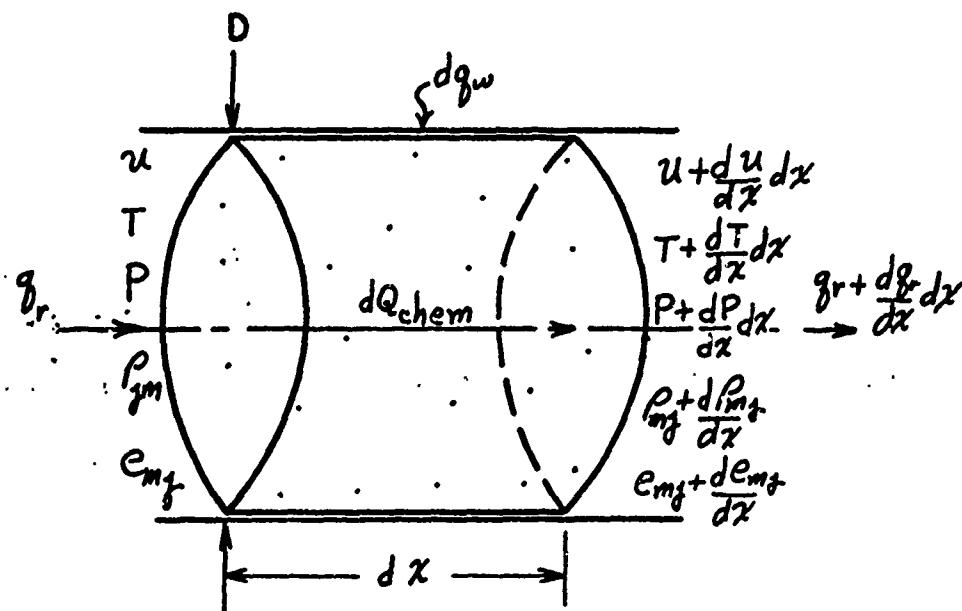
Figure 3. Elemental Control Volume for a Gas-Particle
Mixture of m Species Flowing Through a
Cylindrical Combustion Chamber at
Velocity u

The equations for continuity, momentum and energy were:

Continuity.

$$u \sum_m \sum_j \rho_{mj} = (1 + F/A) \rho_{air} u = constant \qquad (C-9)$$

Where m and j described the chemical species and phase states, respectively.

Momentum. Neglecting the viscous and body forces, the momentum equation for one-dimensional flow is

$$\sum_m \sum_j \rho_{mj} u \frac{du}{dx} = - \sum_m \sum_{j=g} \frac{d P_{mj}}{dx} \qquad (C-13)$$

Where only the gaseous species contribute to the pressure field.

Energy.

$$\sum_m \sum_j \rho_{mj} c_{p_{mj}} u \frac{dT}{dx} = \left[1 - (1 - \tfrac{2}{3} P_{v_{8 O_2}})(C_{O_2})_o \psi \right] u \frac{d P_{air}}{dx} - \nabla \cdot \vec{q} + \dot{Q}_{chem} \qquad (C-21)$$

The term $\sum_m \sum_j \rho_{mj} c_{p_{mj}}$ describes the volumetric specific heat of the multiphase flow. This term was evaluated in Appendix D and was determined to be

$$\sum_m \sum_j \rho_{mj} c_{p_{mj}} = \Theta \rho_{air} c_{p_{air}}$$

where $\qquad \Theta = 1 + 0.31 \phi \qquad (D-8)$

The pressure term in Eq C-21 is approximately equal to the change in the kinetic energy. For flow velocities less than

sonic, the change due to kinetic energy is small when compared to the combustion heating and heat transfer from the flame; thus, it can be neglected. The heat transfer term consists of both radiant and conductive energy transfers with both longitudinal and radial components. The radial energy transfer from the combustor walls was considered as a single energy source, neglecting angular dependence Eq C-21 can be written

$$\Theta \rho_{air} c_{p_{air}} u \frac{dT}{dx} = \Gamma_{air} \frac{d^2T}{dx^2} - \frac{dq_r}{dx} - \frac{1}{r} \frac{d}{dr}(r q_w) + \dot{Q}_{chem} \qquad (4)$$

Axial Heat Transfer

Even though the axial transfer of energy is a combined process of conduction and radiation, one of these processes may be much larger, just as a significant energy change by heat transfer overshadows the changes due to kinetic energy. To determine the relative importance of the axial conduction versus the radiation heat transfer, the surface integral describing heat transfer in Eq C-14 can be evaluated over the volume encompassing the entire heat up zone. The boundary conditions for this volume are ambient temperature T_0 at the combustor entrance and a temperature at or greater than the self-sustained ignition temperature T_i at the boundary between the heat up zone and the combustion zone. Past investigators have established T_i to be near 1900°K. The radiant heat transfer at these surfaces would be σT_0^4 and σT_F^4, respectively, where the combustion temperature T_F is an average temperature of the flame zone. Integrating

the heat transfer surface integral between these extremes
and noting that the surface areas are constant yields

$$-\iint_S \vec{q} \cdot d\vec{S} = -\iint_S \vec{q}_c \cdot d\vec{S} - \iint_S \vec{q}_r \cdot d\vec{S}$$

$$= -\left[(q_c S)_i + (q_c S)_o \right] - \left[(q_r S)_i + (q_r S)_o \right]$$

$$= \left[\Gamma_{air} \frac{T_i - T_o}{x_i - x_o} + \sigma T_F^4 - \sigma T_o^4 \right] S \tag{5}$$

Taking the ratio of the radiant transfers to conductive
transfers in Eq 5 and assuming $T_i = T_F = 2000°K$ with
$\sigma = 1.355 \times 10^{-12}$ cal/cm^2-sec-K^4 and $\Gamma_{air} = 1.2 \times 10^{-4}$
cal/cm-sec-K

$$q_r/q_c = \frac{\sigma (T_F^4 - T_o^4)(x_i - x_o)}{\Gamma_{air}(T_i - T_o)}$$

$$\cong \frac{(1.355)(16.)(x_i - x_o)}{(1.2)(1.7)(10^{-1})}$$

$$= (x_i - x_o) \times 10^2$$

When the heat up distance $(x_i - x_o)$ is on the order of a
centimeter, the radiant transfer is much greater than that
of conduction. To obtain a self-sustained flame, Ortwerth
and Wilkinson (Ref 17) required a minimum combustor length
of 15 centimeters, much greater than one centimeter. There-
fore, it was concluded that the conductive heat transfer
could be neglected.

The radiant energy transfer into an elemental control
volume of the gas-particle mixture, in which Eq 4 applies,

is absorbed or reflected by the solid particles. The
particles also emit radiant energy which is reflected by the
surrounding particles. In the combustion zone, the solid or
gaseous combustion products could also contribute to the
absorptions, emissions and scattering of the radiant energy.
Thus, whether the elementary volume is within the heat up or
combustion zone, the gas-particle mixture will behave like an
absorbing, emitting and scattering media. Applying the above
boundary conditions, the axial radiant energy transfer and
its derivative were developed in Appendix E for the gray gas
media. Invoking the optically thin approximation assumption,
$-dq_r/dx$ can be written

$$-\frac{dq_r}{dx} = 2 k \sigma \left[T_F^4 + T_o^4 - 2T^4 \right]$$

$$= \rho_{air} \, 2 \chi \sigma \left[T_F^4 + T_o^4 - 2T^4 \right]$$

(E-9)

Where T_F is the effective temperature of the flame zone, T_o
the initial temperature of the gas-particle mixture and σ
the Stefan-Boltzmann constant. While k and χ are defined
as the volumetric absorption coefficient and the mass
absorption coefficient, respectively.

Absorption Coefficients

The combustion zone, Zone II, was defined as the region
where the cloud reactions became important and the brilliant
green-white flame, that has been described by all investi-
gators of boron combustion appeared. Kasken and Millikan
(Ref 23), John (Ref 24) and Tisher and Scheller (Ref 25)

22

reported the luminosity of the flame to eminate from the gaseous reaction products. John identified the principle visible emitter as BO_2. Thus, while the gases in Zone I were transparent to radiation and the particles made up the absorption coefficient, the gaseous products in Zone II added to the absorption coefficient. This lead to the model for the volumetric absorption coefficients.

For Zone I,

$$k = k_p$$

Where k_p was the absorption coefficient due to the particles in the gas-particle mixture.

For Zone II,

$$k = k_p + k_g$$

Where k_g was the reaction products contribution to the total mixture absorptivity and must be modeled with the assistance of experimental results from this investigation.

The Particle Volumetric Absorption Coefficient

The volumetric absorption coefficient of the suspended particles was modeled after the reciprocal of the mean free path of a gas from molecular theory and was proportional to the total cross-sectional area presented by the particles per unit volume.

$$k_p = Z n \frac{\pi d^2}{4} \tag{6}$$

Where d is the average diameter of the fuel particles, n the number density of particles per unit volume and Z is a dimensionless proportionality factor. The number n can be

calculated by dividing the mass of the solid fuel per unit volume m_f by the mass per particle. For spherical particles this is

$$n = \frac{6(m_f)_o}{\delta_B \pi d_o^3} \qquad (7)$$

Where δ_B is the density of solid boron and d_o the initial particle diameter. Equation 7 can be described in terms of the density of the carrier air ρ_{air} and the equivalence ratio ϕ as

$$n = \rho_{air} \frac{6(F/A)_s \phi}{\delta_B \pi d_o^3} \qquad (8)$$

Substituting Eq 8 into Eq 6, the volumetric absorption coefficient of the particles is then

$$k_p = \frac{3 Z \rho_{air} (F/A)_s \phi (d/d_o)^2}{2 \delta_B d_o} \qquad (9)$$

The combustion efficiency η was defined in Eq A-6a as $(1 + \Lambda)(m_{f_o} - m_f)/m_{f_o}$. For spherical particles, it can be described in terms of the particle diameter ratio

$$\frac{\eta}{1+\Lambda} = 1 - \left(\frac{d}{d_o}\right)^3 \qquad (10)$$

Thus, the volumetric absorption coefficient, Eq 9, may be written as

$$k_p = \frac{3/2 \, \rho_{air} \, Z \, (F/A)_s \, \phi}{\delta_B d_o} \left[1 - \eta/(1+\Lambda)\right]^{2/3}$$

and the mass absorption coefficient as

$$\alpha_p = \frac{\frac{3}{2} \, \overline{Z} \, (F/A)_s \, \phi \, (1-\eta)^{2/3}}{\delta_B \, d_o}$$

Introducing $\eta' = \eta/(1 + \Lambda)$.

Using the values $d_o = 1 \times 10^{-4}$ cm, $\delta_B = 2.34$ gm/cc, $(F/A)_s = 0.115$ and $\sigma = 1.355 \times 10^{-12}$ cal/cm^2-sec-K^4, the coefficient of the radiant heat transfer due to the particles may be evaluated as

$$2\alpha_p\sigma = 2\overline{Z} \times 10^{-9} \, \phi \, (1-\eta)^{2/3} \text{ cal/gm-K}^4\text{-sec} \qquad (11)$$

Or expressed in terms of the oxygen depletion parameter ψ from Eq A-8, Eq 11 may be written

$$2\alpha_p\sigma = 2\overline{Z} \times 10^{-9} \phi \, (1 - \psi/\phi')^{2/3} \text{ cal/gm-K}^4\text{-sec} \qquad (12)$$

Where $\phi' = (1 + \Lambda)\phi$.

Chemical Heat of Reaction

The energy addition per unit volume due to the chemical energy liberated by the combustion process $\dot{Q}_{chem}$, in Eq 4, was equal to the heat of formation of the products per unit mass of fuel multiplied by the rate of fuel consumption, thus,

$$
\begin{aligned}
\dot{Q}_{chem} &= -\Delta h_f^o \, \frac{dm_B}{dt} \\
&= -(m_B)_o \, \Delta h_f^o \, \frac{d}{dt}\left[m_B/(m_B)_o \right] \qquad (13) \\
&= (m_B)_o \, \Delta h_f^o \, \frac{d\eta}{dt}
\end{aligned}
$$

Where $(m_B)_o$ was the mass of boron atomic species in a unit volume and Δh_f^o the energy liberated by the production of B_2O_3 per unit mass of boron.

Equation 13 can be described in terms of the density of the carrier air since the density of the air is the mass of air per unit volume. Thus, the mass of boron in a unit volume divided by the air density ρ_{air} is the boron/air ratio (B/A)

$$\dot{Q}_{chem} = \rho_{air} \, (B/A) \, \Delta h_f^o \, \frac{d\eta}{dt}$$

Expressed in terms of the stoichiometric ratio and the equivalence ratio Eq 13 may be written as

$$\dot{Q}_{chem} = \rho_{air} \, (B/A)_s \, \phi \, \Delta h_f^o \, \frac{d\eta}{dt} \qquad (14)$$

The measurement of the oxygen content of the exhaust gases can be accomplished with ease. However, the determination of the percentage of boron that has reacted would be much more difficult. Therefore, Eq 14 can be written in terms of the oxygen depletion parameter. The equivalence ratio can be combined with the differential of the combustion efficiency in Eq 14 and the chemical energy release rate may be written as

$$\dot{Q}_{chem} = \rho_{air} \, (B/A)_s \, \Delta h_f^o \, \frac{d\phi\eta}{dt}$$

$$\qquad (15)$$

$$= \rho_{air} \, (B/A)_s \, \Delta h_f^o \, \frac{d\psi}{dt}$$

26

In Zone I, the heat up zone, the radial energy addition from the combustor walls must be considered. The source of this energy was chemical reaction from particles reacting on the combustor walls. But since the reactions took place on the walls outside of the control volume, the energy must be transferred back into the control volume. This would be accomplished by a complicated process of the combination of radiant, convective and mass transfers. To simplify the mathematical relations for the process, the radial energy flux generated by the wall reactions was considered as part of the volumetric chemical heating. The energy generated by the chemical reaction in Eq 4 can then be written as the rate of chemical energy released by the combustor wall reaction plus the rate of the chemical energy released from the particles suspended in the air within a control volume.

$$\dot{Q}_{chem} = \dot{Q}_{chem})_w + \dot{Q}_{chem})_{cloud}$$

This relation may be stated in terms of the oxygen depletion rate; therefore, Eq 15, which is a general expression, can be written as

$$\dot{Q}_{chem} = \rho_{air} (B/A)_s \, \Delta h_f^{\circ} \left[\left(\frac{d\psi}{dt} \right)_w + \left(\frac{d\psi}{dt} \right)_{cloud} \right] \tag{16}$$

Where $(d\psi/dt)_w$ was the rate of oxygen depletion on the combustor walls and $(d\psi/dt)_{cloud}$ the oxygen depletion rate for the suspended particles reacting in the carrier gas.

The heat of formation for the product B_2O_3 decreases as the temperature increases due to the change in the phase of B_2O_3 from liquid to gaseous. To reflect this change in the heat of formation term, Δh_f^o was expressed as a function of the heats of formation for the liquid and gaseous products.

$$\Delta h_f^o = \Delta h_f^o(\ell) - P_{v_{B_2O_3}}\left[\Delta h_f^o(\ell) - \Delta h_f^o(g)\right] \tag{17}$$

Where $P_{v_{B_2O_3}}$ was the partial pressure of B_2O_3 in atmospheres at ambient pressure. The value for $P_{v_{B_2O_3}}$ postulated by Edelman and Economos (Ref 21) was

$$P_{v_{B_2O_3}} = Exp\left[19 - 44000/T\right]$$

The values for $\Delta h_f^o(\ell)$ and $\Delta h_f^o(g)$ were taken from the JANAF tables (Ref 22):

$$\Delta h_f^o(\ell) = 13.9\ Kcal/gm_B$$

$$\Delta h_f^o(g) = 9.36\ Kcal/gm_B$$

thus

$$\Delta h_f^o = 13.9 - Exp\left[19 - 44000/T\right]4.54\ Kcal/gm_B \tag{18}$$

Wall Reaction Rate Model

The reaction on the combustor walls, $(d\Psi/dt)_W$, would be proportional to the rate at which the particles impact the walls, the temperature of the combustor walls, the temperature

of the particles before impact and the condition and thickness of the oxide deposits on the walls. It could also be affected by the velocity of the air across the deposit surface. The temperature of the walls and the condition of the wall deposits would be difficult to establish and the velocity of the air will increase as the particle temperature increases. Therefore, for a simplified relation, the wall reaction rate was assumed to be proportional to the equivalence ratio ϕ and the particle temperature,

$$\left(\frac{d\psi}{dt}\right)_w = g\,T\phi \qquad\qquad (19)$$

Where g is a constant of proportionality with units of $(\text{sec-K})^{-1}$. In Zone II, the energy generated by the reactions of the particles suspended in the gas-particle mixture was assumed to be the dominant chemical energy source and the wall reactions were neglected.

Particle Reaction Rate Model

The reaction rate for the wall combustion processes was modeled from experimental results while the cloud combustion process for the suspended particles was modeled from single particle combustion models of previous investigators (Refs 9, 10, 11 and 12). The present model for suspended particles differs from past models in that the reaction temperature was assumed to increase as the combustion process proceeded. All other models have assumed a constant reaction temperature. The constant temperature assumption may be correct for the nonadiabatic combustion of

particles radiating their thermal energy to the surroundings
at ambient temperature or for liquid particles burning with
a diffusion flame where most of the thermal energy is
required to vaporize the liquid fuel. However, the present
combustion system was a dense cloud of solid particles burn-
ing in an insulated chamber to approximate an adiabatic
combustion process. The boron particles may be molten at
the combustion temperatures but the volatility of the
particles was assumed to be so low that the combustion
process may be represented as a surface reaction as depicted
in Fig 4.

For a solid fuel reacting with a gaseous oxidizer, the
rate of consumption of the solid material is proportional
to the surface area of the solid and the concentration of
the oxidizer in the surroundings. For a spherical solid
particle burning in air, the empirical first-order diffusion
limited reaction rate is described in Appendix I as

$$- \frac{dm_B}{dt} = 4 n \pi r^2 \, C_{O_2} \, M_B \, \frac{K(T)}{r} \qquad (20)$$

Where m_B was the mass of boron per unit volume, n was the
number of fuel particles per unit volume, r the radius of
the particle, C_{O_2} the concentration of oxygen in air, M_B the
molecular weight of boron, and $K(T)$ a temperature dependent
proportionality coefficient in moles/cm-sec.

The mass of a spherical particle of boron can be
expressed in terms of the particle diameter d, thus, Eq 20
may be written as

─────── Diffusion of Product
Oxides away from the
Particle Surface

─ ─ ─ ─ Diffusion of Oxygen to
the Particle Surface
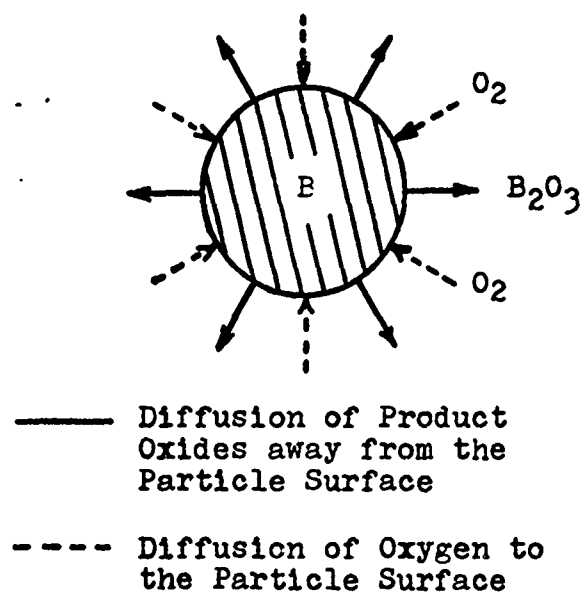
Figure 4. Heterogeneous Surface Reaction Model
for Solid Shperical Particles
Suspended in the Carrier Gas

$$-\frac{d}{dt}\left[\delta_B \, n \, \frac{\pi d^3}{6}\right] = 2 \, n \pi \, d \, C_{O_2} \, M_B \, K(T) \qquad (21)$$

For constant temperature reaction and an unlimited source of oxygen, Eq 21 can be integrated to obtain

$$d_0^2 - d^2 = \frac{8 \, C_{O_2} \, M_B \, K(T)}{\delta_B}(t - t_0)$$

$$= \beta_{diff}(t - t_0) \qquad (22)$$

Where $\beta_{diff} = 8(C_{O_2})_0 \, M_B \, K(T)/\delta_B$. Equation 22 is the d^2 law for diffusion limited reaction of a fuel particle or droplet and β_{diff} is defined as the d^2 law evaporation rate constant.

For gas-particle mixtures near the stoichiometric mixture, the oxygen concentration is no longer constant but varies with the combustion efficiency. Nondimensionalizing Eq 21 by dividing this relation by d_0^3 and multiplying and dividing by the initial concentration of oxygen $(C_{O_2})_0$, one obtains

$$-\frac{d}{dt}\left[\delta_B \, n \, \frac{\pi}{6}\left(\frac{d}{d_0}\right)^3\right] = \frac{2 \, n \, \pi}{d_0^2} \, M_B \, (C_{O_2})_0 \, K(T)\left(\frac{d}{d_0}\right)\left[\frac{C_{O_2}}{(C_{O_2})_0}\right] \qquad (23)$$

For a constant combustion temperature, only the oxygen concentration and the particle diameter ratios change with time. These ratios can be expressed as functions of the combustion efficiency by using the relations developed

1. Eqs 10 and A-8. Substituting these relations into Eq 23, it can be expressed in terms of the combustion efficiency as

$$\frac{d\eta}{dt} = \frac{12(1+\Lambda)M_B(C_{O_2})_o K(T)(1-\eta')^{1/3}(1-\phi\eta)}{\delta_B d_o^2} \qquad (24)$$

Now, to extend this analysis to a temperature dependent model, the proportionality coefficient $K(T)$ was expressed as an Arrhenius equation

$$K(T) = A e^{-E_a/RT} \qquad (25)$$

Where E_a and A are the Arrhenius activation energy and the Arrhenius pre-exponential constant, respectively. The pre-exponential constant A has a temperature dependence in the more exact theories; but unless very accurate experimental measurements are made, this is difficult to detect. The temperature dependence of the exponential term normally dominates in most reaction systems; therefore, the term A was considered as a constant.

Replacing the proportionality factor $K(T)$ in Eq 25 with the Arrhenius expression, the temperature dependent particle reaction model for a diffusion limited reaction rate and a finite oxygen source expressed in terms of the combustion temperature and combustion efficiency was

$$\frac{d\eta}{dt} = \frac{12(1+\Lambda)(C_{O_2})_o M_B A (1-\eta')^{1/3}(1-\phi\eta) Exp[-E_a/RT]}{\delta_B d_o^2} \qquad (26)$$

Equation 26 may   ' tten in terms of ψ as

$$\frac{d\psi}{dt} = \frac{12(C_{O_2})_o M_B A}{\delta_B d_o^2} \phi' (1-\psi/\phi')^{1/3} (1-\psi) Exp\left[-E_a/RT\right] \quad (27)$$

Where $\phi' = (1 + \Lambda) \phi$ and $(C_{O_2})_o$ was the initial oxygen concentration, moles O_2/moles air, equal to 0.21. This relation was for the particles reacting in the particle cloud with the reaction limited by a diffusion process.

Equation 27 can be simplified as

$$\frac{d\psi}{dt} = A'_{diff} \phi' (1-\psi/\phi')^{1/3} (1-\psi) Exp\left[(E_a/R)(\frac{1}{2320} - \frac{1}{T})\right] \quad (28)$$

Where $A'_{diff} = 12(C_{O_2})_o M_B A Exp\left[-E_a/R2320\right]/\delta_B d_o^2$ with units of $(sec)^{-1}$.

The Residence Time Parameter

The reaction rate model for the combustion process, Eqs 19 and 28, has been defined as a function of residence time t; while the increase in temperature of the combustion process, Eq 4, was expressed as a function of the axial distance from the combustor entrance. For a steady process, the relation between the axial distance and time is

$$dx = u \, dt$$

or

$$dx/u_o = (u/u_o) dt \quad (29)$$

Using the continuity equation, Eq 29 can be written

$$\left(\frac{u}{u_0}\right)dt = \frac{dx}{u_0} = \frac{(\rho_{air})_0}{(\rho_{air}u)_0}\cdot dx = d\xi \qquad (30)$$

Where $\xi = \left[(\rho_{air})_0\, x/(\rho_{air}u)_0\right]$ is defined as the residence time parameter.

The velocity ratio can be written as a function of temperature. From the analysis in Appendix F

$$\frac{u}{u_0} = \left[\frac{1+(1+F/A)\gamma M_N^2}{1+(1+F/A)(\gamma M_N^2)_0}\right]\frac{T}{T_0} \qquad (F\text{-}12)$$

If the Mach number is neglected, significant error would not be introduced for Mach numbers much less than one. Thus, for the present investigation, Eq 30 becomes

$$\frac{u}{u_0}\, dt \cong \frac{T}{T_0}\, dt = d\xi \qquad (31)$$

The energy equation Eq 4, along with the relations developed for the radiant heat transfer Eq E-9 and the chemical energy release Eq 16, comprises the one-dimensional combustion model for the gas-particle mixture. These equations apply from the beginning of the heat up zone through the flame zone. This model may be written in terms of the residence time parameter ξ as

$$\Theta\, \rho_{air}\, c_{\rho_{air}}\, \frac{u}{u_0}\, \frac{dT}{d\xi} = 2\rho_{air}\, x\, \sigma\, (T_F^4 + T_0^4 - 2T^4)$$

$$+ \rho_{air}\, (B/A)_s\, \Delta h_f^0\, \frac{u}{u_0}\, \left[\left(\frac{d\psi}{d\xi}\right)_w + \left(\frac{d\psi}{d\xi}\right)_{cloud}\right] \qquad (32)$$

Here we have neglected the conductive heat flux. The first term on the right represents the gradient of the axial radiant heat flux, the first portion of the second term represents the radial heat flux and the last portion represents the volumetric heating due to the combustion of fuel particles in suspension.

Multiplying Eq 32 by T_o/T (noting that $u/u_o \cong T/T_o$) and dividing by $\Theta \rho_{air} c_{p_{air}}$, the combustion model for the temperature rise as a function of the residence time parameter is

$$\frac{dT}{d\xi} = \frac{2 \mathcal{X} \sigma T_o}{\Theta c_{\rho_{air}} T} (T_F^4 + T_o^4 - 2T^4) + \frac{(B/A)_s \Delta \dot{h}_f}{\Theta c_{\rho_{air}}} \left[\left(\frac{d\psi}{d\xi}\right)_w + \left(\frac{d\psi}{d\xi}\right)_{cloud} \right] \quad (33)$$

The Combustion Model for Zone I

In Zone I, it was assumed that the gases were transparent to the radiant heat transfer and only the solid particles in the mixture absorbed the radiation. The absorption coefficient $\mathcal{X}$ is only that due to the particles. The dominant chemical reaction in this zone was the reaction at the combustor wall while the reactions on the suspended particles became increasingly important as the temperature approached the self-sustained ignition temperature. The implicit functions and constants of Eq 33 can now be evaluated and expressed as functions of the equivalence ratio, the oxygen depletion parameter and temperature. Using the numerical values for $c_{p_{air}}$ and $(B/A)_s$ of 0.257

cal/gm-K and 0.1046, respectively, and the expression $2 \mathcal{X}_p \sigma$ developed in Eq 12, then

$$\frac{2 \mathcal{X}_p \sigma T_0}{c_{\rho_{air}}} = 2.33 \mathcal{Z} \times 10^{-6} \phi \left(1 - \frac{\psi}{\phi} \right)^{2/3} (\sec{-K^2})^{-1} \quad (34)$$

Using the numerical expression for the chemical heat of formation for B_2O_3, Eq 18, the coefficient for the chemical energy term in Eq 33 was calculated to be

$$\frac{(B/A)_s \Delta \mathring{h}_f}{c_{\rho_{air}}} = 5650 - Exp\left[19 - 44000/T \right]/1850 \; {}^\circ K \quad (35)$$

The simplified expression for the chemical reaction rate on the wall was developed from the relation established in Eq 19 and can be written in terms of the residence time parameter ξ as

$$\left(\frac{d\psi}{d\xi} \right)_w = \frac{T_0}{T} \left(\frac{d\psi}{dt} \right)_w = g \, T_0 \, \phi \quad (36)$$

The model for the reaction rate of the particles suspended in the carrier air is described in Eq 28. This relation can be written in terms of the residence time parameter ξ as

$$\left(\frac{d\psi}{d\xi} \right)_{cloud} = \frac{A'_{diff} T_0 \phi'}{T} \left(1 - \frac{\psi}{\phi'} \right)^{1/3} (1 - \psi) Exp\left[(E_a/R)(\frac{1}{2320} - \frac{1}{T}) \right] \quad (37)$$

Equation 33 is the general expression of the model for the combustion of a gas-particle mixture. This relation, together with Eqs 34 through 37, represents the gas-particle

mixture before vigorous combustion takes place. This model
accounts for reaction of fuel particles on the combustor
walls, the initial stages of the energy release from the
particles in suspension and neglects axial conductive heat
transfer. The carrier air is assumed transparent to
radiation by considering absorption and emission of radiant
energy by the fuel particles alone.

The Combustion Model for Zone II

In Zone II, the suspended particle reaction
$(d\psi/d\xi)_{cloud}$ was the principal reaction; the wall reaction
$(d\psi/d\xi)_w$ was assumed to play a minor role in the reaction
processes and was neglected. The luminous products added
to the luminosity of the flame and were included in the
absorptivity term of the heat transfer. A control volume
within this zone was assumed to be in thermal equilibrium
with the rest of the flame; its only thermal exchange was
with the cold gas-particle mixture approaching the flame.
For Zone II, the equation for the rate of temperature rise
Eq 33 was then

$$\frac{dT}{d\xi} \cdot \frac{2(\chi_P + \chi_g)T_0}{\Theta c_{p_{air}}T}\sigma(T_0^4 - T^4) + \frac{(B/A)_s \Delta h_f^o}{\Theta c_{p_{air}}} \left(\frac{d\psi}{d\xi}\right)_{cloud} \quad (38)$$

Where the relations established in Eqs 34, 35 and 37 are
still valid.

The parameters affecting the combustion model have been
identified and its theoretical analysis may be accomplished
with Eqs 33 through 38. Next, an experimental parametric
study of the steady state, self-sustained boron/air

combustion will be required to determine the characteristics of the boron combustion process. The parameters to be evaluated are: the fuel/air equivalence ratio ϕ, oxygen depletion parameter ψ, the local gas-particle temperature T, the Arrhenius equation activation energy E_a and pre-exponential constant A, the effective flame temperature T_F, the combustor wall reaction rate constant g, the particle absorption proportionality factor Z, the combustion product contribution to the flame absorptivity χ_g, and the combustor residence time parameter ξ.

The parametric study was accomplished at different values of the residence time parameter ξ and the equivalence ratio ϕ. The residence time parameter ξ was varied by changing the combustor length L and the air mass flux. The equivalence ratio ϕ was determined by metering the fuel flow for the corresponding air mass flow. The oxygen depletion parameter and the gas-particle temperature were determined for the various values of ξ and ϕ. The oxygen depletion values were measured from exhaust gas samples by mass spectrography and the temperatures were evaluated from absorption-emission data. The rest of the parameters were evaluated using the combustion model to determine the best correlation to the measured data.

III. APPROACH AND EXPERIMENTAL APPARATUS

A system was developed that permitted a high degree
of control over the fuel particle flow for a self-sustained
boron/air combustion flame. The system consisted of dry,
filtered, compressed air and boron particles. The air supply
was metered through a central duct. The air was then divided
with a portion of the air directed through a particle mill
with the main flow of air going directly to a combustion
chamber. The air directed through the particle mill re-
joined the main flow upstream of the combustion chamber.
Boron fuel was prepared by pressing Trona amorphous boron
into cylindrical pellets. The pellets were placed into a
fuel cylinder and fed into the particle mill at a given rate
to obtain the desired flow rate of boron particles. The
particles were entrained in the air flow that was directed
through the particle mill and carried to the main flow. The
particle laden flow was injected longitudinally along the
center line of the inlet duct 46 centimeters upstream from
the combustion chamber to allow for mixing the particles and
air before they entered the combustor. The boron/air mixture
was initially ignited by a hydrogen/air pilot flame. Once
the boron combustion was established, the pilot flame was
turned off and the self-sustained boron flame would stabilize
at near atmospheric pressure. After the flame had reached
steady state combustion, data on flame temperature and
exhaust gas oxygen content were taken. A diagram of the
test apparatus is shown in Fig 5.

A Compressed Air Supply
B Constant Pressure Chamber
C Particle Mill Fluidizing Air
D Variable Speed Drive
E Fuel Feed Piston
F Fuel Pellet Chamber
G Particle Mill
H Repowdered Fuel Flow
I Hydrogen Supply

J Igniter Tube
K Combustor
L Combustor Length
M Spectrometer
N Focusing Lens
O Tungsten Lamp
P Pressure Gauge
Q Turbine Flow Meter
R Gas Valves
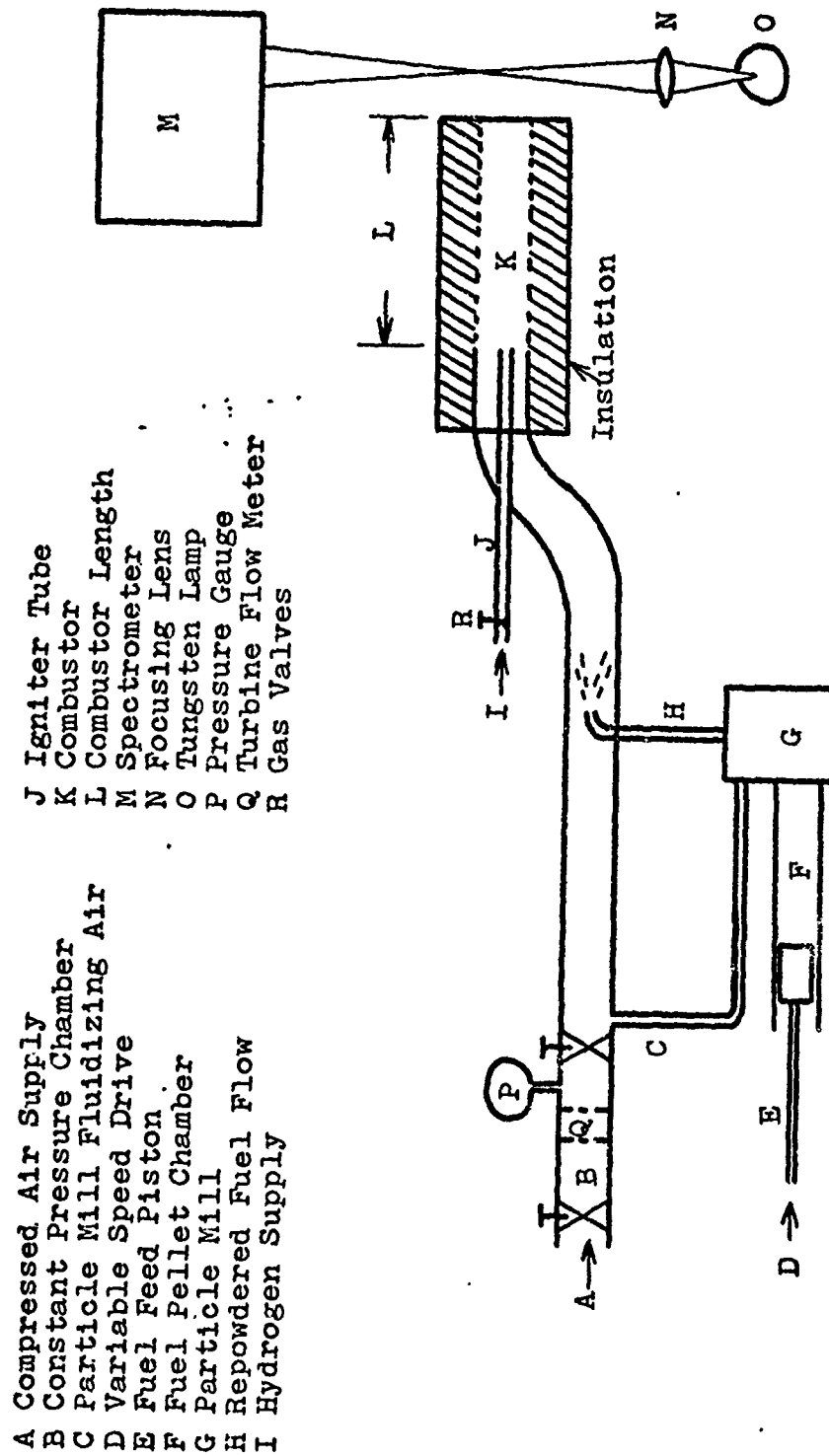
Figure 5. Schematic Diagram of the Test Apparatus

Test Matrix

The characteristics of self-sustained combustion at near atmospheric pressure were investigated. The combustion chambers used were constant area tubes with no restrictions at the exit. Combustor tubes up to 76 centimeters in length were used to vary the combustion residence time. The length of the combustor was measured from the exit plane back to the igniter tube tip. The fuel-to-air loading effects were determined by varying the fuel/air equivalence ratio from 0.5 to 2.0. The effects due to mass flux of the air were investigated over the range of 0.098 to 6.35 gm/cm^2-sec for combustor diameters of 1.9 to 7.62 centimeters.

The primary tests for combustion efficiency and temperature were accomplished using 1.9-centimeter diameter zirconia tubes. The other combustors were used to evaluate the ease of initiating steady state combustion, the effects of combustor heat loss, the changes in the wall deposits with air mass flux and the effect of combustor length on combustion efficiency. The listing of the combustors and test parameters is as follows:

Combustor Material	ID (cm)	$(\rho u)_{air}$ (gm/cm^2-sec)	Length (cm)
Thin-Walled Stainless Steel	2.54	0.488-3.42	0. -40
	5.08	0.195-0.488	20. -61
	7.62	0.098-0.195	20. -76
Graphite	2.54	0.977	15.2-61
Zirconia	1.9	1.71 -6.35	22.8-56
	2.54	0.488-3.42	30.5-76

Combustor Materials

The tubular steel chambers were fabricated from 247 stainless steel. The graphite burner was made from stabilized graphite by the University of Dayton under a contract for the AF Materials Laboratory. It consisted of 7.62-centimeter OD graphite cylinders with a 2.54-centimeter inner core. The graphite cylinders were incased in a 7.62-centimeter pipe and held in place by end flanges; the exit end flange was spring loaded to allow for thermal expansion.

The zirconia chambers were formed with water base zirconia cement. Glass wool fibers were mixed into the cement to provide a matrix binder. Waxed paper was wrapped around a length of metal tube to form the inside diameter of the combustor and the plaster mixture was trowelled around the metal tube in layers of approximately 0.6 to 1.0-centimeter thicknesses until a five-centimeter thick chamber wall was built up. Each layer was allowed to cure at room temperature before the next layer was applied. After the plaster had cured, the metal tube was removed and a steel tube was inserted into the combustor entrance to enable the combustor to be connected to the upstream tubing. The waxed paper burnt away immediately upon applying the initial pre-heat leaving only an insulated combustor.

Fuel System

A fuel system was developed to provide a method for obtaining a steady uniform flow of fuel particles and measuring the fuel flow rate. This system consisted of amorphous

boron pressed into cylindrical pellets and fed into a particle mill at a known rate.

Feed System. The feed system was composed of a tubular fuel chamber and a worm gear driven piston. The worm gear was driven by a one hp variable speed electric motor. The speeds of the piston throughout its range of operation were checked periodically during the experimental investigation. The maximum deviation of the speeds at any motor potentiometer setting was 5% with the root mean square deviation less than 1%. The rate of fuel flow was calculated from the speed of the piston drive multiplied by the density per unit length of the fuel pellets.

Particle Mill. The particle mill consisted of an aluminum chamber and a row of circular wire brushes, as shown in Fig 6. Three Osborne ringlock No. 2679 brushes with a 5.3-centimeter diameter, 11-μ diameter steel wire and a 1.525-centimeter arbor hole were used. The brushes were rotated at a constant speed of 6000 RPM. The aluminum chamber was constructed so that there were a minimum of void spaces for dust accumulation. A chevron seal around the drive shaft precluded the loss of fuel particles and air. To determine the effectiveness of the particle mill returning the amorphous boron back to its original particle size, a sample of the amorphous boron as it was received and a sample of repowdered particles were analyzed for size distribution. A Stokes flotation analysis of these samples was performed by the Chemistry Laboratory of the AF Aerospace Research Laboratories. The results from their analysis is shown in

END VIEW

SIDE VIEW
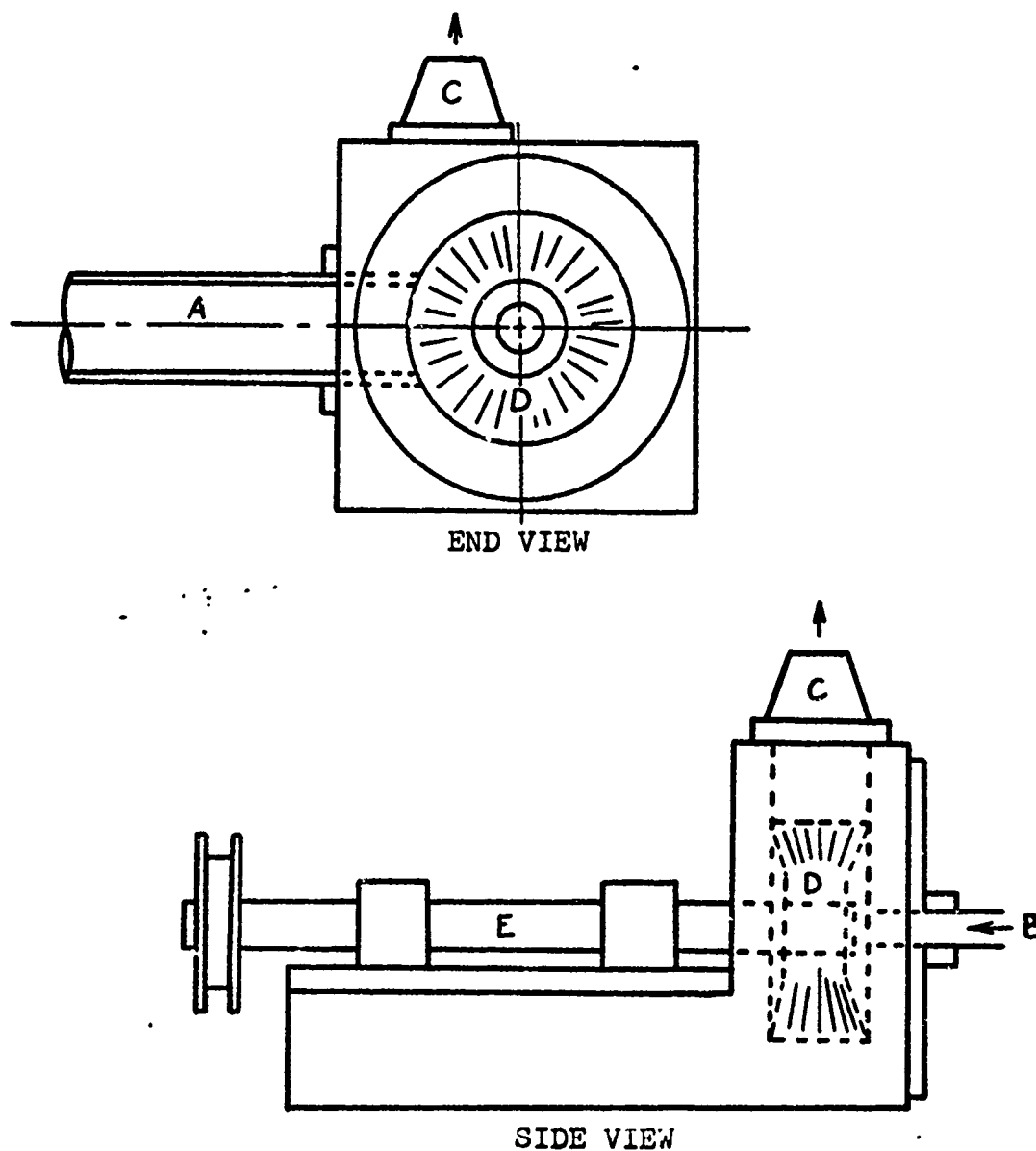
A Fuel Pellet Feed Chamber
B Air Flow into the
   Particle Mill Chamber
C Particle Laden Air Flow
   to Combustion Chamber
D Wire Brushes
E Arbor Drive

Figure 6. Boron Particle Mill

Fig 7 as the accumulat   fraction of the sample mass with
particle diameters less than that indicated on the abscissa.
The repowdered boron had a smaller size distribution than
did the original amorphous boron. Assuming spherical
particles, the number of fuel particles within a diameter
class was determined from the mass of fuel in each class.
The average particle diameter was then calculated from this
information. The calculated average particle size for the
repowdered boron was 1.25 μ while the original amorphous
powder had an average particle size of 1.75 μ.

Fuel Preparation. The fuel pellets were fabricated by
mixing tap water with Trona amorphous boron powder until a
thick, smooth paste was obtained. The paste was placed in
a teflon lined mold and pressed slowly on a metallurgical
press to 6000 psi to remove the excess water and boron
trioxide. The pressure was applied slowly to equalize the
pressure within the mold to obtain a homogeneous density.
The pellets were extruded from the mold and allowed to dry
at the room atmosphere. After they were thoroughly dried,
they were weighed on a chemical balance scales and measured
to obtain their linear density. The residual moisture
content of a sample pellet was checked by the Fuels Branch,
AF Aero Propulsion Laboratory, Wright-Patterson AFB, Ohio,
and was found to be that of the surrounding atmosphere.

Igniter Flame. An igniter tube, constructed of 0.64-cm
stainless steel tubing, was located at the aft end of the
combustor aligned parallel with the combustor center line
as shown in Fig 5. Hydrogen, passed through this tube, was
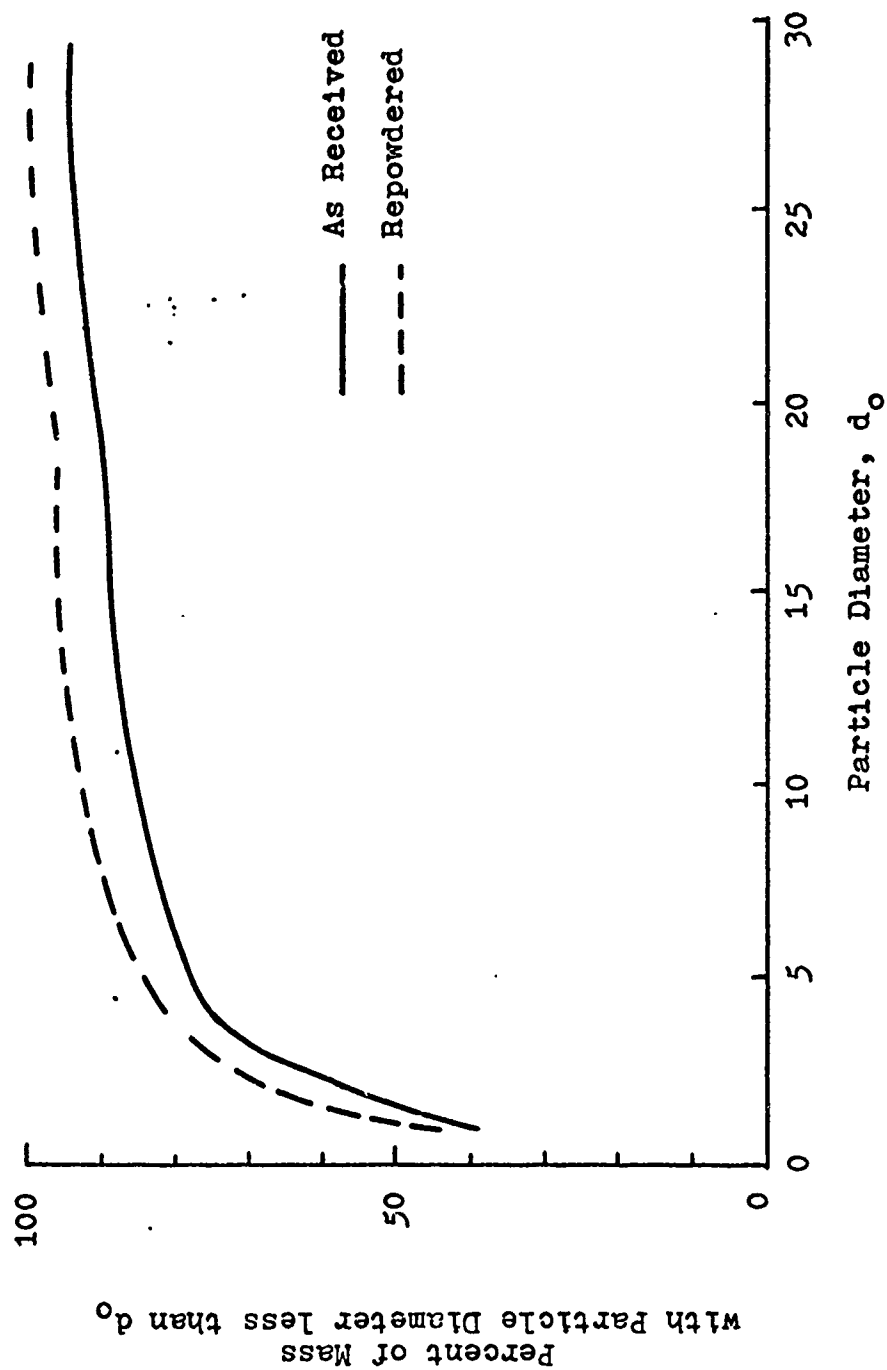
Figure 7. Particle Size Distribution of Trona Amorphous Boron

used to preheat the combustor walls and to ignite the boron particles. The test procedure was to ignite the hydrogen flame at a reduced air flow then stabilize the air mass flow to the desired test condition. When the air flow was stabilized, the boron particle flow was introduced. Once the boron flame was established, the hydrogen was turned off.

Instrumentation

Air Flow. A GL-8 Cox turbine type flow meter was used to measure the air flow rate. The flow meter was calibrated at the gas flow facilities at Newark AFS, Ohio and Tinker AFB, Oklahoma against a known air volumetric flow at 20, 30 and 40 psi. The meter output was converted to an analog signal and displayed on a Brown recorder. The air pressure in the constant pressure chamber was adjusted to the desired test condition and monitored on a calibrated Heise pressure gauge.

Fuel Flow. A variable speed, one hp, electric motor was used to drive the fuel piston. The motor RPM was controlled by a calibrated potentiometer. The piston drive speed and potentiometer settings were correlated by a stop watch.

Temperature Measurement. The luminous flame emissions were scanned using a Warner-Swasey 501 Rapid Scan Spectrometer, both in scanning mode and as a monochrometer. In the scanning mode, the spectrum from 0.4 to 0.65 μ was monitored. The boron oxide emission peak at 0.518 μ was monitored monochromatically. The spectrometer signal was enhanced through photomultipliers and displayed on an

oscilloscope. Absorption d ta of the flame were obtained by viewing a calibrated tungsten lamp through ie flame. Absorption-emission information was obtained by chopping the light from the tungsten lamp. The data were recorded on Type 52 Polaroid film. The method of calculating the flame temperatures from this data is given in Appendix G.

Exhaust Gases Measurement. Exhaust gas samples were collected through a vacuum operated 0.64-centimeter stainless steel probe. The samples were trapped in glass sample bottles with high vacuum valves. Oxygen/nitrogen and nitrogen/argon ratios were determined by the High Energy Chemistry Branch at the AF Aerospace Research Laboratories using mass spectroscopy.

IV. RESULTS AND DISCUSSION

Numerous test runs were performed; some from which data were collected and others were made to observe the appearance of the flame, the combustor wall deposits or the effects of the combustion process on the combustor materials. The test runs were reproducible and the technique for establishing the self-sustained flame became apparent. Self-sustained flames of particulate boron and air could not be established for any test condition without boron reacting on the combustor walls. The difficulty of establishing steady flames increased as the fuel/air ratio decreased and at equivalence ratios less than 0.5, a steady self-sustained flame could not be established. Although the equivalence ratio at 0.7 could be established as a steady self-sustained flame with complete burning of the boron, the emissivity of a 2.54-centimeter diameter flame was too weak and irratic to measure the temperature. As the fuel/air ratio was increased, the flames were increasingly easier to establish with the partially burned boron particles of fuel rich flames burning to completion in the exhaust plume. But above an equivalence ratio of three, the white exhaust cloud, characteristic of complete combustion, became dark brown to black which indicated many of the particles did not ignite and unburned boron was present in the exhaust plume.

The combustion process investigated here was for one fuel particle size distribution (with an average diameter near one μ) and no information was derived for the influence of different particle diameters. However, the solids

loading in the gas-particle mixture was varied to determine
the effect of the fuel/air equivalence ratio on the combus-
tion characteristics. The data for the oxygen content and
temperature of the exhaust gases at the combustor tube exit
are tabulated in Tables IV, V and VI of Appendix J for
equivalence ratios 1, 1.5 and 2. These data were obtained
from 1.9-centimeter and 2.54-centimeter diameter combustors
with lengths varying from 15 to 76 centimeters and are
portrayed in Figs 8 through 27. They indicated the results
wore reproducible and a steady, self-sustained, boron powder
combustion flame could be established.

The discussion is arranged in three parts: (a) the
experimentally measured characteristics are presented to
show that this combustor design technique for boron/air
combustion resulted in rapid complete reaction with a high
thermal energy release, (b) these characteristics are
compared to the analytical combustion model of this study to
illustrate the relative importance of the heat producing and
transfer mechanisms and the empirically determined character-
istic values, and (c) discussion of some characteristics of
the combustion process.

Fuel Pellets

The fuel pellets obtained from the fuel fabrication
process were 1.75 centimeters in diameter with density near
0.9 gm/cc. This procedure resulted in uniform density
pellets. Approximately 10% of the pellets were weighed and
measured, these had an rms deviation of less than 2% from the
average among the pellets. Most of this variation was

caused by the compressibility of the press mold teflon liner which allowed the pellet diameter to vary slightly.

Gas-Particle Mixture

The uniformity of the gas-particle flow was checked by measuring the attenuation of the intensity of the calibrated tungsten lamp. The tungsten lamp was viewed through the gas-particle flow by the Warner-Swasey Rapid Scan Spectrometer as shown in Fig 5. Oscilloscope traces of the wave length spectrum from 0.4 to 0.65μ were photographed with $\frac{1}{2}$-second exposure. This was accomplished for particle loadings corresponding to fuel/air equivalence ratios of 0.1 to 1.0 with no broadening of the oscilloscope trace. This indicated that the gas-particle flow was steady for all particle loadings checked. The average diameter of the particles in the gas-particle mixture was calculated using the absorption coefficient developed in Eq 9, it was determined to be near $\frac{1}{2}$ micron for the proportionality constant Z equal to one. This compares well with the 1.25μ average diameter calculated by the AF Aerospace Research Laboratory from a Stokes flotation analysis.

Combustion Efficiency

The combustion efficiency for the gas-particle mixture was evaluated by measuring the change in the oxygen content of the carrier gas. This was accomplished by obtaining the ratio of nitrogen to oxygen from mass spectrographic data of the cooled exhaust gases and comparing it to the nitrogen/oxygen ratio of air. This method assumed there were no nitrogen reactions of any consequence and the primary

oxygen reactions were with the boron. To assure that this assumption was true, nitrogen/argon, NO/argon and NO_2/argon ratios of the mass spectrographic data were made. There was no change in the nitrogen/argon ratio as shown in Table VII of Appendix J, where the values obtained for this ratio were within the natural scatter of the data. The data for NO and NO_2 were too small to be noted. Thus, assuming no nitrogen reactions, the exit oxygen depletion parameter was

$$\psi_E \doteq 1 - (m_{O_2})_E / (m_{O_2})_o = 1 - \left(\frac{c_{O_2}}{c_{N_2}}\right)_E / \left(\frac{c_{O_2}}{c_{N_2}}\right)_o \qquad (A-8)$$

The validity of any gas sampling data is always in question. The major reason for this is the quenching of the sample. For solid particles reacting in a gas, the rate of quenching would be slower than for a gaseous reaction. The sampling procedure for a particle system was further complicated since the particles were either molten or had molten oxides on their surfaces. These particles adhered to the gas probe causing restrictions of the flow into the probe or deflection of the exhaust plume away from the probe. The internal restrictions caused by the solids collecting within the probe were reduced by adding a helium purge gas system to the sampling probe. These solids were removed by purging the probe after the sample was taken. The sampling time to ensure a representative sample of the exhaust gases was reduced by purging the probe just prior to taking a sample. Rapid quenching of the boron reaction was

believed to take place because boron reacts vigorously only
above 1800 to 2000°K with almost no reaction below 1000°K.
Thus, the oxygen content in the sample was assumed to be
approximately the same as that of the exhaust gas from which
it was obtained.

Correlation of the Exhaust Gas Data

The exhaust gas data were collected from different
length combustors and at various mass fluxes of the carrier
air. The combustor length was measured from the pilot
burner tip to the combustor exit and the air mass flux was
calculated from the total air flow into the system. The
oxygen depletion parameter values ψ were plotted against
the combustor residence time parameter ξ , defined in Eq 31,
to determine the trends for the combustion efficiency, as
shown in Figs 8 and 9. The data at $\phi = 1.5$ was so similar
to that at $\phi = 2.0$, it was plotted with the data for 2.0.

At low air mass fluxes, the oxygen depletion data
collected were shifted toward the longer residence times.
This gave the indication of lower reaction rates for the low
gas flows. However, this shift of the data was not caused
by a lower reaction rate but was due to excessive deposits
of boron and its oxides in the upstream end of the combustor.
These deposits filled in the volume at the entrance of the
combustion chamber and created a shortened combustor. This
tendency of the particles to agglomerate at the entrance of
the combustor decreased as the air mass flux increased until
above approximately 1.5 gm/cm^2-sec the wall deposits were
uniform. Thus, the majority of the test runs recorded were
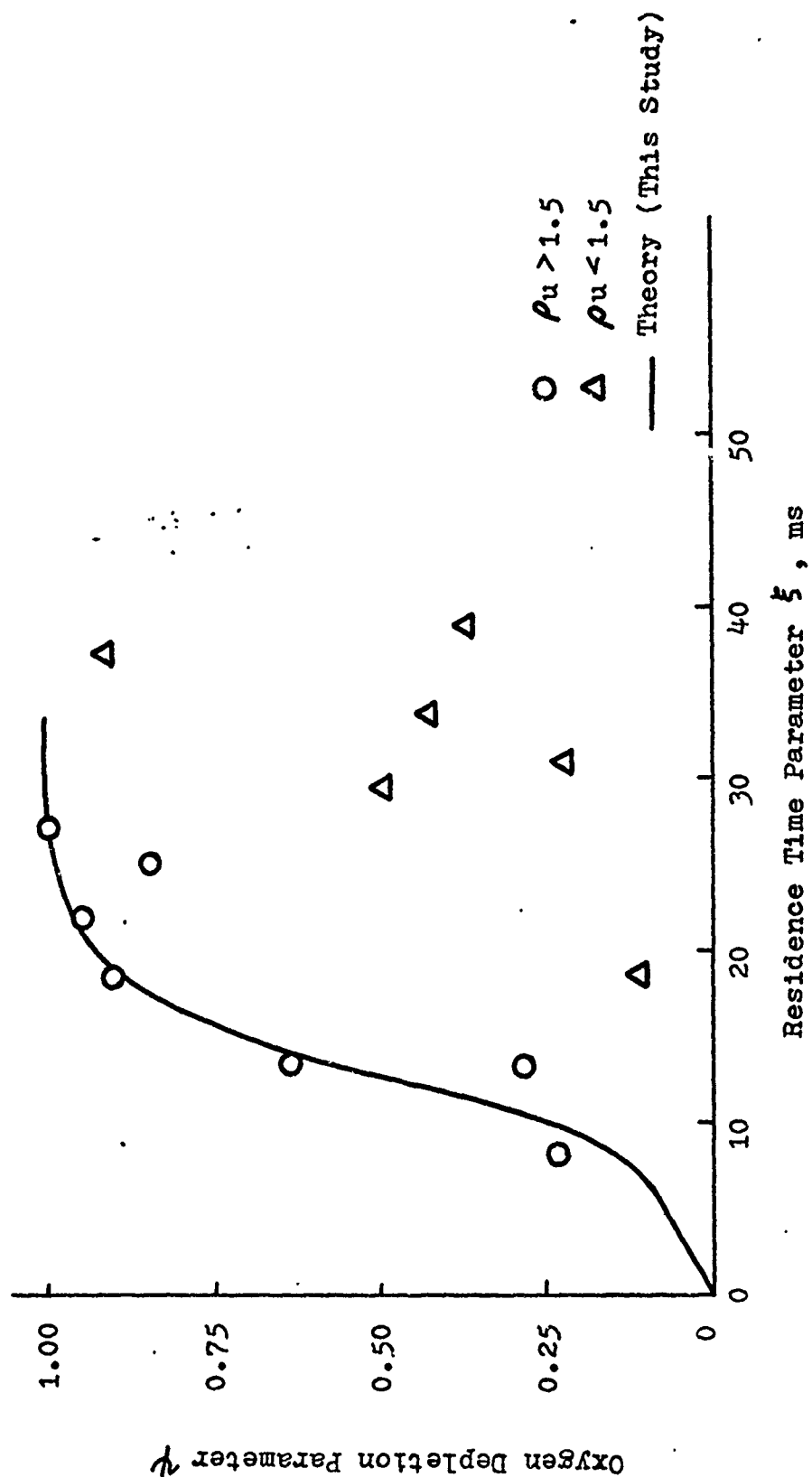
DS/ME/74-2

Figure 8. Effect of Air Mass Flux on Combustion Efficiency at $\phi = 1$
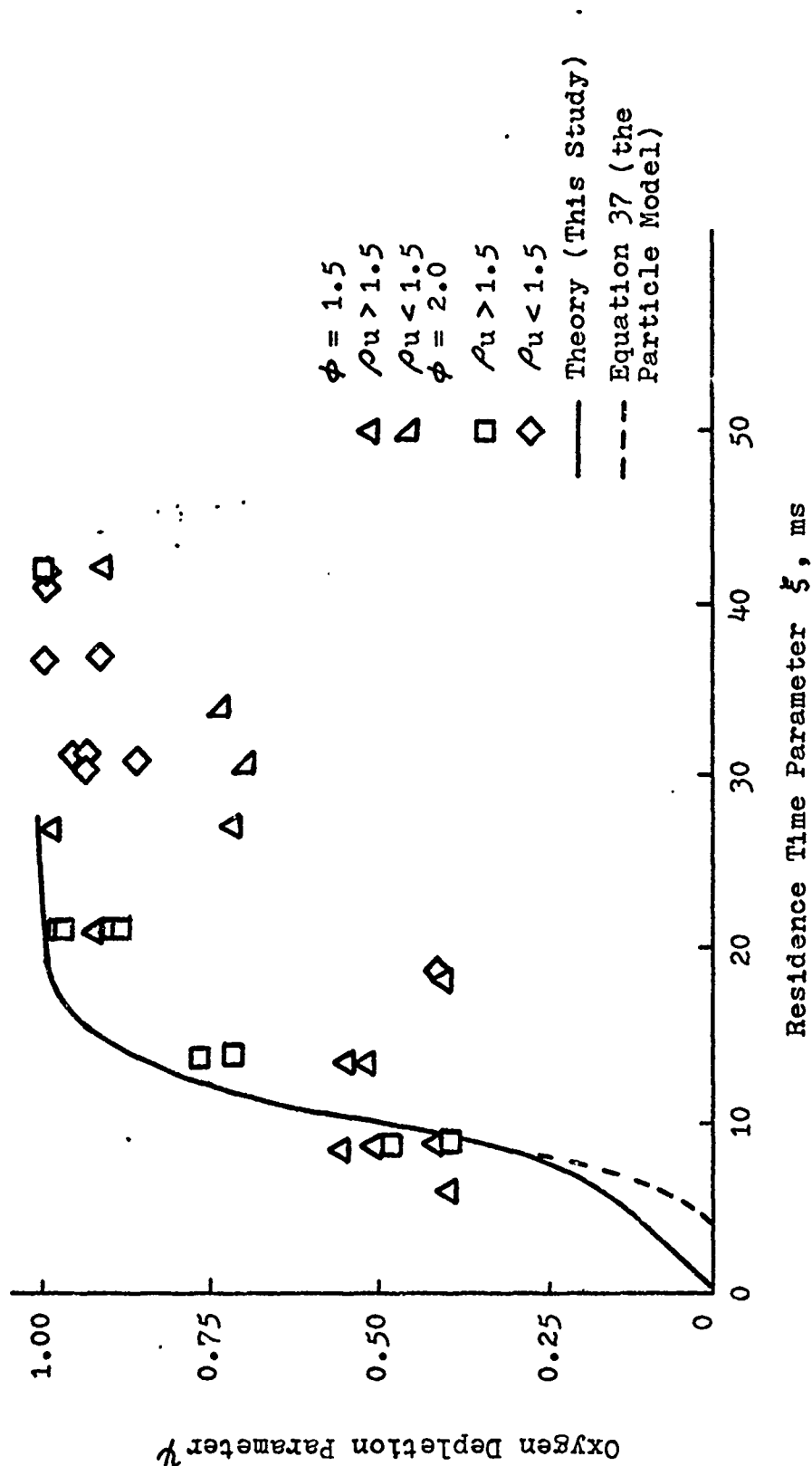
Figure 9. Effect of Air Mass Flux on Combustion Efficiency at $\phi = 1.5$ and 2.0

near 3 gm/cm^2-sec to insure the uniformity of the wall deposits.

Data were collected only for tests where a stable luminous flame was visible at the exit plane. For this condition, the minimum oxygen depletion value was 0.1 at ϕ = 1.0 and approximately 0.4 for equivalence ratios of 1.5 and 2.0. This corresponded to a value of the residence time parameter of 8.6 as listed in the tables of data for a 1.9-centimeter diameter chamber, 22.8 centimeters in length. With increased residence time, 90 to 100% of the oxygen was consumed for residence time parameter values greater than twenty milliseconds. Even though the higher values of oxygen depletion were obtained more rapidly at an equivalence ratio of 2.0, the oxygen depletion rates from the onset of the luminous flame to complete consumption of the oxygen were very similar for both equivalence ratios of 1.0 and 2.0. The greatest deviation in the oxygen depletion was at ξ of 13.4 for an equivalence of one. This was at the steepest slope for the reaction and a slight change in the flame front would account for most of the deviation.

Correlation of the oxygen depletion data with the real time combustor residence time indicated that the stable luminous flame was established in approximately two milliseconds and the reaction was complete in four milliseconds. This was evaluated from data at an equivalence ratio of 2.0 in Fig 10; the times would not be significantly different for equivalence ratios of 1.0 and 1.5. The combustor residence time was calculated from the
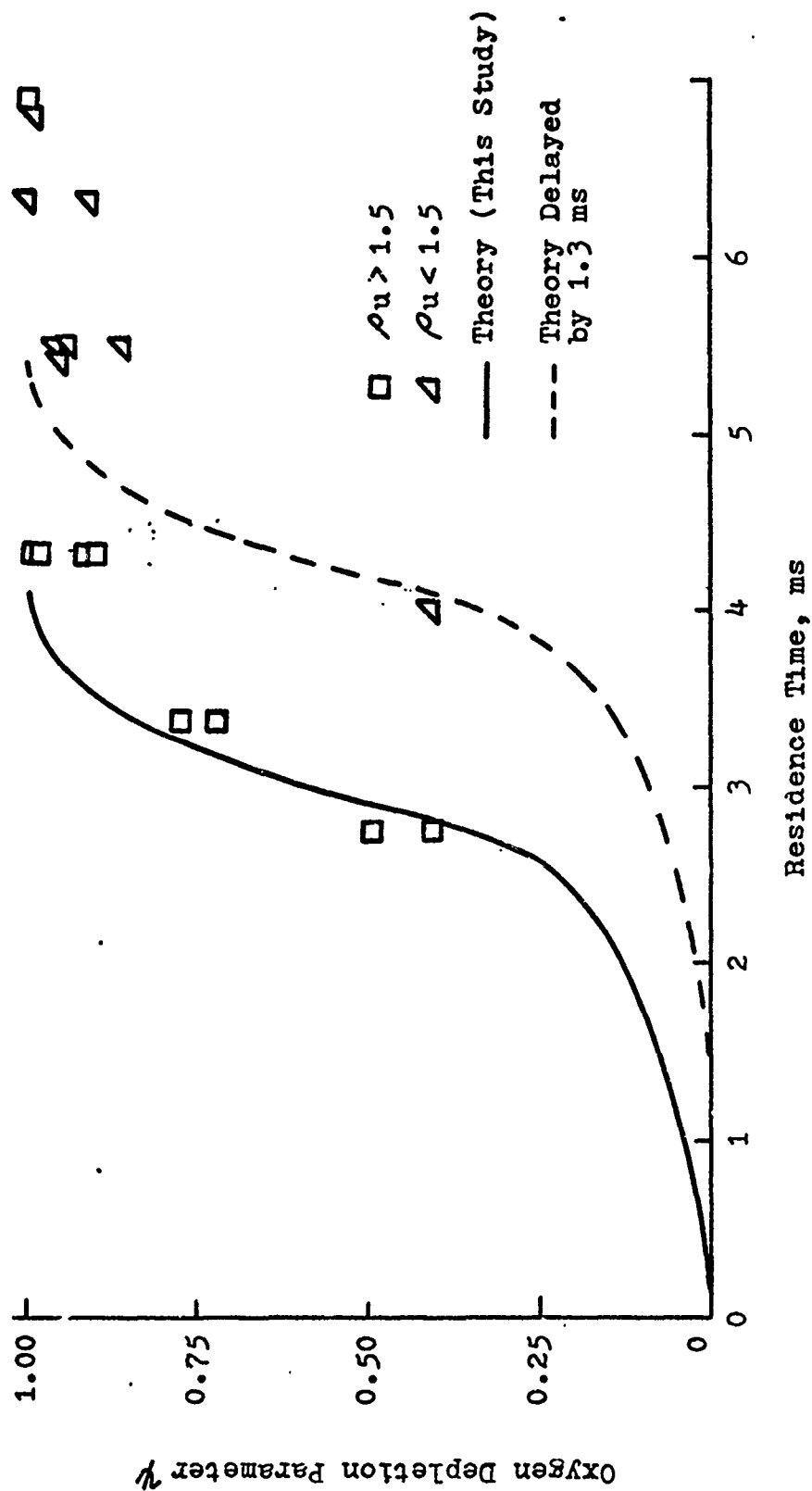
Figure 10. Variation of Oxygen Depletion with Actual Residence Time at $\phi = 2.0$

residence time parameter by integrating Eq 31 with the temperature values obtained from Fig 21 using straight line segments connecting the average values of the temperature data.

Temperature Measurements

Because the flame temperatures encountered were much too high for thermocouple measurements and due to the solids in the flame zone, a noninterference measurement was used. The boron flames are highly luminous, therefore, an absorption-emission measurement system, described by Beyermann (Ref 27), was adopted. This system utilized Planck's law of radiation and is theoretically applicable only to gaseous media.

The theoretical methods for applying the absorption-emission technique to temperature calculation are shown in Appendix G. The flame temperature at the combustor exit was calculated using Eq G-4. This technique required the monochromatic radiant intensity of a known temperature source, the emitted intensity of the test flame and a measure of the attenuation of the known source through the test flame. The monochromatic absorptivity of the flame is proportional to the difference in the alternating absorption-emission intensity signals while the flame intensity is proportional to the lower (emission) intensity, Fig 29.

Typical absorption-emission data for equivalence ratios of 1.0 and 2.0 at 0.518 μ are shown in Figs 11, 12 and 13, where the emitted intensity of the flame is the lower signal and the flame plus the intensity of a controlled tungsten lamp viewed through the flame is the upper signal. The
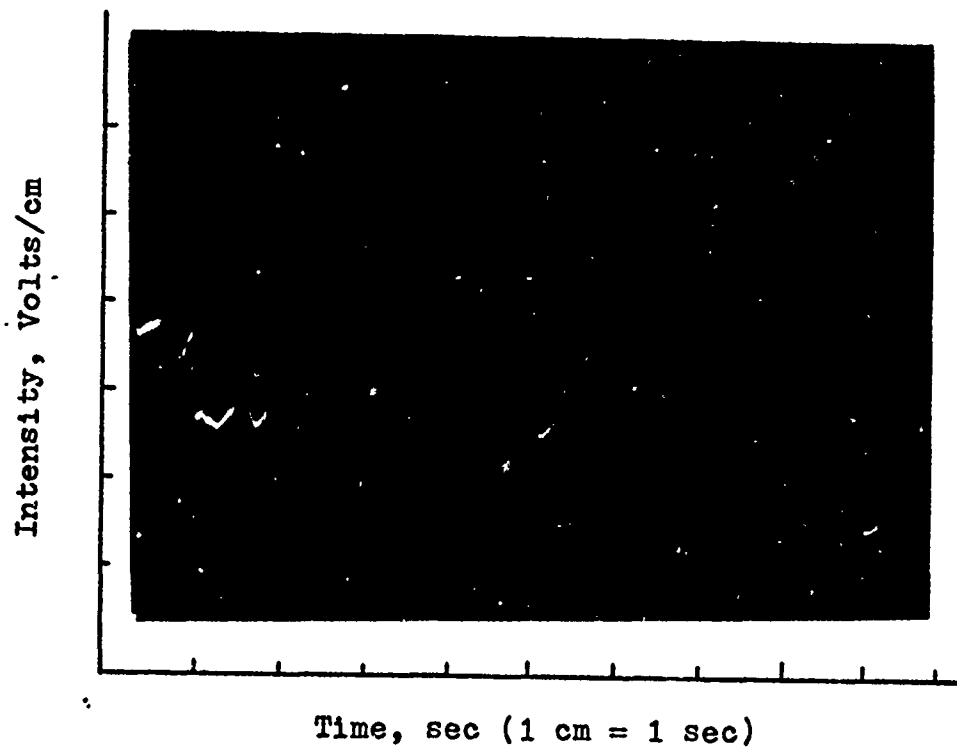
Figure 11. Spectrometric Data of the Flame Emissions
from 1.9-cm ID Zirconia Combustor at
$\lambda = 0.518 \mu$ for $\phi = 2$ at $\xi = 8.62$ ms

Time, sec (1 cm = 1 sec)
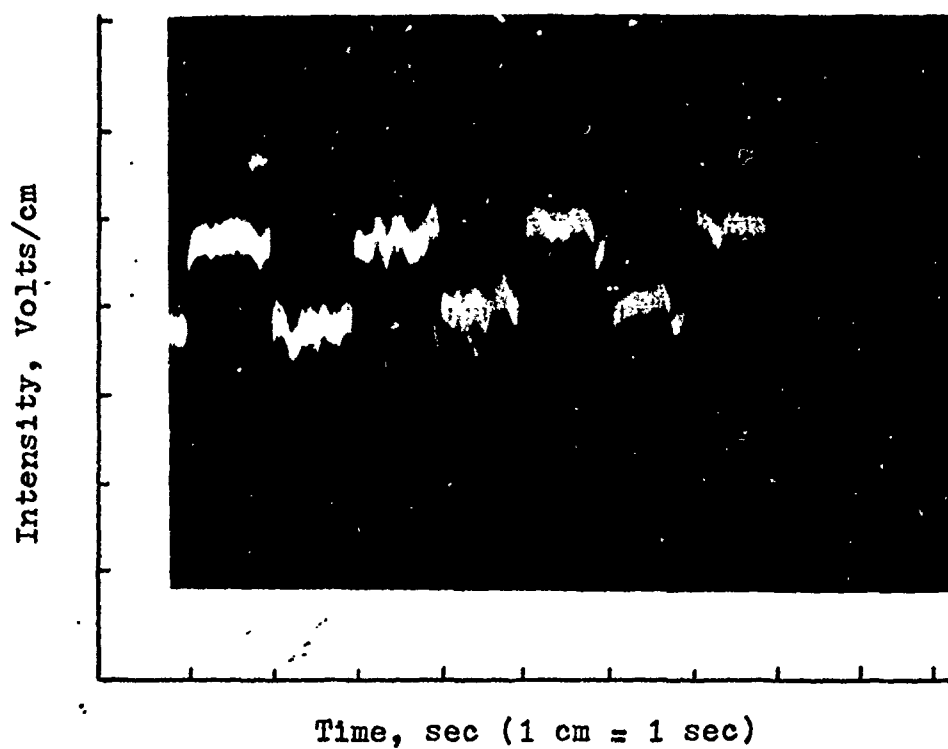
Figure 12. Spectrometric Data of the Flame Emissions
from 1.9-cm ID Zirconia Combustor at
$\lambda = 0.518 \mu$ for $\phi = 2$ at $\xi = 21.1$ ms
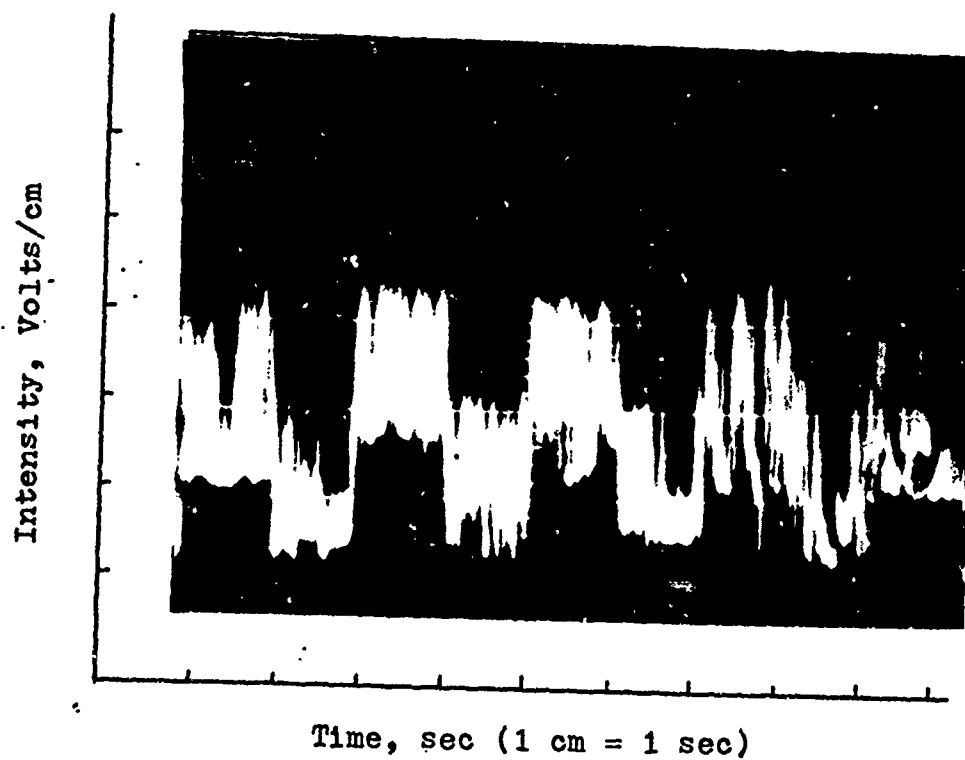
Figure 13. Spectrometric Data of the Flame Emissions from 1.9-cm ID Zirconia Combustor at $\lambda = 0.518\mu$ for $\phi = 1$ at $\xi = 34.1$ ms

chopped signal from the tungsten lamp provided the known
temperature calibration scale. As can be seen from Figs 11
through 13, the signal-to-noise ratio was quite high
especially for equivalence ratios near unity. Equivalence
ratios less than one produced signals that were too weak and
irratic to deduce a temperature. The noise level of the
flame signal also increased with increasing temperature.
There was very little broadening of the signal between the
emission and absorption scans; this indicated that the
monochromatic absorptivity of the flame was constant.

To calculate a temperature from this data, there was
uncertainty as to what portion of the signal should be used
to evaluate the flame emissivity and intensity. Flame
temperatures were calculated from the spectrometric data
using various positions within the broadened signals to
evaluate the change in calculated temperature. The
uncertainty in the calculated temperature was proportional
to the flame temperature and inversely proportional to the
equivalence ratio. The maximum variation in a calculated
flame temperature was 50°K at approximately 2200°K for an
equivalence ratio of two and over 1000°K for a flame at an
equivalence of one near 3000°K.

During the test runs at high combustion efficiency for
an equivalence ratio of one, the zirconia chamber would
become so molten that sections of the chamber wall were
blown from the combustor. It was only at an equivalence of
one that this condition occurred. After these tests, the
combustor wall near the exit had a layer of light gray

material on yellow zirconia ceramic, as represented by the

sketch in Fig 14. The gray material could only be melted

by an oxyacetylene torch adjusted to its hottest flame

(near 3000°K) and impinging directly on a specimen of the

substance. These materials were analyzed by the Air Force

Materials Laboratory. The bright yellow ceramic was identi-

fied as cubic zirconia and the light gray material as pure

monoclinic zirconia.

The melting point of monoclinic zirconia was reported

in Table II of Appendix J to be 2900°K and a flame tempera-

ture of 2940°K was calculated for the first maximum

stoichiometric test from absorption-emission data using the

maximum signal peaks. With this information as a calibration

point, all the temperature information was calculated using

the maximum signals.

The cause for the fluctuations in the flame signal in

Figs 11 through 13 is not known. It could arise from

several sources, the most probable are: blocking of the

flame emissions by the condensing oxides on the periphery of

the flame, scattering of the signal by solids in the flame,

more dense oxides surrounding the particles, or natural

fluctuations from one emission peak to another. The

frequency of the fluctuation increased and the amplitude

decreased with increasing equivalence ratios; thus, the

unburned boron or oxides surrounding the particles could

cause the fluctuations. However, the greatest amplitude of

the fluctuations occurred at high combustion efficiency at

an equivalence of one where all the fuel particles should
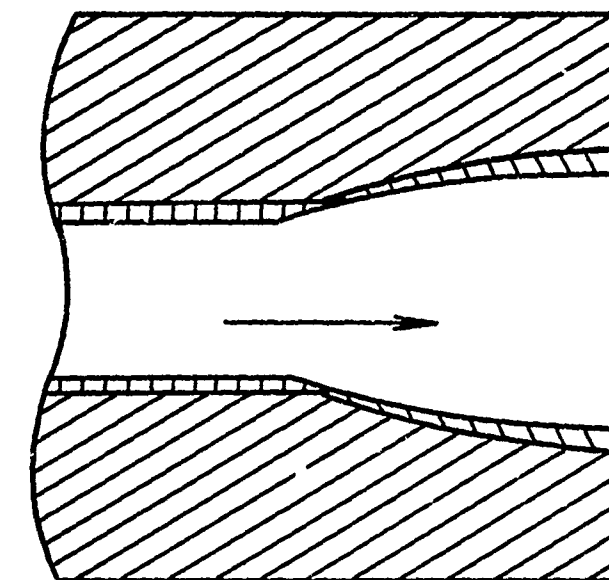
Triclinic Zirconia Ceramic

Monoclinic Zirconia Ceramic

Boron Oxide Deposit

Figure 14. Condition of the Zirconia Combustor after
a Maximum Efficiency Test Run at $\phi = 1.0$

have burned up and all constituents of the exhaust plume should have become gaseous. The boron oxide absorption-emission spectra for the observed flame signals is described in the literature as "fluctuation bands" without explanation of their definition of fluctuation (Refs 23, 24 and 25).

Figure 15 shows a typical spectra of the boron/air flame at an equivalence of one and the emission lines are identical to those described in the literature. This spectra was taken in the rapid scan mode of the Warner-Swasey Spectrometer at two milliseconds per scan; the exposure time was twenty milliseconds. The lower signals were the flame emissions and the upper signals were of the flame and the reference tungsten lamp. The emission fluctuations were clearly illustrated here and the steady nature of the fluctuations was shown in Figs 11, 12 and 13 where the 0.518μ line was scanned at one centimeter per second. The maximum emission signal was produced by the line at approximately 0.518μ . As can be seen, this maximum emission signal was much greater than the continuum emissions; thus, the gaseous emissions were the dominant portion of the signal. The oxides condensing on the periphery of the plume would be much cooler than the core of the exhaust flow. If this was the primary cause of the fluctuations, then the best explanation of the flame signal would be that the hot core of the flame was seen as the maximum portion of the signal and would best describe the exhaust temperature.

The change in the exhaust temperature with increasing combustor residence time was correlated to the combustion
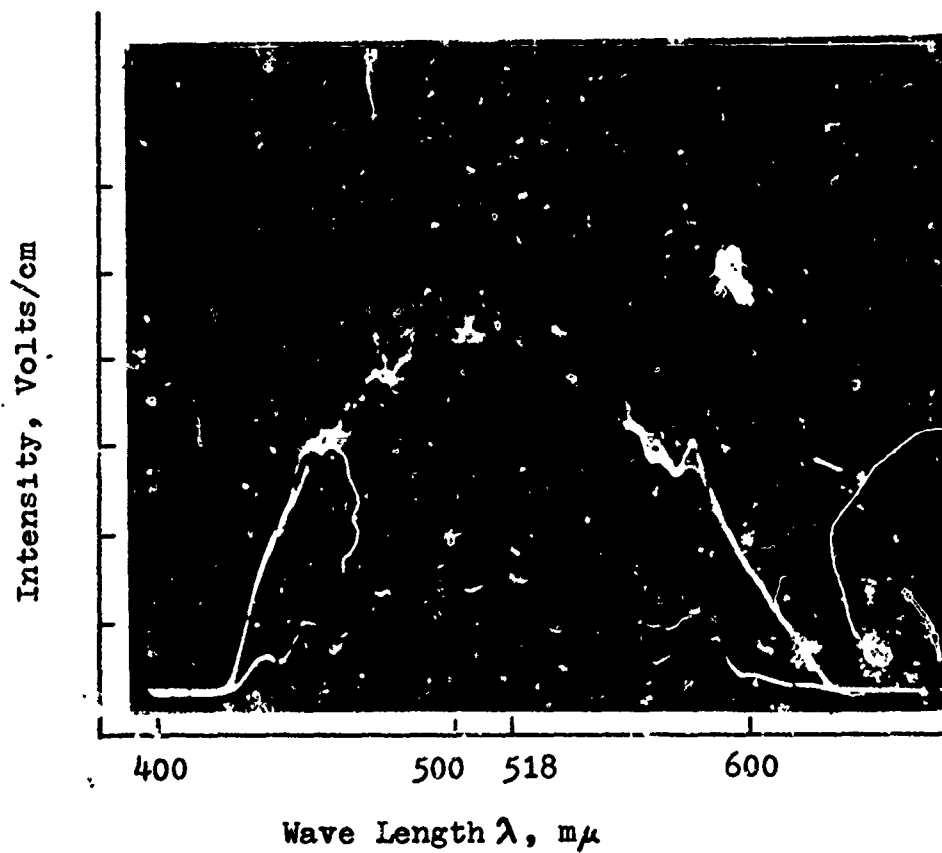
Figure 15. Typical Oscilloscope Trace at Exhaust Plane
Showing a Characteristic Boron Flame Spectra
for Maximum Flame Temperature at $\phi = 1$

model from this study, Eqs 33 through 38, for an equivalence

of one in Fig 16 and for an equivalence of two in Fig 17

with the residence time parameter ξ. The calculated

temperature data at the different values of the residence

time parameter were taken from zirconia combustors with the

same lengths and air mass fluxes and thus represented the

spread of the data. The minimum temperatures measured were

from $2100^\circ K$ to $2200^\circ K$. These were not the minimum tempera-

tures for the luminous flames but were the minimum exhaust

temperatures for a steady, self-sustained flame to become

stabilized in the tubular combustors. The fluctuation

characteristics of the flame signal in Fig 11 indicated that

that particular flame was not stable. The temperature

continued to increase as the residence time parameter was

increased with the maximum temperature approaching the

adiabatic flame temperature for B_2O_3 as shown in Fig 18.

Further trends in the temperature increase for $\phi = 2$ in

Fig 17 indicated that the temperature rose rapidly to

asymptotically approach the B_2O_3 adiabatic flame temperature.

With further increase in combustor length and well above

combustor lengths for complete oxygen depletion, the temper-

ature began a second increase above the maximum temperature

for B_2O_3. This second rise indicated a possible boron

nitride reaction; however, due to the large source of

nitrogen in the air, this was not substantiated by a change

in the N_2/argon ratio. This trend was duplicated for

68
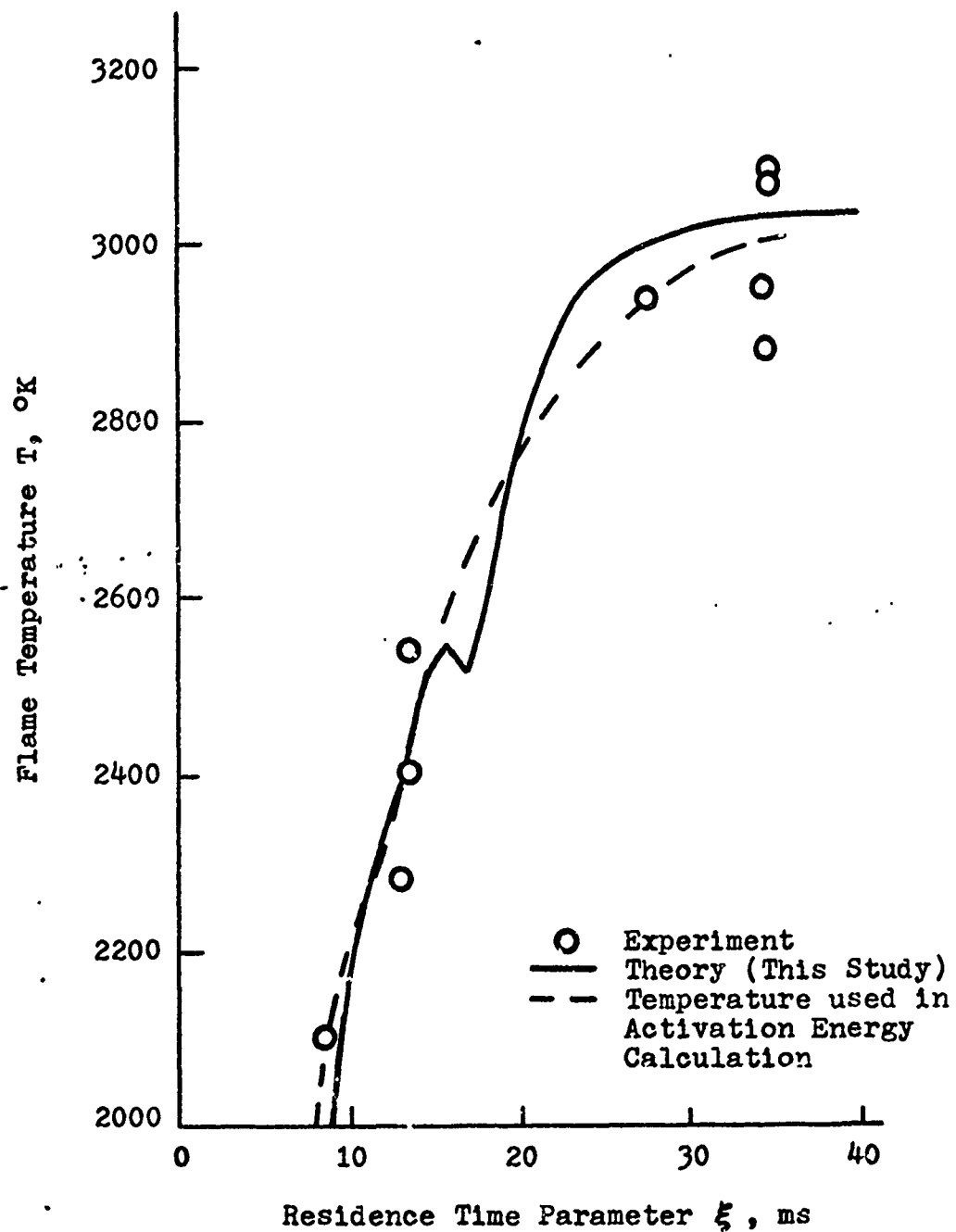
Figure 16. Variation of Temperature with Combustor Residence Time Parameter at $\phi = 1$
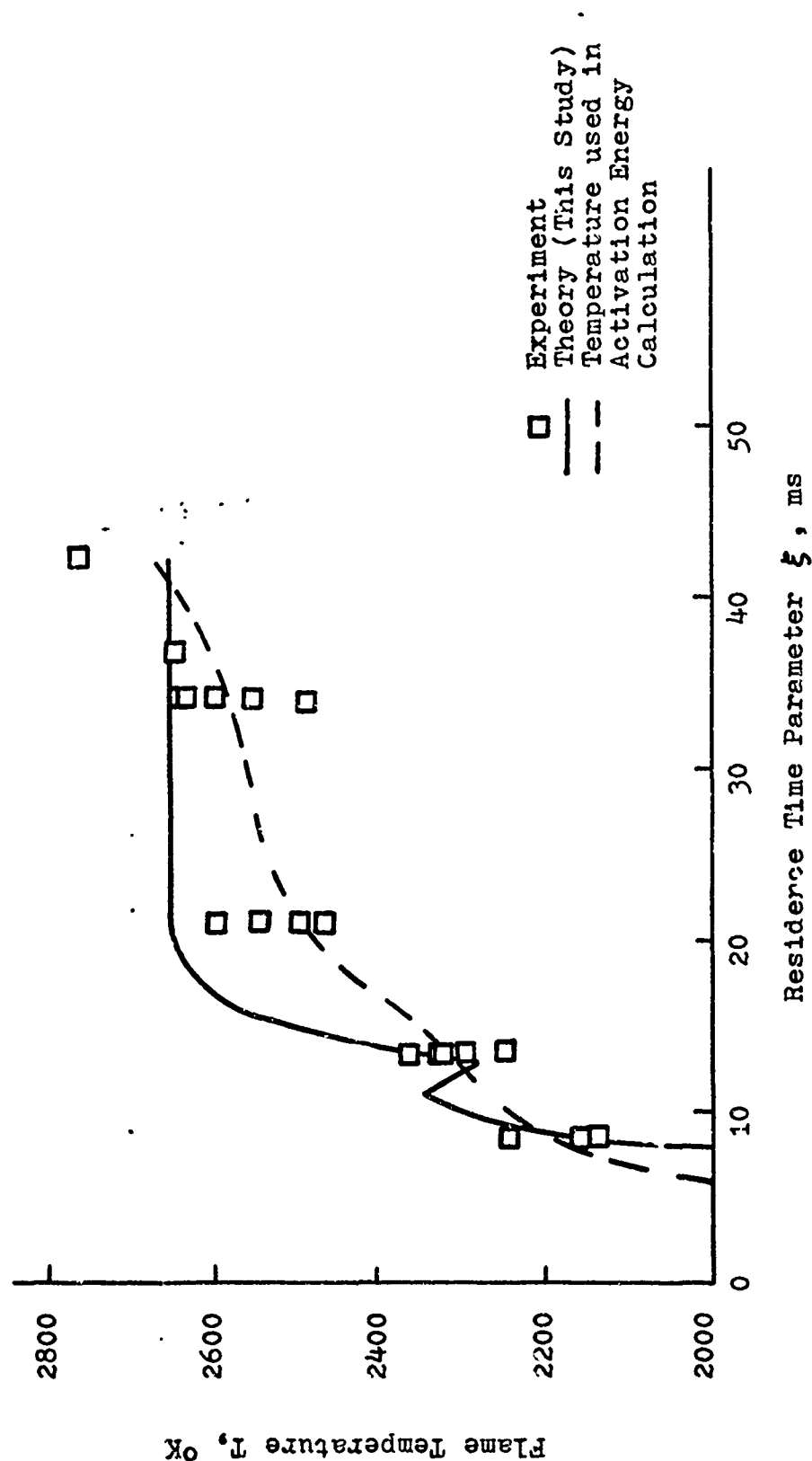
Figure 17. Variation of Temperature with Combustor
Residence Time Parameter at $\phi = 2$
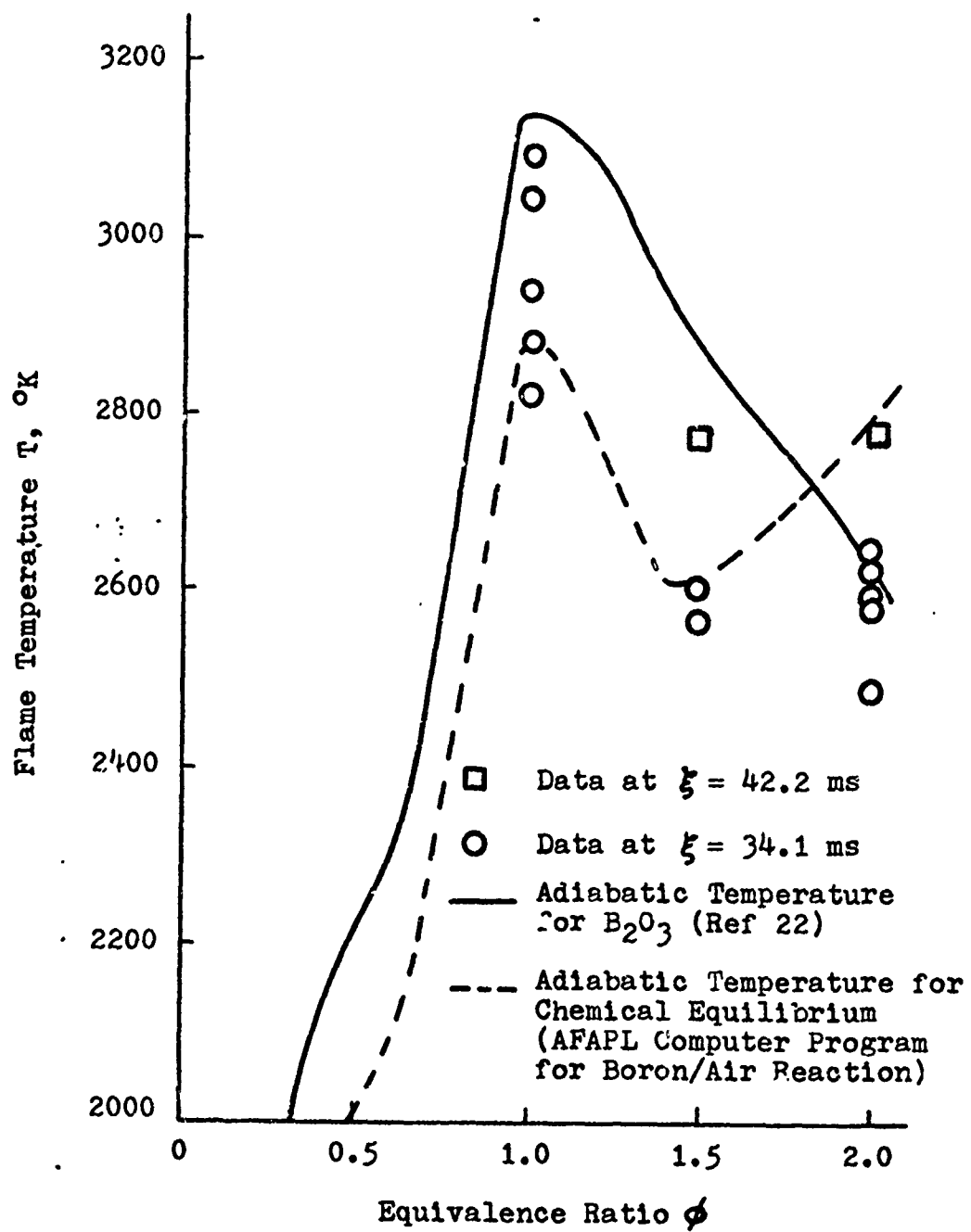
Figure 18. The Influence of the Equivalence Ratio
on the Maximum Combustion Temperature

$\phi = 1.5$, in Table V of Appendix J, but was not present in the stoichiometric fuel/air ratio.

Maximum Flame Temperatures

The flame temperatures for test runs at high combustion efficiency or runs where the combustor residence time was more than sufficient to yield 95 to 100% oxygen depletion were plotted versus equivalence ratio in Fig 18. These temperature data were collected from the zirconia combustors where the combustion process was near adiabatic. The experimentally determined temperatures were compared to theoretical predictions for adiabatic temperatures obtained at equilibrium conditions and for boron trioxide as the only product. Some of the temperatures deduced from the data at $\phi = 1.0$ and 1.5 fell between the two curves indicating that the chemical heat release was greater than that predicted by the equilibrium process. Since the maximum measured temperatures at these equivalence ratios were greater than the adiabatic flame temperature for equilibrium but less than the adiabatic flame temperature for B_2O_3, the preferred reaction product appeared to be B_2O_3.

Combustion Model

The next sections of this discussion examine the phenomena observed during the experimental investigation that verify the theoretical model formulated in chapter two and evaluate the parameters identified in the theoretical analysis. The phenomena were the role of the heat flux from the flame in the heat up of the gas-particle mixture; the importance of the combustor wall reactions and their

attendant radial heat flux; and the contribution to the flame
absorption coefficient due to the combustion products. The
parameters, listed on page 39, chapter two, were evaluated
by correlating the experimental results with the theoretical
analysis. The results for the theoretical model were
arrived at by solving Eqs 33 through 38 using a Runga-Kutta
technique. The associated Fortran Program is listed in
Appendix H.

Temperature and oxygen depletion parameter data for
ϕ of 1.0, 1.5 and 2.0 were correlated in Fig 19; the
adiabatic temperature for B_2O_3, as calculated from the JANAF
tables, was included as a comparison. At the low oxygen
depletion values, the measured temperatures were greater
than those which could be obtained by the adiabatic process
indicating that external energy was supplied. At the higher
oxygen depletion values, the temperature deviation was less
pronounced with the higher equivalence ratios coinciding
with the adiabatic temperature trend; the measured
stoichiometric temperatures continued to approach the
adiabatic values with the maximum measured temperatures less
than the maximum adiabatic temperature.

These temperatures indicated that energy to heat the
gas-particle mixture above the adiabatic values was supplied
by the heat transferred from the flame. The mass flux of
air necessary for the flame to supply all of the energy
required to heat the oncoming particles to ignition was
calculated using the relation developed by Essenhigh and
Csaba (Ref 19)
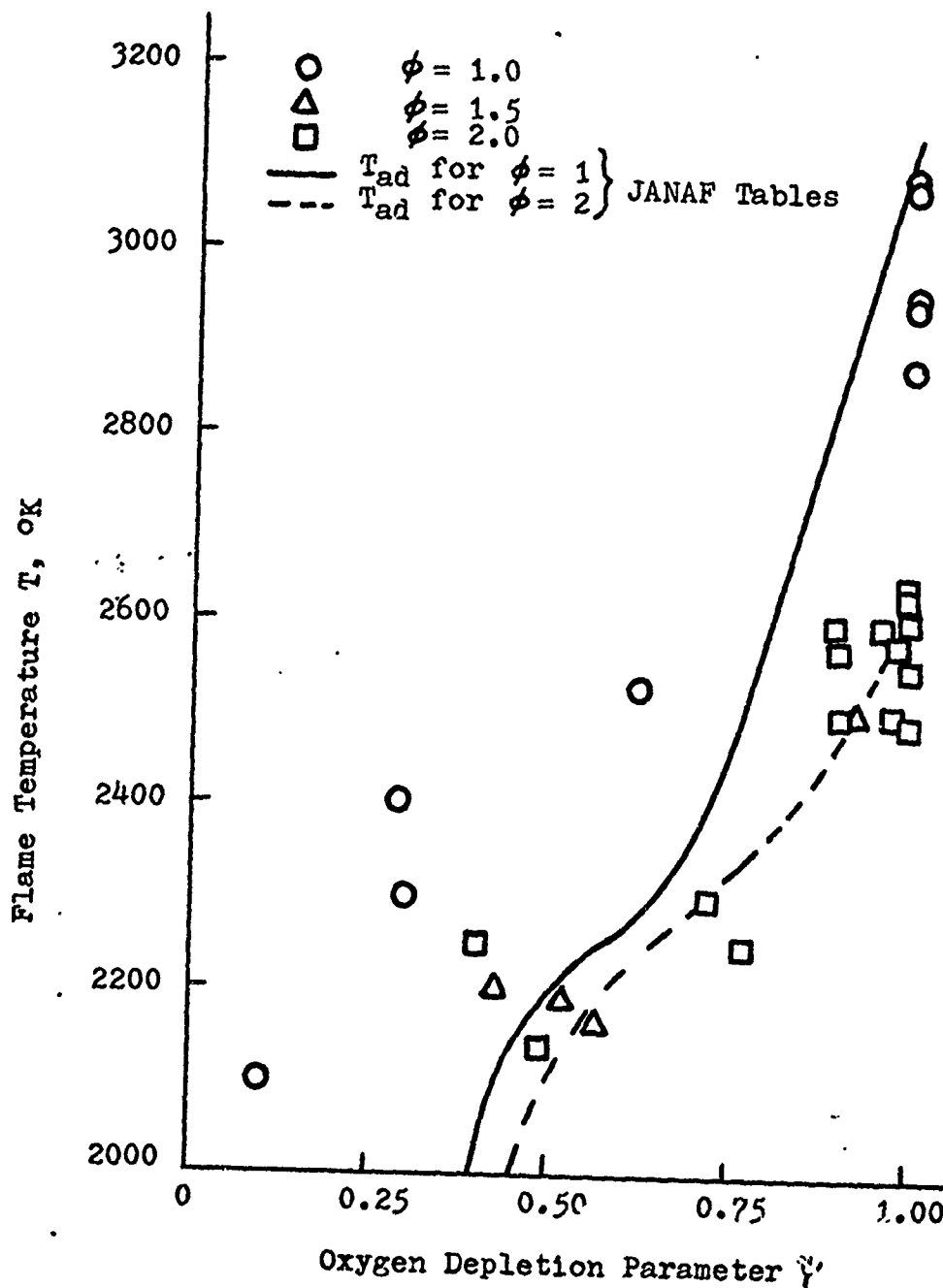
Figure 19. Comparison of Measured Temperatures with the
Theoretical Adiabatic Temperatures for B_2O_3
as the only Reaction Product

$$(\rho u)_{air} = \frac{\epsilon_F \sigma T_F^4}{\Theta c_{p_{air}} (T_i - T_o)} \cong 0.1 \, gm/cm^2\text{-}sec$$

When $T_F = 2500°K$, $T_i = 1850°K$ and $\epsilon_F = 1$.

This value of the mass flux of air would be the maximum
possible since it assumed the flame to be a black body.
This value would be increased by a factor of two if the
adiabatic flame temperature at ϕ of 1.0 was used; however,
the mass flux of air would still be a factor of ten less
than that used in this investigation. Therefore, it was
concluded that heat addition from boron reacting on the
combustor wall was required to stabilize the flame.

Radiation Stabilized Flame

Tests were made to determine whether the radiation from
the luminous flame could support the gas-particle mixture
heat up to ignition temperature without the wall reactions.
A boron flame with a hydrogen pilot flame was established
in a 7.62-centimeter steel chamber at an air mass flux of
0.1 gm/cm^2-sec with a fuel particle loading for an equiv-
alence ratio of two. However, a self-sustained flame could
not be stabilized without the presence of radiant wall
deposits. The combustor wall deposits were initiated by
preheating the walls. Once the walls were coated with a
radiating layer of boron and its oxides, the flame emissivity
increased sufficiently so that the hydrogen pilot could be
turned off. The boron continued to be heated to ignition.
As the combustion of the boron continued to increase in

intensity, the thickness of the luminous flame increased, increasing the emissivity of the flame.

With increased flame luminosity, the flame front flashed back through the oncoming gas-particle mixture to become stabilized at the chamber entrance. This demonstrated that the heat flux from the flame could cause the flame to propagate into a boron particle cloud.

Combustor Wall Reactions

To determine the characteristics of the wall deposits and to ascertain that they were primarily burning boron and not molten oxides heated by the flame, a series of tests were made without a flame being established. This was accomplished by positioning the igniter tube near the exit of a steel chamber at an air mass flux of 1.76 gm/cm^2-sec and an equivalence ratio of one. A brilliant green-white flame was established in what would be the hydrogen flame but it would extinguish when the hydrogen pilot was turned off. The igniter tube was retracted into the steel tube until a short deposit was formed. The flame would extinguish as soon as the pilot flame was removed but the deposit layer continued to glow a bright red as long as the powder flow was sustained. This process was repeated until a deposit length of approximately 20 centimeters was formed. The deposit would continue to glow under a sustained fuel flow without the green-white flame, only red streaks of partially ignited boron were observed in the exhaust dust. The steel tube with these deposits glowed a bright red in color. The color temperature of the tube was observed

using a pyrometer with the measured temperature almost
uniform at 2000°F. This indicated that for a uniform
thickness deposit, the heat flux from the reactions inside
the tube was not constant along the tube. By increasing the
fuel flow, the boron cloud could be ignited and burn as the
characteristic green-white flame.

Evaluation of the Heat Up Zone (Zone I)

The values of oxygen depletion and temperature were
measured at the exit of different lengths of combustors.
However, for the combustion model, it was assumed that the
combustor lengths at which the data were taken corresponded
to the various locations along a single combustor. In the
combustion model, the upstream conditions were affected by
the downstream conditions. The same downstream conditions
did not exist for the shorter combustors where the reaction
was not complete but were replaced by a luminous exhaust
plume. The exhaust plume characteristics as seen by the
oncoming gas-particle mixture were assumed to be similar to
those of the confined flame for this model.

No experimental measurements were taken in the heat up
region of the gas-particle mixture. Nor was there any
attempt to measure the temperature at which the reaction of
the particles within the mixture became self-sustaining.
However, temperature and oxygen depletion parameter data
were measured near the minimum residence time parameter
necessary to sustain a steady luminous flame. The para-
metric values of the average flame temperature T_F, the
proportionality factor Z, and the wall reaction model

77

$(d\psi/d\xi)_w$ were evaluated using Eqs 33 through 37 to approach these measured values. These parameters were interrelated where an assumption of a value for Z less than unity would require an increase in the values for T_F or $(d\psi/d\xi)_w$. Correlated with data at equivalence ratios of 1.0 and 2.0, the resulting values for Z equal to one were: T_F equal to 2900°K for ϕ of 1.0 and 2400°K for ϕ of 2.0 and $(d\psi/d\xi)_w = 0.014\phi$ ms^{-1} or $g = 4.67 \times 10^{-2}$ (sec-K)$^{-1}$. These results were compared to the experimental measurements in Figs 20 and 21.

The absorption coefficient proportionality factor Z is a measure of the particle absorptivity and Z approximately equal to one indicated that the boron particles approach black body absorptivity. This value of Z was the same as that assumed for the cold gas-particle mixture, page 52. This result yields an absorption coefficient k near unity at room temperature. But, the absorption coefficient is proportional to the air density and decreases as the mixture temperature increases. Therefore, as the gas-particle mixture approaches the self-sustained temperature, where the major radiant energy transfer from the flame is applied, the absorption coefficient is much less than unity and the optically thin limit, assumed for this model, is approached.

The equivalence ratio dependence of the heating due to the wall reaction and the radiant energy transfer from the flame provided an explanation for the difficulty in obtaining a self-sustained flame in fuel lean or extremely fuel rich mixtures. The energy release from the wall reactions,
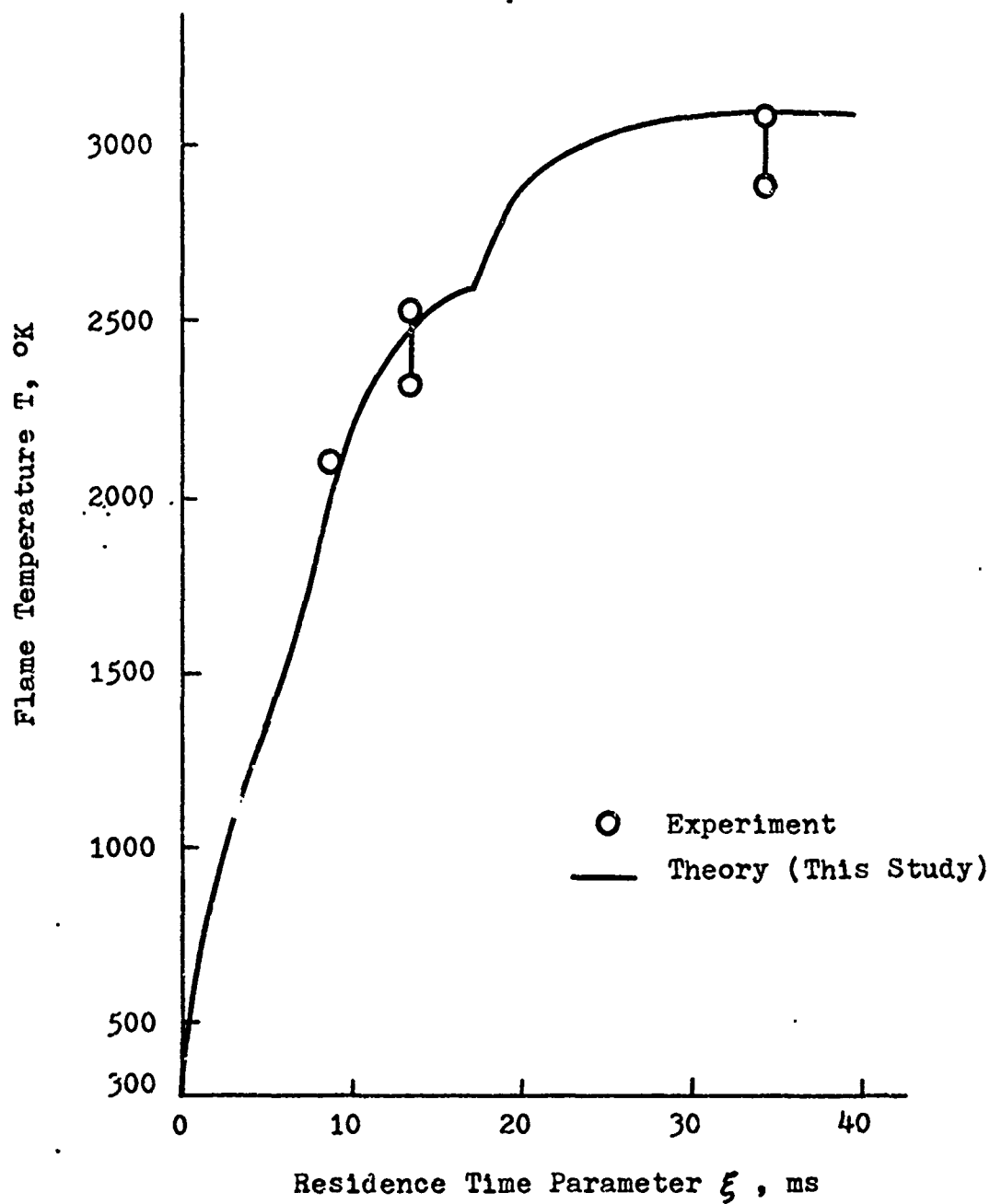
Figure 20. Comparison of the Temperature of the
Combustion Model to Experiment at $\phi = 1$
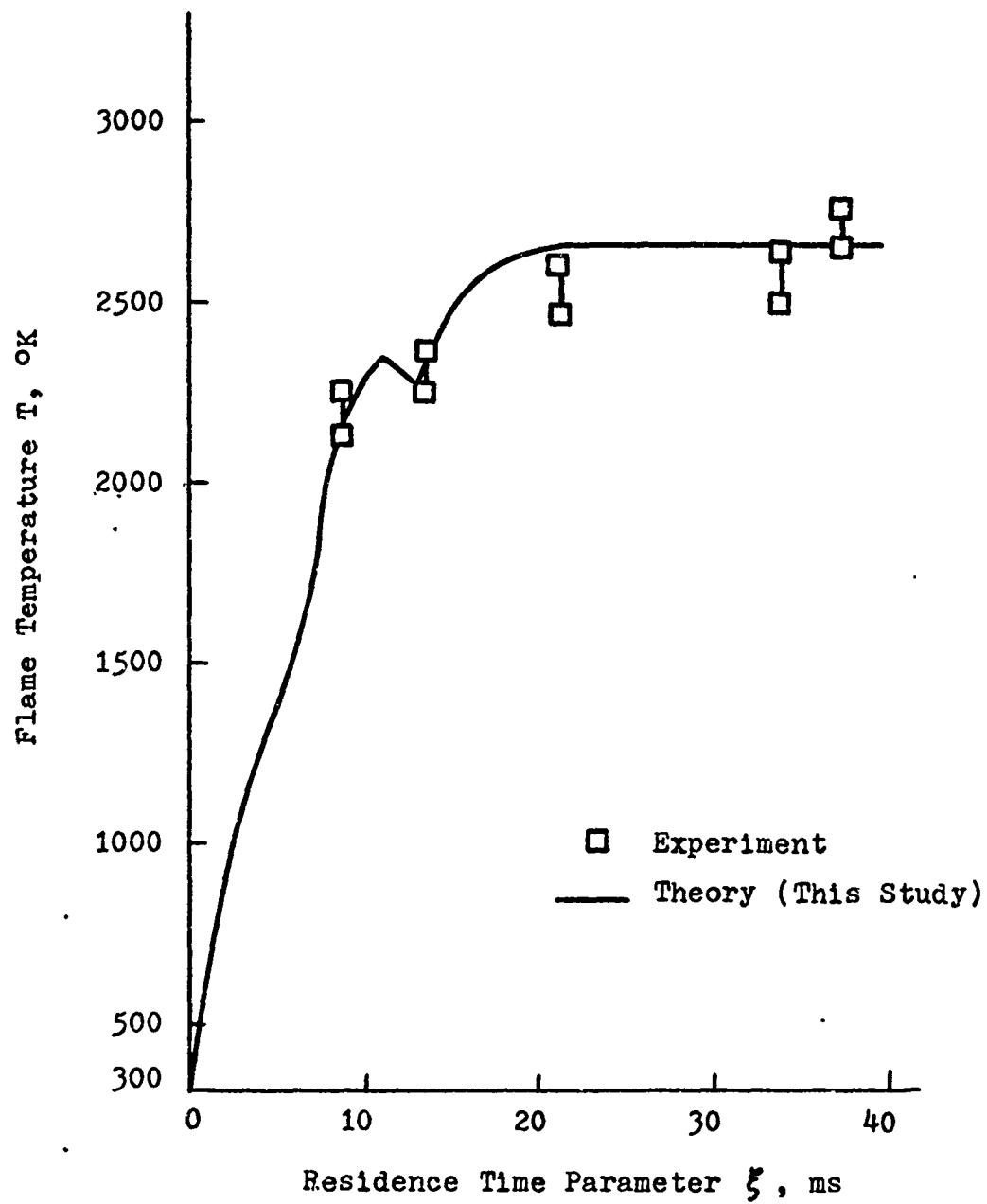
Figure 21. Comparison of the Temperature of the
Combustion Model to Experiment at $\phi = 2$

so necessary for a self-sustained flame decreased as the
equivalence ratio was decreased. Also, the adiabatic flame
temperature shown in Fig 18 approaches 2200 to 2100°K,
the minimum temperature necessary for self-sustained combus-
tion, as the equivalence ratio is decreased below 0.5 or
increased above 3.0.

Particle Reaction Model

By correlating the measured oxygen depletion and temper-
ature data with Eq 37, the constants A' and E_a/R were
evaluated. The value for the activation energy is quite
insensitive to change with values of E_a/R from 10^4 to
5×10^4 °K giving similar oxygen depletion rates. These
trends and the dependence of ϕ on E_a/R are shown in Figs
22 and 23 for A' of 1423 sec^{-1}. The correlations were
calculated using an average of the measured temperatures
with E_a/R of 2×10^4 giving the best correlation to the
oxygen data. The Arrhenius pre-exponential constant A was
then evaluated in Appendix I and was calculated to be
9.04×10^{-3} moles of air/cm-sec.

Combustion Model for the Flame Zone (Zone II)

Temperature calculations using the equations for the
combustion model for Zone I, Eqs 33 through 37, were
continued after the cloud particle reactions became the
dominant source of energy. This resulted in calculated
temperatures well above the measured values. Much of this
was due to the form of the radiant heat transfer term which
continued to be a heat source until the average flame
temperature was reached and did not provide a mechanism to

81
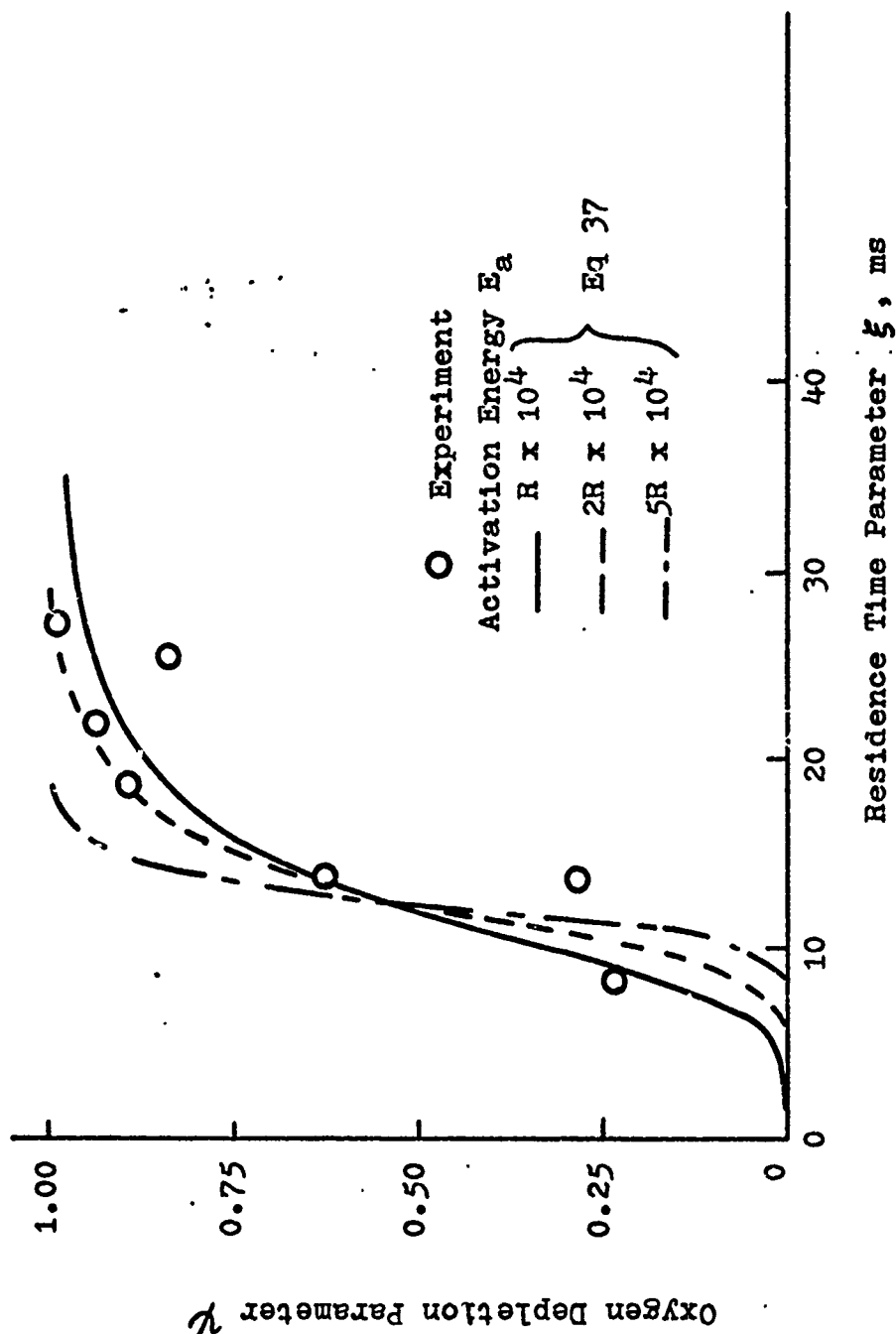
Figure 22. Variation of the Oxygen Depletion for the Cloud Reaction Model with Activation Energy at $\phi = 1$
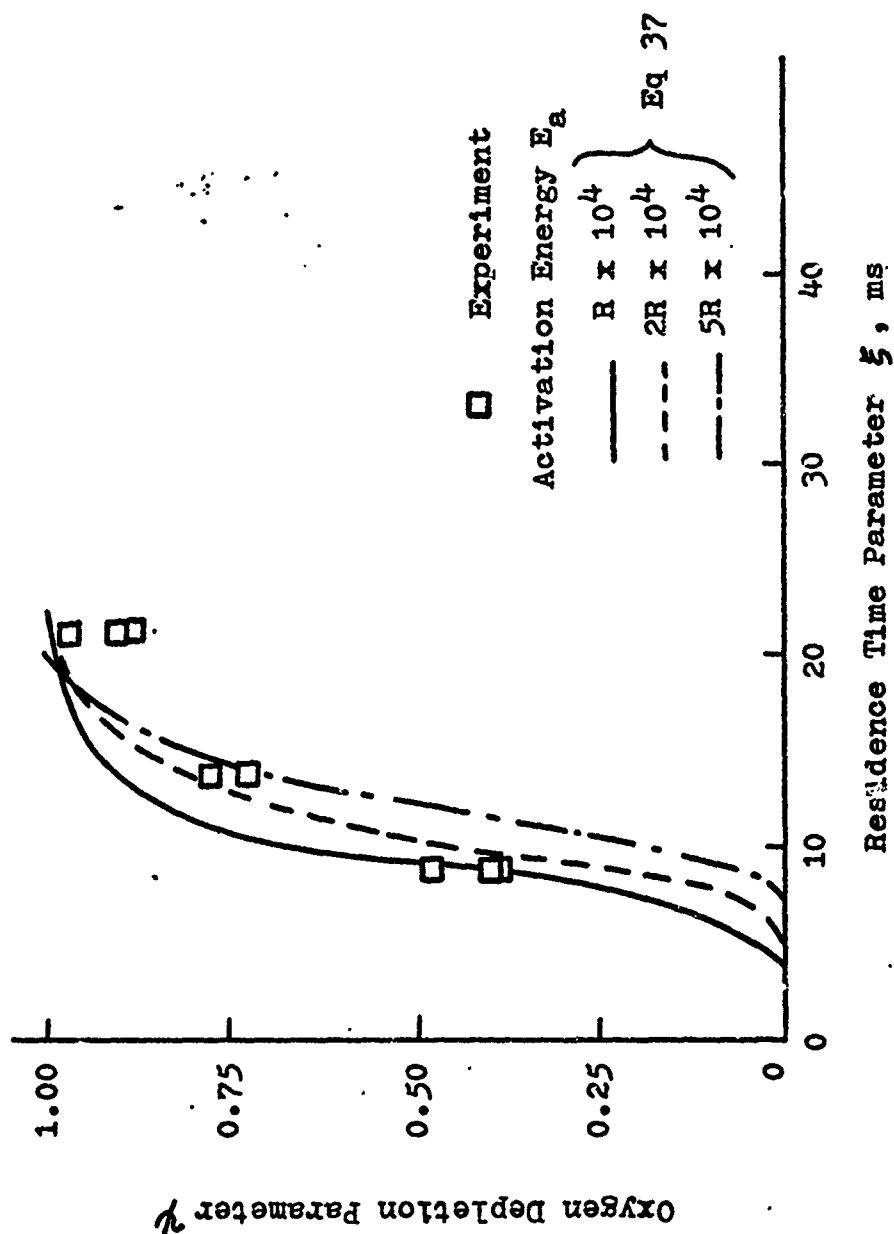
Figure 23. Variation of the Oxygen Depletion for the Cloud Reaction Model with the Activation Energy at $\phi = 2$

transfer energy to the oncoming cloud. The rate of increase in measured temperature was less than the rate of increase in adiabatic temperature at the higher oxygen depletion values, as seen in Fig 19, indicating an energy loss from the flame zone at this point. The boron flame is very luminous and as indicated in Fig 15, the luminosity resulted from continuum radiation as well as from radiating gases. The fuel particles, especially for the fuel rich flames, and the reaction products, condensed and gaseous, contributed to the flame luminosity.

Equation 38, along with Eqs 34, 35 and 37, was evaluated for the flame zone to determine the contribution of the reaction products to the flame mass absorption coefficient χ_g. The value of χ_g for temperatures less than 2100°K was considered negligible. At 2100°K, χ_g was a maximum indicating the transition from Zone I to Zone II. Its value decreased steadily with increasing ψ to become negligible above the oxygen depletion value of 0.8. The linearized relation for χ_g, used for the flame zone calculation in Appendix H to correlate the experimental data, was calculated to be

$$\chi_g = 9\left[1 + 0.58(\phi - 1)\right](3 - T/1000) \times 10^3 \ cm^2/gm \qquad (39)$$

This value is considerably larger than the particle mass absorption coefficient χ_p used in the correlation which was

$$\mathcal{X}_\rho = 0.736 \, \phi \, (1 - \psi/\phi)^{2/3} \times 10^3 \, cm^2/gm \qquad (40)$$

The calculated temperatures and oxygen depletion values were compared to measured data in Figs 8, 9, 16, 17, 20 and 21. The predicted oxygen depletion values at equivalence ratios of 1.0 and 2.0 and temperature trends at ϕ of 1.0 agreed with the measured values very well. The calculated temperatures compared to the measured values in Figs 17 and 21 for an equivalence ratio of 2.0 indicated that the flame emissivity was underestimated at 2100°K to 2200°K and over-estimated near 2300°K. The flame emissivity was considered negligible above ψ of 0.8 in the calculations and this resulted in an overprediction of the temperature rise.

The sudden increase of the combustion model flame emissivity corresponded to the rapid rise in the reaction rate of the suspended particles and the decrease in emissivity followed the reaction rate as the oxygen was consumed. The measured values for the gaseous absorption coefficient at $\lambda = 0.518 \, \mu$ followed this trend. This result is shown in Figs 24 and 25. The measured values of the absorption coefficient at 0.518μ were less than the values calculated using Eq 39. This was as expected since the measured values were at one wave length while the calculated values were for the entire spectrum. Both the measured and calculated absorption coefficients indicated
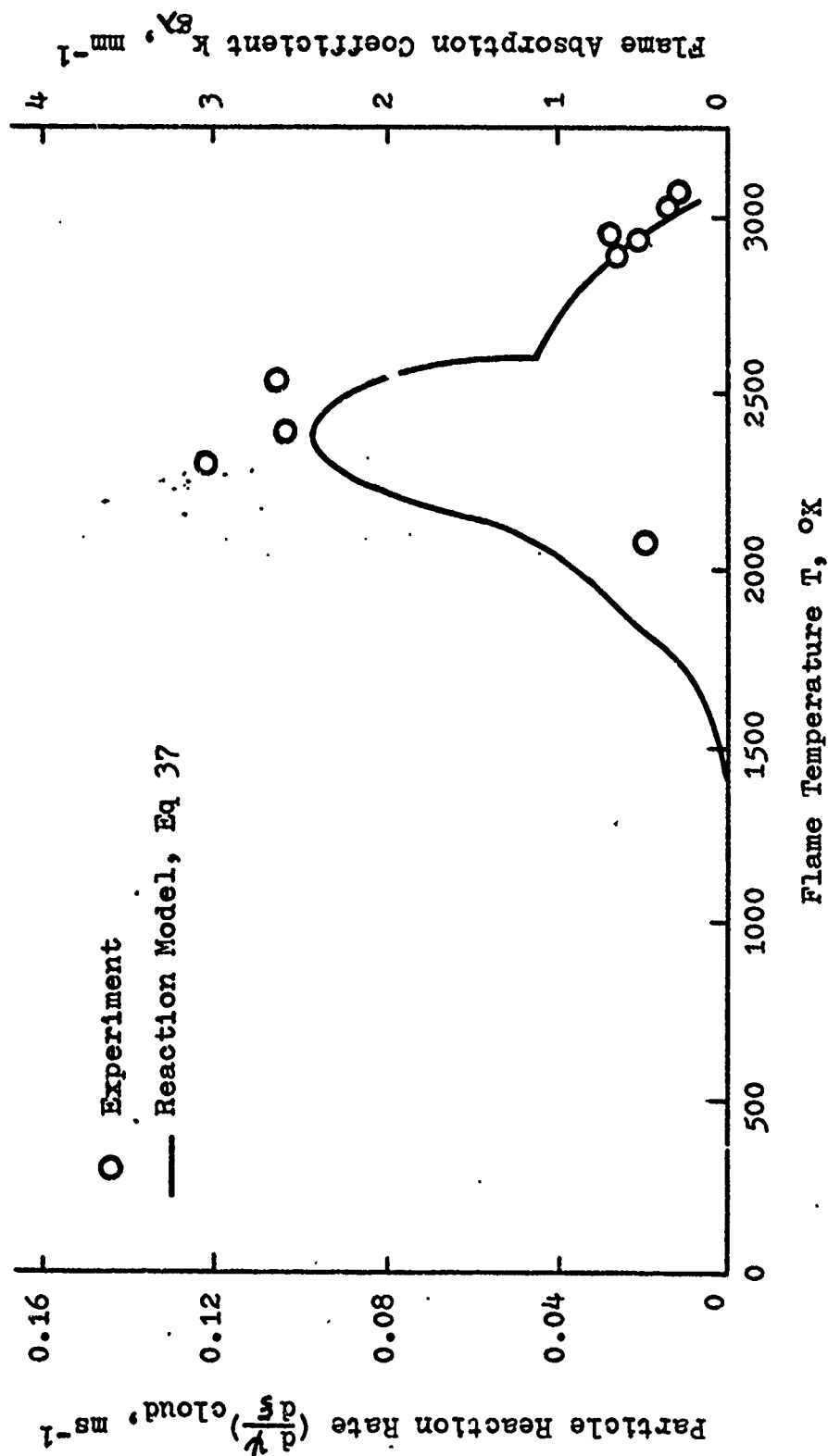
Figure 24. Comparison of the Reaction Rate at $\phi = 1$ as Calculated from Combustion Model to the Gaseous Emissivity at $\lambda = 0.518\mu$
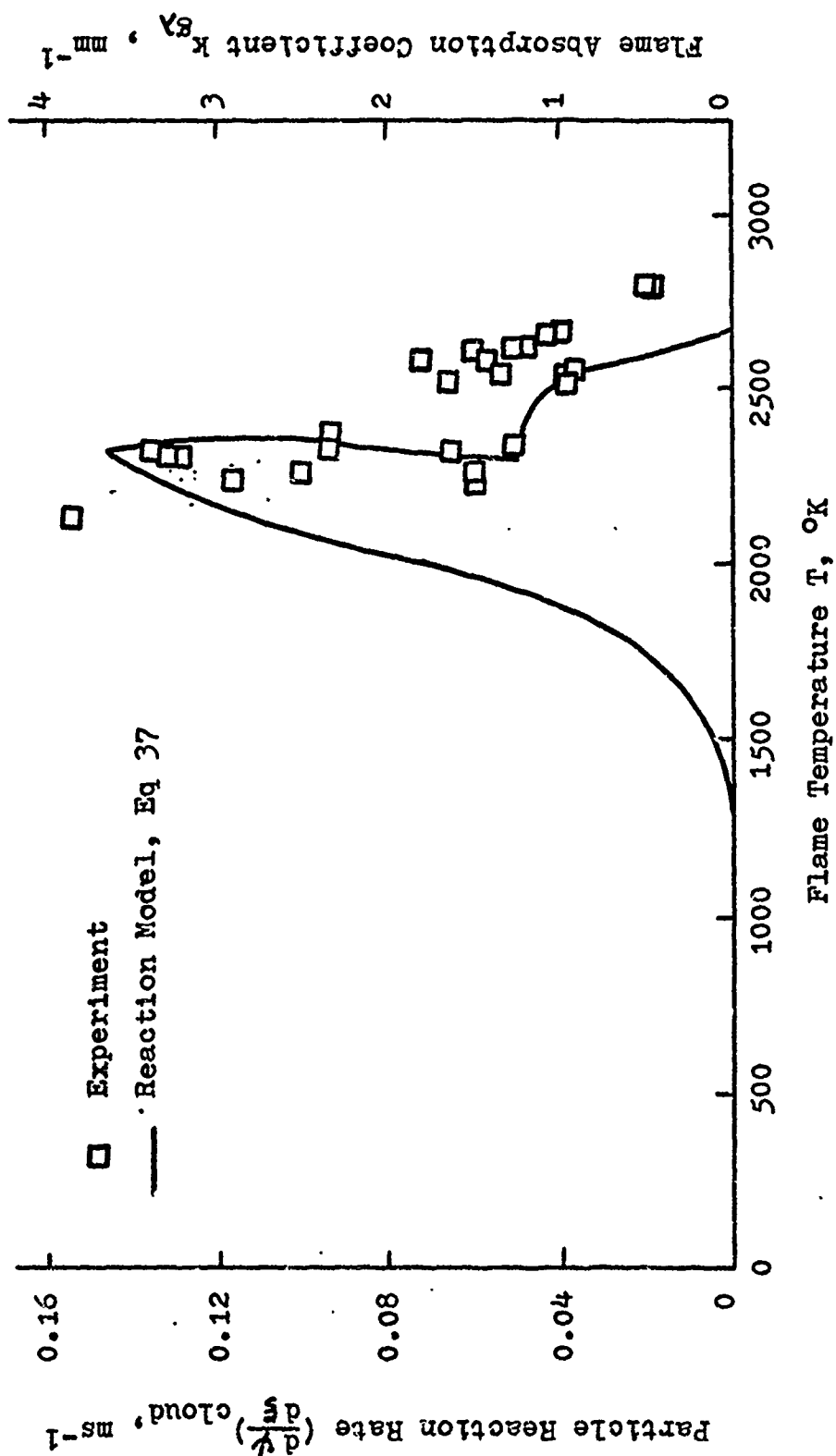
Figure 25. Comparison of the Reaction Rate at $\phi = 2$ as Calculated from Combustion Model to the Gaseous Emissivity at $\lambda = 0.518\mu$

87

that the maximum radiant emissions for a boron flame
occurred just above the minimum temperature necessary for
self-sustained flames (2100 to 2200°K).

Gaseous Emissivity

John (Ref 24) attributed the absorption-emission lines
from 0.4 to $0.6\,\mu$ to BO_2 only and not from gaseous B_2O_3.
Thus, the value of the absorption coefficient at $0.518\,\mu$
was a measure of the concentration of the BO_2 species. The
gaseous absorption coefficient at $0.518\,\mu$ followed the
particle reaction rate closely indicating that the concentra-
tion of BO_2 was proportional to the reaction rate and a
possible short-lived intermediate reaction species. A
further indication of this was the correlation of the
volumetric absorption coefficient to $1/T$ in Fig 26. The
data from 2200°K to 3000°K for all equivalence ratios were
correlated by least squares for a slope equal to 2×10^4.
This slope corresponded to the empirical activation energy
calculated for the reaction.

Combustor Wall Deposits

The growth of the wall deposits and the stability of
the self-sustained flame was achieved much faster when the
chamber walls were preheated. During combustion, the
deposits glowed a brilliant red-white and were molten.
After the deposits cooled, they had a very hard, brittle,
porous structure with a dark brown to black coloration.
Samples of these deposits were analyzed by the Air Force
Materials Laboratory which reported the major species to be
B_2O_3 with traces of B_6O and BN.
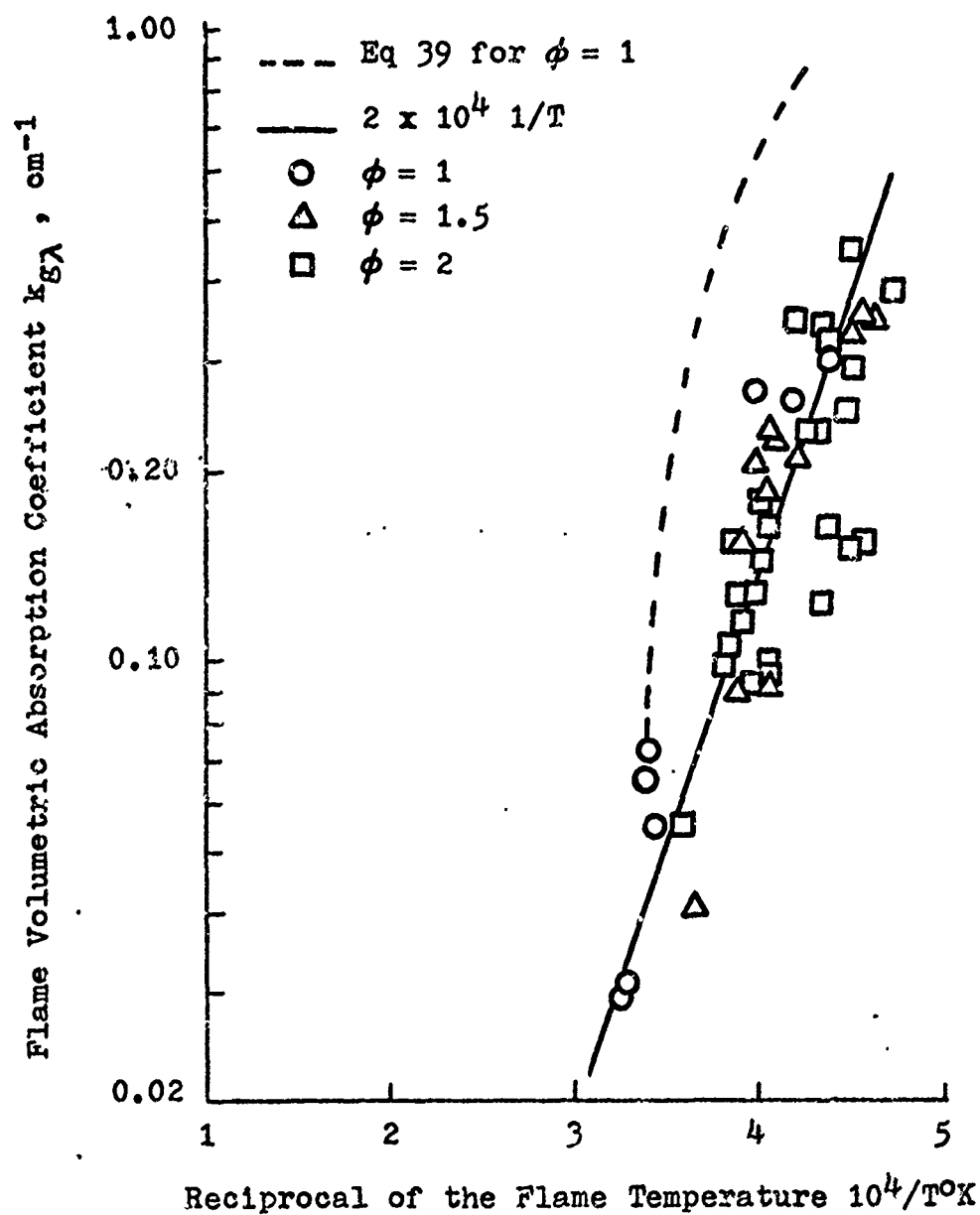
Figure 26. Variation of the Flame Absorption
Coefficient at $\lambda = 0.518\mu$ with the
Reciprocal of the Flame Temperature,
$k_{g\lambda} = 4.71 \times 10^{-5} \text{ Exp } [2 \times 10^4/T]$.

The thickness of the deposits appeared to be dependent on the air mass flux and the thermal conductance of the combustor materials. The thickness of the deposit layer was greater in the stainless steel chambers and the least in the zirconia combustors. It was difficult to characterize the wall deposits in the graphite chamber as they did not stabilize but continued to pour out of the burner exit in the molten state.

For the zirconia combustors at the highest air mass flux test conditions, the entire deposit thickness from the upstream end to the exit of the combustor was uniform with a smooth inside surface. As the air mass flux was decreased below 1.5 gm/cm^2-sec, the upstream entry section deposit thickened until only a very small entry hole remained. These entry deposits in the zirconia chambers were identical to those in the stainless steel tubes. This condition was stable and the tubes did not completely close off even after numerous repeated runs. Immediately downstream of this small entry port, the deposits thinned rapidly to a minimum where the flame was fully established. This thinner deposit layer occurred as the self-sustained flame became stabilized. At the beginning of each repeated run, the oxide deposits would become molten and sluff off to establish the steady combustor conditions. When this occurred in the 2.54-centimeter stainless steel tubes, it resulted in the failure of the tube and prevented high efficiency combustion.

The dependence on the thermal conductance was also observed in the zirconia chambers. A layer of the zirconia

plaster under the boron deposits would become molten and form cubic zirconia ceramic. This ceramic layer would thicken during repeated runs. The boron oxide deposits were approximately 0.15 centimeters thick after an initial run and would thicken to almost 0.6 centimeters after five to ten repeated runs for a total burner life of ten to fifteen minutes at 3 gm/cm^2-sec air mass flux. This change in the cross-sectional area of the combustor due to the wall deposits was not apparent in the data collected. Therefore, this condition may be primarily an effect of the cooled deposits as there was no way to observe the deposits during a combustion run.

Evaluation of the Evaporation Rate Constant

The evaporation rate constant β_{diff}, defined in Eq 22, was the major parameter with which previous investigators characterized the combustion process of solid fuel particles. This parameter was calculated in Appendix I to be $\beta_{diff} = 2/3 \, A'_{diff} \, d_o^2$ at T = 2320°K. For particles with an average diameter of one micron, β_{diff} was found to be equal to 949 μ^2/sec for a diffusion limited reaction. Particle burning times measured by Maček and McLain (Refs 9 and 11) suggested an evaporation rate constant of 2.3 x 10^4 to 9 x 10^4 μ^2/sec or twenty to one hundred times greater than that given in Appendix I. Particle agglomerations in the present investigation could account for much of this discrepancy and the average combustion temperature could also have some effect. Assuming that the differences in the combustion temperature and the agglomeration effects were

small, the agreement in the evaporation rate constants would
be much better if the reaction rate process was limited by
the chemical reaction and not by diffusion. This would
yield evaporation rate constants from 400 to 2000 μ/sec
from Maček's and McLain's data and 474 μ/sec from the
present investigation. There is some evidence that this may
be the case. Maček's data at 2280°K and 2430°K gas tempera-
tures for the 35 and 44 micron particles correlates best for
the linear burning law. Sheer (Ref 26) measured the
reaction rate of 99% pure boron powder at 425°C to 495°C and
reported an activation energy of 40 Kcal/mole for that
reaction. This reaction temperature was low enough that the
reaction rate should have been limited by chemical reaction
rather than diffusion. This was the same value for the
activation energy deduced in the present investigation.
Since there is no significant difference in the analysis
between the chemical limited and the diffusion limited rate
processes for a one particle size distribution, there was
no way to resolve this question in this investigation.
Because the diffusion process was the concensus of the
previous investigators, it was used in the present analysis.

Diagnosis of Past Combustion Problems

All attempts in the past to use boron as a fuel additive
have had difficulties in making the boron burn within the
combustor. These problems have been the difficulty in
igniting the boron and slow boron reaction rates (Ref 5).
The results of this investigation established residence times
for stable combustion and complete oxygen consumption to be

approximately two milliseconds and four milliseconds, respectively.

The improvements observed in this investigation point out the two main difficulties that have plagued past attempts to obtain high combustion efficiency at atmospheric pressure--particle agglomerations and energy losses from the flame. The agglomeration problem was solved by the dry cloud of boron particles from the particle mill. The dispersed particles decreased the particle agglomerations. The insulated combustors with the boron and its oxide deposits on the combustor walls reduced the heat losses from the flame and aided in the rapid heat up to ignition of the suspended fuel particles. The reduction of energy loss from the flame enabled the flame to burn at a higher temperatu⌐ This caused the reaction to proceed faster and eliminated the inhibiting oxide coating on the fuel particles.

The method of preparing the fuel aided in providing cleaner fuel particles. The boron oxide is soluble in water and was washed away when the boron powder was pressed into solid pellets. The closely packed pellets did not oxidize as rapidly as a dry packed powder would have. The wire brush particle mill stripped these cleansed particles from the pellet surface and delivered them to the combustor before they had time to oxidize.

V. CONCLUSIONS

This research was conducted to aid the understanding of multiple particle combustion of boron. The specific objective was to deduce an analytical combustion model for steady state, self-sustained combustion of an air/boron particle mixture and to demonstrate its validity experimentally. A combustion model was deduced that accounted for: (a) the energy mechanisms required to heat the gas-particle mixture to the ignition temperature, (b) the energy loss mechanism from the flame zone by unconsumed fuel particles and the combustion products, and (c) the temperature dependent particle reaction rate.

The steady state, self-sustained combustion of boron in air was established and investigated to evaluate the parameters identified in the analysis. The experimental combustion process, operating in the stoichiometric to fuel rich regime, achieved high values of oxygen depletion and energy release.

From this investigation, it was concluded that:

1. The analytical model for one-dimensional flow agreed with the measured characteristics of temperature and oxygen depletion for particulate boron combustion in constant area combustors at combustion pressure near atmospheric.

2. The combustion system design techniques of dry powdered boron and insulated combustors used in this study resulted in rapid burning and high combustion efficiency. Complete depletion of oxygen within four to five milliseconds was measured for equivalence ratios ϕ between one and two.

3. The primary combustion product of boron and air was B_2O_3. This was indicated by measured combustion temperatures near the adiabatic flame temperature for B_2O_3 and above the temperatures possible for a chemical equilibrium process.

4. The reaction rate for the particle burning process was temperature dependent and followed an Arrhenius equation with activation energy of 40 Kcal/mole and pre-exponential constant of 9.04×10^{-3} moles of air/cm-sec.

5. The evaporation rate constant for the particle correlated best for chemical limited rather than for diffusion limited combustion. The value for the chemical limited reaction was calculated to be 474 μ/sec. For diffusion limited combustion this constant was calculated to be 949 μ^2/sec.

6. When the gas-particle mixture became luminous from combustion heating, the absorption coefficient $\cancel{x}$ was increased ten fold.

7. The highest flame luminosity occurred at flame temperatures just above the minimum necessary for self-sustained flames (2100 to 2200°K).

8. The calculated absorption coefficient for the flame was proportional to the absorption coefficient measured at the 0.518 μ wave length.

9. The flame absorption coefficient, measured at 0.518 μ, was proportional to the theoretical reaction rate of the combustion process which suggested the primary absorbing species may be a short-lived intermediate species.

10. The absorption-emission technique for deducing high temperatures provided an accurate method for the measurement of luminous multiphase flame temperatures. The oscilloscope traces of the flame emissions had large fluctuations in intensity; but, the maximum level of the signal represented the temperature of the flame.

11. Self-sustained boron/air combustion in constant area combustors was not possible without some of the boron adhering to and burning on the combustor walls. However, at very low air mass fluxes (on the order of 0.1 gm/cm^2-sec) it was possible to propagate the flame into the cold gas-particle mixture.

12. Thickening of the wall deposit at the combustor entrance occurred for air mass fluxes less than 1.5 gm/cm^2-sec; this resulted in decreased combustor volume. Air mass fluxes above 1.5 gm/cm^2-sec produced uniform wall deposits.

13. Past combustion problems, the difficulty to ignite the boron particles and the slow combustion reaction rates, were resolved with this combustion system. These problems were primarily due to particle agglomerations and energy losses from the flame. The agglomeration problem was solved by the dry cloud of dispersed particles from the particle mill and the combustors constructed of high thermal resistant materials with the boron and boron oxides on the combustor walls reduced the energy losses from the flame and aided in the rapid heat up to ignition of the suspended particles.

RECOMMENDATIONS FOR FURTHER INVESTIGATIONS

As in any investigation, there were almost as many
questions raised as there were answered. The following
topics are among those questions that have arisen in the
course of this study.

1. Determination of the pressure dependency of the
boron/air system. The present investigation was conducted
at atmospheric pressure but most combustion systems of
interest are at either subatmospheric pressure for high
altitude flight or at elevated pressures for sea level, high
Mach flight speeds. The boiling point of boron trioxide
would be changed and could change the reaction limiting
phenomena. Increased air density would cause a correspond-
ing increase in the fuel loading per unit volume, this
could shift the optical limit toward the thick region.
Thus, this combustion system could exhibit very different
properties during high pressure combustion.

2. Evaluate larger combustor geometries to determine
the changes in the effects of the wall deposits, wall
reactions and flame emissions. An increase in the combustor
diameter affects the ratio of the combustor volume to surface
area, which could affect the wall reaction to flame emission
ratio for the energy required to heat up the cold particle
cloud. The Reynolds number change for the same air mass
flux could change the character of the wall deposits and
reactions. The two-dimensional effects caused by the larger
diameter particle cloud could completely alter the combustor
length parameter.

3. Further investigation of the absorption-emission technique for measuring the temperature of luminous flames containing liquids and solids is needed to evaluate the accuracy of the system in these environments. The assumptions made in the present study were: (a) thermal equilibrium between the particles (liquid or solid) and the gases in the flow, (b) translational and molecular temperature equilibrium of the gases, (c) the temperature measurements taken at the gaseous emission peak were not affected by the particle continuum emissions, and (d) scattering and reflection extinction and/or enhancement mechanisms were neglected. The comparison of flame emissions and calibrated source attenuation phenomena at different wave lengths may aid in determining the validity of these assumptions. Of particular interest would be the comparison of the data at wave lengths where the gaseous species are highly absorbing to wave lengths where the gases are transparent. These measurements, in conjunction with alternate measurement techniques would be necessary.

4. Evaluation of minimum length dump combustors or other recirculating flow geometries on reaction efficiency. This system may require two-dimensional and three-dimensional analyses of multiphase reacting flows. The spherical particle assumption may be applicable to thermal radiation absorption but the irregular shapes of the particles should be considered for the solid particle species dispersion and the momentum transfer between the gases and solids. A simpler analysis could be to correlate the combustor

geometries, the gas flow properties and the solid loading ϕ to the minimum combustor length necessary for high combustion efficiency.

5. Investigate the BO_2 concentration in boron flames to determine its relationship to the reaction rate and ignition delay time. The single particle investigations have correlated the visible emissions from the particle to the minimum ignition temperature, ignition delay and to the time necessary to completely consume the particle. Kaskin and John (Ref 24) have identified these visible emissions to eminate from the BO_2 molecule and not from the final combustion product B_2O_3. The present investigation has shown the absorption coefficient of these emissions to be proportional to the boron/air reaction rate. An investigation into these phenomena could yield understanding of the order of the reaction rate kinetics, the temperature and concentration of BO_2 required to give visible emissions and the phase relationships between BO_2 and B_2O_3 in nonchemical equilibrium reacting systems.

6. Determine the dominant mode for limiting the combustion of multiparticle boron/gas mixtures. This investigation would require uniformly distributed particle clouds of different sized fuel particles or particle distributions with different average diameters. Previous investigators have assumed a diffusion limited process for the combustion of single particles while the chemical limited process correlates the present data best. Talley (Ref 15) characterized the combustion process for large particles of

boron. He found that below the boiling point of B_2O_3 the rapid reaction of the boron was limited by the diffusion of the oxide vapor away from the reacting surface. Once the boron was free of condensed oxides on its surface, the combustion limiting process would be either chemical or diffusion of the oxidants to the reacting surface. At much higher temperatures, the diffusion of boron vapor away from the surface would be a limiting process.

REFERENCES

1. Markstein, G. H., "Combustion of Metals", <u>AIAA Journal</u>, Vol. 1, No. 3, p. 550, March, 1963.

2. Pinns, N. L., W. T. Olson, H. C. Barnett and R. Breitwieser, "NACA Research on Slurry Fuels", NACA Report 1388, 1958.

3. Schadow, K., "Boron Combustion Characteristics in Ducted Rockets", The Combustion Institute, Western States Section, WSS/CI preprint No. 71-19, 1971.

4. Sarner, S. F., <u>Propellant Chemistry</u>, Reinhold, Chapter 8, 1966.

5. Discussions at the Boron Workshop at AFIT, Wright-Patterson AFB, Ohio, October, 1969.

6. Cassel, H. M., A. K. Das Gupta and S. Guruswamy, "Factors Affecting Flame Propagation Through Dust Clouds", Third Symposium on Combustion, Flame and Explosion Phenomena, Williams and Wilkins, 1949.

7. Cassel, H. M. and I. Liebman, "The Cooperative Mechanism in the Ignition of Dust Dispersions", <u>Combustion and Flame</u>, Vol. 6, pp 9-19, 1962.

8. Gordon, D. A., "Combustion Characteristics of Metal Particles", <u>ARS Solid Propellant Rocket Research</u>, M. H. Summerfield, Ed., Vol. 1, pp 271-278, 1960.

9. Maček, A. and J. Semple, "Combustion of Boron Particles at Atmospheric Pressure", <u>Combustion Science and Technology</u>, Vol. 1, p. 181, 1969.

10. Kelley, C. M., R. E. Williams and A. Takemoto, "Combustion Kinetics of Particulate Boron", Project Squid, TR Den-1-PU, Sept., 1970.

11. McLain, W. H. and L. A. Cotugno, "The Ignition and Combustion of Single Boron Particles in Air at Ambient Pressure", AFOSR, TR-71-2215, Aug. 1971.

12. Bryant, J. T. and N. J. Siffel, "Amorphous Boron Dust Flames", <u>Combustion Science and Technology</u>, Vol 3, pp 145-151, 1971.

13. Uda, Robert T., "A Shock Tube Study of the Ignition Limit of Boron Particles", AFIT Thesis, GA/ME/69-1.

14. Jones, James T., "Boron Ignition Limit Curve as Determined by a Shock Tube Study", AFIT Thesis, GA/ME/70-1.

15. Talley, C. P., "The Combustion of Elemental Boron", ARS Solid Propellant Rocket Research, M. H. Summerfield Ed., Vol. 1, pp 279-285, 1960.

16. Simmons, J. A. and W. Baumann, "Ignition of Boron Particles Theory and Experiment", Western States Section of the Combustion Institute, Paper # 71-20, presented at the 1971 Spring meeting.

17. Discussions with Dr. P. J. Ortwerth and D. Wilkinson at the Aero Propulsion Laboratory, Wright-Patterson AFB, Ohio, Sept., 1969.

18. Nusselt, W., V.D.I., Vol. 68, p. 124, 1924.

19. Essenhigh, R. H. and J. Csaba, "The Thermal Theory for Plane Flame Propagation in Coal Dust Clouds", Ninth Symposium on Combustion, Academic Press, p. 111, 1963.

20. Sparrow, E. M. and R. D. Cess, Radiation Heat Transfer, Brooks/Cole, Chapter 7, 1966.

21. Edelman, R. B. and C. Economos, "Gas Generator Fueled Scramjet Program", AFAPL TR-70-84, Part III, p. 40, Jan., 1971.

22. JANAF Thermodynamic Tables, The Dow Chemical Company, Midland, Michigan, Dec. 31, 1972.

23. Kaskan, W. E. and R. C. Millikan, "Source of Green Bands from Boron-Containing Flames", J. Chem. Phy., April-June, Vol. 32, p. 1273, 1960.

24. John, J. W., "The Absorption Spectrum of BO_2", Canadian Journal of Physics, Vol. 39, July-Dec., 1961.

25. Tischer, R. L. and K. Scheller, "The Luminous Characteristics of Cyanogen-Oxygen-Boron Trichloride Diffusion Flames", Combustion and Flame, Vol. 12, p. 367, 1968.

26. Boron, Metallo-Boron Compounds and Boranes, R. M. Adams, Ed., Interscience Publishers, p. 273, 1964.

27. Beyermann, W. E., "Noninterference Instrumentation for Scramjet Combustors", The Marquardt Corporation, AFAPL TR-67-166, March, 1968.

28. Lewis, B. and G. von Elbe, Combustion, Flames and Explosion of Gases, Academic Press, p. 625, 1961.

29. Larrabee, R. D., "The Spectral Emissivity and Optical Properties of Tungsten", PB Report 144929, 1957.

DS/ME/74-2

30. Mulcahy, M. F. R. and I. W. Smith, "Kinetics of
    Combustion of Pulverized Fuel: A Review of Theory
    and Experiment", _Rev. of Pure and Appl. Chem._,
    Vol. 19, p. 81, 1969.

31. Aris, Rutherford, _Vectors, Tensors and the Basic
    Equations of Fluid Mechanics_, Prentice-Hall, 1962

APPENDIX A

CHEMICAL EQUATION AND DEFINITION OF CHEMICAL RATIOS

The molar chemical equation assuming no nitrogen reactions and air composed of oxygen and nitrogen only is

$$a_1 B + a_2 (O_2 + \chi_0 N_2) \rightarrow a_{ij} B_i O_j + a_3 B + a_4 O_2 + a_2 \chi_0 N_2 \quad \text{(A-1)}$$
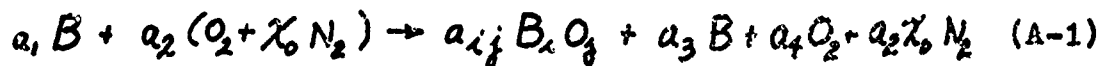
The stoichiometric equation would then be

$$(a_1 - a_3) B + (a_2 - a_4)(O_2 + \chi_0 N_2) \rightarrow a_{ij} B_i O_j + (a_2 - a_4)\chi_0 N_2 \quad \text{(A-2)}$$
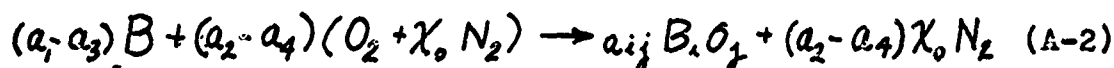
From these equations, the following terms may be defined:

$$(B/A) = \frac{a_1 M_B}{a_2 (M_{O_2} + \chi_0 M_{N_2})} \quad \text{(A-3)}$$

$$(B/A)_s = \frac{(a_1 - a_3) M_B}{(a_2 - a_4)(M_{O_2} + \chi_0 M_{N_2})} \quad \text{(A-4)}$$

$$\phi \equiv (B/A)/(B/A)_s = \left[\frac{a_1}{(a_1 - a_3)}\right]\left[\frac{(a_2 - a_4)}{a_2}\right] \quad \text{(A-5)}$$

$$\eta \equiv \left[(m_B)_0 - m_B\right]/(m_B)_0 = (a_1 - a_3)/a_1 \quad \text{(A-6)}$$

$$1 - m_{O_2}/(m_{O_2})_o = (a_2 - a_4)/a_2 \qquad \text{(A-7)}$$

Combining Eqs A-5, A-6 and A-7, one obtains

$$\psi \equiv 1 - m_{O_2}/(m_{O_2})_o = \phi \eta \qquad \text{(A-8)}$$

Since B_2O_3 is the only combustion product considered, a_{ij} is equal to zero for all i, j except $i = 2$ and $j = 3$. For this case, $(a_1 - a_3)/(a_2 - a_4) = 4/3$. The fuel used in this investigation had 10% impurities by weight; thus, the actual fuel-to-air stoichiometric ratio was 110% of the boron/air ratio. The boron/air ratio by weight for B_2O_3 as the only product is $(B/A)_S = 0.1046$, then $(F/A)_S = 0.115$.

APPENDIX B

GAS PHASE VOLUMETRIC AND MASS CHANGES

The change in the mass and molecular weight of the boron/air reaction can be calculated using the chemical equation for an incomplete reaction quenched at some time t after the start of the reaction.

$$(N_B)_o \, B + (N_{O_2})_o \, O_2 + (N_{N_2})_o \, N_2 \rightarrow N_{B_2O_3} \, B_2O_3 + N_B \, B + N_{O_2} \, O_2 + (N_{N_2})_o \, N_2 \quad (B\text{-}1)$$

Where N_m is the number of moles of species m.

For conservation of the elementary chemical species, the right side of Eq B-1 is subject to the following constraints:

$$2N_{B_2O_3} + N_B = (N_B)_o$$

$$\tfrac{3}{2} N_{B_2O_3} + N_{O_2} = (N_{O_2})_o \quad (B\text{-}2)$$

Using the definitions for the combustion efficiency η and oxygen depletion parameter ψ, introduced in Appendix A, the first relation of Eq B-2, the total number of moles on the right side of Eq B-1 can be expressed in terms of the initial molar conditions

$$N_T = (N_{N_2})_o + (N_{O_2})_o - \psi (N_{O_2})_o + (N_B)_o - \eta (N_B)_o + \tfrac{2}{3} \psi (N_{O_2})_o$$

$$= (N_{air})_o + (N_B)_o - \eta (N_B)_o - (1 - \tfrac{2}{3}) \psi (N_{O_2})_o \quad (B\text{-}3)$$

Where

$$(N_{air})_o = (N_{N_2})_o + (N_{O_2})_o$$

and

$$N_{B_2O_3} = \tfrac{2}{3}\,\psi\,(N_{O_2})_o$$

Due to its high boiling point, $3930^\circ K$, boron can be assumed to remain in the solid state with negligible partial pressure throughout the entire reaction process. However, B_2O_3, which boils at $2320^\circ K$, would have a significant partial pressure and could be completely vaporized at high reaction efficiency. Thus, the number of moles in the gas phase in Eq B-3 is

$$N_{T_g} = (N_{air})_o - (1 - \tfrac{2}{3}P_{v_{B_2O_3}})\psi(N_{O_2})_o$$
$$= \left[\, 1 - (1 - \tfrac{2}{3}P_{v_{B_2O_3}})(C_{O_2})_o\,\psi\,\right](N_{air})_o \qquad (B\text{-}4)$$

Where $P_{v_{B_2O_3}}$ was the partial pressure of B_2O_3 and ranged from zero to one and $(C_{O_2})_o$ was the mole fraction of oxygen in air with a value of 0.21.

At low values of the oxygen depletion parameter ψ, the partial pressure of B_2O_3 would be small. At high values of reaction efficiency ($\psi \sim 1$), the partial pressure would approach unity. Thus, Eq B-4 can be written

$$N_{T_g} = (1 - 0.21\psi)(N_{air})_o \quad ; \quad \psi \ll 1$$
$$= (1 - 0.07\psi)(N_{air})_o \quad ; \quad \psi \simeq 1 \qquad (B\text{-}5)$$

The change of mass within the gas phase can be calculated by multiplying the number of moles by its molecular weight. From Eq B-4, this becomes

$$m_{T_g} = \sum_m N_{m_g} M_m = (N_{air})_o M_{air} - (1 - \tfrac{2}{3} P_{V_{B_2O_3}} \frac{M_{B_2O_3}}{M_{O_2}})(N_{O_2})_o M_{O_2} \psi$$

$$= \left[1 - (1 - \tfrac{2}{3} P_{V_{B_2O_3}} \frac{M_{B_2O_3}}{M_{O_2}})(O_2/air)_o \psi \right](m_{air})_o$$

$$= (1 - 0.23 \psi)(m_{air})_o \; ; \; \psi << 1 \qquad (B-6)$$

$$= (1 + 0.103 \psi)(m_{air})_o \; ; \; \psi \simeq 1$$

Where $(O_2/air)_o$ is the mass fraction of oxygen in air with a value of 0.23 and M_m is the molecular weight of species m.

The changes in the equation-of-state for the gaseous elements can be determined using Eq B-4

$$P_{T_g} = \sum_m P_{m_g} = \frac{1}{V} \sum_m N_{m_g} RT = \sum_m \rho_{m_g} R_{m_g} T$$

$$= \frac{1}{V} \left[1 - (1 - \tfrac{2}{3} P_{V_{B_2O_3}})(c_{O_2})_o \psi \right] N_{air} RT$$

$$= \left[1 - (1 - \tfrac{2}{3} P_{V_{B_2O_3}})(c_{O_2})_o \psi \right] \rho_{air} \underline{R} T \qquad (B-7)$$

From this analysis, the volumetric and mass characteristics of the gaseous elements do not vary significantly from that of air. For gaseous B_2O_3, the maximum changes were seen to be 7% with respect to volume, 10% in mass with an increase in the molecular weight of 12%. For no gaseous B_2O_3, the mass and volumetric changes would be at a maximum; however, there would be almost no change in the molecular weight.

APPENDIX C

DEVELOPMENT OF THE CONSERVATION EQUATIONS

The conservation equations for a flowing system were developed using the Reynolds Transport Theorem (Ref 31). The Reynolds Transport Theorem states that for a quantity F that can be described per unit mass of the substance within a closed volume, the change of F with respect to time within the volume is equal to the change of F at each point within the volume plus the flux of F across the boundary surfaces S containing the volume. Stated in vector form, the Reynolds Transport Theorem is

$$\frac{d}{dt}\iiint_V \rho F \, dV = \iiint_V \frac{\partial}{\partial t}(\rho F)dV + \iint_S \rho F \vec{v}\cdot d\vec{S} \qquad (C-1)$$

For steady flow conditions, there is no change in any quantity within a volume fixed in space, thus, for steady flow, Eq C-1 is

$$\frac{d}{dt}\iiint_V \rho F \, dV = \iint_S \rho F \vec{v}\cdot d\vec{S} \qquad (C-2)$$

Invoking the Divergence Theorem, the surface integral may be stated as a volume integral

$$\iint_S \rho F \vec{v}\cdot d\vec{S} = \iiint_V \nabla\cdot(\rho F \vec{v}) \, dV \qquad (C-3)$$

In a multispecies, multiphase system, each phase or species within the phase may have a different velocity. Thus, for a flow system of this type, the flow properties in

109

DS/ME/74-2

Eq C-3 must be expressed in terms of each species m and phase j

$$\iint_S \sum_m \sum_j \rho_{mj} F_{mj} \vec{v}_{mj} \cdot d\vec{S} = \iiint_V \sum_m \sum_j \nabla \cdot (\rho_{mj} F_{mj} \vec{v}_{mj}) \, dV \qquad (C-4)$$

The Conservation of Mass

Since there are no sources or sinks of mass even in a reacting system, the mass is conserved and the integrals of Eq C-4 are identically zero for $F = 1$. Then

$$\iint_S \sum_m \sum_j \rho_{mj} F_{mj} \vec{v}_{mj} \cdot d\vec{S} = 0 \qquad (C-5)$$

For one-dimensional flow, the only velocity component is the axial velocity u and the flow properties are constant across any cross section perpendicular to the flow, then Eq C-5 can be integrated to yield

$$\sum_m \sum_j \left[(\rho_{mj} u_{mj})_2 S_2 - (\rho_{mj} u_{mj})_1 S_1 \right] = 0$$

or

$$\sum_m \sum_j (\rho_{mj} u_{mj}) S = constant$$

and for a constant area duct

$$\sum_m \sum_j \rho_{mj} u_{mj} = constant \qquad (C-6)$$

When the velocities of all species and phases are assumed to be identical, there is no slip between the solid or liquid particles and the carrier gas. This implies that there was conservation of the elementary molecular or atomic

110

species as well as conservation of mass. Thus, there was no change in the fuel/air ratio within any given volume fixed in the combustor space. For a reacting flow, the individual chemical species are not conserved but the sum of all species m is conserved. Thus, Eq C-6 can be written

$$u \sum_m \sum_f \rho_{mf} = Constant \qquad (C-7)$$

Initially, before any reactions take place, the mass of the gas-particle mixture is solid boron particles and air

$$u \sum_m \sum_f \rho_{mf} = u_o \left[(m_B)_o + (m_{air})_o \right]$$
$$= (1 + F/A)(\rho_{air})_o u_o \qquad (C-8)$$

Since the fuel/air ratio remains constant within the combustor space, Eq C-7 can be expressed in terms of the air before the reaction had started.

$$(\rho_{air})_o u_o = u \sum_m \sum_f \rho_{mf} / (1 + F/A) = \rho_{air} u = Constant \qquad (C-9)$$

The Momentum Equation

The rate of change of momentum of a flow system is equal to the summation of the forces acting upon it. For a horizontal flow system, the gravitational forces can be neglected and neglecting the viscous forces, only the pressure forces P acting on the surface of the volume must be considered. The momentum per unit mass is the velocity,

111

thus, Eq C-4 when $F = \vec{v}$ is

$$\iint_S \sum_m \sum_j (\rho_{mj} \vec{v}_{mj}) \vec{v}_{mj} \cdot d\vec{S} = \iint_S \sum_m \sum_{j=g} \vec{\vec{P}}_{mj} \cdot d\vec{S} \qquad \text{(C-10)}$$

Where only the gas phase contributes to the pressure tensor.

Using the Divergence Theorem and rearranging, Eq C-10 becomes

$$\iiint_V \nabla \cdot \sum_m \sum_j \left[\rho_{mj} \vec{v}_{mj} \vec{v}_{mj} - \vec{\vec{P}}_{mj} \right] dV = 0 \qquad \text{(C-11)}$$

Assuming that all properties within the integral are valid at each point within the integral and noting from Eq C-6 that $\sum_m \sum_j \rho_{mj} \vec{v}_{mj}$ is a constant, the differential representation of the momentum equation C-11 can be written

$$\sum_m \sum_j \left[\rho_{mj} \vec{v}_{mj} \nabla \cdot \vec{v}_{mj} + \nabla P_{mj} \right] = 0 \qquad \text{(C-12)}$$

Where $\nabla \cdot \vec{\vec{P}} = -\nabla P$

For one-dimensional flow and no slip flow between the phase states, Eq C-12 becomes

$$\sum_m \sum_j \left[\rho_{mj} u \frac{du}{dx} + \frac{dP_{mf}}{dx} \right] = 0 \qquad \text{(C-13)}$$

Equation C-13 must be summed over all phases not just the gaseous one. To take the solid and liquid phases separately would imply that these velocities are zero since they do not contribute to the total pressure. To maintain the velocity of the particles approximately equal to that of

the gases will require energy extraction from the gases.
Thus, the solids will contribute to the pressure gradient
in multiphase flows.

The Energy Equation

The rate of charge of energy within a volume is equal
to the energy source or sink caused by chemical reaction
$\dot{Q}_{chem}$, work due to pressure, plus the heat flow into the
volume and minus the heat flow out of the volume. For each
phase j of a flow system, the energy per unit mass of species
m is $(e_{mj} + v_{mj}^2/2)$ and since the heat flux inward is positive,
the integral energy equation can be written

$$\frac{d}{dt}\iiint_V \sum_m \sum_j \rho_{mj}\left(e_{mj} + \frac{v_{mj}^2}{2}\right)dV = -\iint_S \vec{q}\cdot d\vec{S} + \iiint_V \dot{Q}_{chem}dV \tag{C-14}$$
$$-\iint_S \sum_m \sum_{j=g} P_{mj}\vec{v}_{mj}\cdot d\vec{S}$$

Where e_{mj} is the internal energy per unit mass of species m
in phase j and $\vec{q}$ was the combined heat fluxes shown in Fig 3.

Using the Divergence Theorem to express the surface
integrals as volume integrals, Eq C-14 can be written

$$\iiint_V \left\{\sum_m \sum_j \rho_{mj}\vec{v}_{mj}\cdot\nabla\left(e_{mj} + \frac{v_{mj}^2}{2}\right) + \nabla\cdot\vec{q} - \dot{Q}_{chem} + \sum_m \nabla\cdot P_{mg}\vec{v}_{mg}\right\}dV = 0 \tag{C-15}$$

Assumption (b) of the flow model states that the number
of solid particles was constant in any given volume of the
gas-particle mixture, thus, Eq C-15 is valid for every small
volume as well as the integral volume. For one-dimensional

113

flow and the velocity and temperature independent of the system phase states, the differential element of Eq C-15 becomes

$$\sum_m \sum_j \rho_{mj} u \frac{d}{dx}\left(e_{mj}+\frac{u^2}{2}\right) + \nabla \cdot \vec{q} - \dot{Q}_{chem} + \sum_m \frac{d}{dx}(P_{mg}u) = 0 \quad (C\text{-}16)$$

Expanding the pressure work term in Eq C-16

$$\sum_m \frac{d}{dx}(P_{mg}u) = \sum_m P_{mg}\frac{du}{dx} + u\sum_m \sum_{j=j}\frac{dP_{mj}}{dx} \quad (C\text{-}17)$$

The derivative of the velocity can be obtained by differentiating Eq C-9. Substituting Eqs C-9 and C-13 into C-17, one obtains

$$\sum_m \frac{d}{dx}(P_{mg}u) = -\left(\sum_m P_{mg}\right)\frac{u}{\rho_{air}}\frac{d\rho_{air}}{dx} - \sum_m \sum_j \rho_{mj} u^2 \frac{du}{dx} \quad (C\text{-}18)$$

Equation C-18 can be expanded further using the equation-of-state for air and rearranging the last term.

$$\sum_m \frac{d}{dx}(P_{mg}u) = -\left(\sum_m P_{mg}\right)u\left[\frac{1}{P_{air}}\frac{dP_{air}}{dx}-\frac{1}{T}\frac{dT}{dx}\right] - \sum_m \sum_j \rho_{mj} u\frac{du^2/2}{dx} \quad (C\text{-}19)$$

Substituting Eq B-7 into Eq C-19, the pressure work term may be expressed as

$$\sum_m \frac{d}{dx}(P_{mg}u) = -\left[1-(1-\tfrac{2}{3}P_{\frac{g O_3}{2}})(C_{O_2})\psi\right]u\frac{dP_{air}}{dx} + \sum_m \rho_{mg}R_{mg}\frac{dT}{dx}$$

$$-\sum_m \sum_j \rho_{mj} u\frac{du^2/2}{dx} \quad (C\text{-}20)$$

Substituting Eq C-20 into Eq C-16, collecting terms and using the definitions $(c_v)_s = (c_p)_s = c_s$, $(c_p)_g = (c_v)_g + R_g$ and $de_{mj}/dx = c_{v_{mj}} dT/dx$, Eq C-16 can be simplified to

$$\sum_m \sum_j \rho_{mj} c_{p_{mj}} u \frac{dT}{dx} = \left[1 - \left(1 - \tfrac{2}{3} \rho_{V_{2O_3}}\right)(c_{O_2})_\bullet \psi \right] u \frac{dP_{air}}{dx} - \nabla \cdot \vec{q} + \dot{Q}_{chem} \quad \text{(C-21)}$$

APPENDIX D

DETERMINATION OF THE VOLUMETRIC SPECIFIC HEAT

The total volumetric specific heat, $\sum_m \sum_f \rho_{mf} c_{p_{mf}}$, is a measure of the energy stored within the gas-particle mixture per degree of temperature per unit volume. Even though, from the analysis in Appendix B, the gas phase volume and molecular weight did not vary significantly as the boron/oxygen reaction proceeded, the specific heat capacity of the gas-particle mixture must be evaluated to determine whether the change due to the reaction product, B_2O_3, was significant. Since the mass within the control volume for steady state condition was conserved, the atomic species was also conserved and the phase states can be expanded into the chemical species m. Expanding the total volumetric specific heat in terms of the mass of the chemical species per unit volume,

$$\sum_m \sum_f \rho_{mf} c_{p_{mf}} = \left[\left(m_{N_2} \right) c_{p_{N_2}} + m_{O_2} c_{p_{O_2}} + m_B c_{p_B} + m_{B_2O_3} c_{p_{B_2O_3}} \right] \quad (D-1)$$

The fuel mass contained impurities as well as boron. The impurities consisted of various metal oxides, Table III of Appendix J; however, the percentage of each impurity was small. So to simplify the analysis, it was assumed that the heat capacity of the fuel was identical to pure boron.

Now

$$m_{air} = \left(m_{N_2} \right)_o + \left(m_{O_2} \right)_o \quad (D-2)$$

and

$$m_{air} \, c_{p_{air}} = (m_{N_2}) \, c_{p_{N_2}} + (\dot{m}_{O_2}) \, c_{p_{O_2}} \qquad (D\text{-}3)$$

From conservation of the elemental species, the mass of B_2O_3 can be expressed in terms of the change in the mass of boron and oxygen. From Eq B-2, the mass of B_2O_3 is

$$m_{B_2 O_3} = N_{B_2 O_3} \, M_{B_2 O_3}$$
$$= \tfrac{2}{3} \left[(N_{O_2})_o - N_{O_2} \right] M_{B_2 O_3} \qquad (D\text{-}4)$$

Using the definition for the oxygen depletion parameter ψ, derived in Appendix A, Eq D-4 can be written

$$m_{B_2 O_3} = \tfrac{2}{3} \psi \, (N_{O_2})_o \, M_{B_2 O_3}$$
$$= \tfrac{2}{3} \psi \left[\frac{M_{B_2 O_3}}{M_{O_2}} \right] (N_{O_2})_o \, M_{O_2} \qquad (D\text{-}5)$$
$$= 1.45 \, \psi \, (m_{O_2})_o$$

Since $M_{B_2O_3} = 69.6$ and M_{O_2} is 32 gm/mole.

Substituting these relations, obtained in Eqs D-2, D-3 and D-5, into Eq D-1

$$\sum_m \sum_f m_{mf} \, c_{p_{mf}} = (m_{N_2})_o c_{p_{N_2}} + (m_{O_2})_o c_{p_{O_2}} - (m_{O_2})_o \, c_{p_{O_2}} + m_{O_2} c_{p_{O_2}}$$
$$+ (m_f)_o c_{p_B} - (m_f)_o c_{p_B} + m_f c_{p_B} + 1.45 \, \psi (m_{O_2})_o c_{p_{B_2O_3}}$$

$$= m_{air} \, c_{p_{air}} + (m_f) c_{p_B} - \eta (m_B)_o c_{p_B} + (1.45 \, c_{p_{B_2O_3}} - c_{p_{O_2}}) \psi (m_{O_2})_o$$

Dividing by the volumetric specific heat of air, the ratio of specific heats $\ominus$ is defined as

117

$$\Theta \equiv \sum_{m} \sum_{f} m_{m_f} c_{p_{m_f}} / (m_{air} c_{p_{air}}) \tag{D-6}$$

$$= 1 + (F/A) \frac{c_{p_B}}{c_{p_{air}}} - (B/A) \eta \frac{c_{p_B}}{c_{p_{air}}} + (O_2/A) \psi \left[1.45 \frac{c_{p_{B_2O_3}}}{c_{p_{air}}} - \frac{c_{p_{O_2}}}{c_{p_{air}}} \right]$$

Where $(O_2/A) = (m_{O_2})_o / (m_{air})_o$.

Using the definitions $(B/A) = (B/A)_s \phi$ and $\psi = \phi \eta$,
derived in Appendix A, the ratio of the specific heats Θ,
Eq D-6 may be written

$$\Theta = 1 + (F/A)_s \frac{c_{p_B}}{c_{p_{air}}} \phi + \psi \left\{ (O_2/A) \left[1.45 \frac{c_{p_{B_2O_3}}}{c_{p_{air}}} - \frac{c_{p_{O_2}}}{c_{p_{air}}} \right] - (B/A)_s \frac{c_{p_B}}{c_{p_{air}}} \right\} \tag{D-7}$$

In evaluating Eq D-7 numerically, the following values were
used (Ref 22):

$(F/A)_s = 0.115$; $c_{p_{air}} = 0.257$ cal/gm-K; $c_{p_{B_2O_3}} = 0.353$ cal/gm-K;
$(O_2/A) = 0.23$; $c_{p_B} = 0.69$ cal/gm-K; $c_{p_{O_2}} = 0.173$ cal/gm-K.
Then

$$\Theta = 1 + 0.31 \phi + \psi \left\{ 0.23 \left[0.51 - 0.173 \right] - (0.1046)(0.69) \right\} / 0.257$$

$$= 1 + 0.31 \phi + 0.021 \psi$$

The third term was the change of heat capacity per unit
volume of the mixture due to combustion. Since it was small
compared to the rest of the relation, it was neglected.
Thus, the value for Θ, used in the combustion model was

$$\Theta = 1 + 0.31 \phi \tag{D-8}$$

APPENDIX E

RADIANT ENERGY EQUATIONS OF TRANSFER (REF 20)

The gas-particle mixture was assumed to be a flow of solid particles suspended in the gas and uniformly distributed throughout the gas volume. Before vigorous combustion of the particles took place, the gas was transparent to radiation and only the solid particles absorbed, scattered and emitted radiation. During vigorous combustion, the solid fuel particles, the solid combustion products, as well as the gaseous combustion products could participate in the radiant transfers. Thus, a cloud of solid particles suspended in a gas volume would behave like an absorbing, emitting, scattering gaseous media.

During the heat up phase, the gas-particle mixture would be bounded on the upstream end by a black cavity radiating at the ambient temperature T_o and on the downstream end by a radiating combustion zone that was effectively a black cavity radiating at an average flame temperature T_F, Fig 1. Once the combustion zone was reached, the major heat flux from an elemental layer of the mixture was upstream toward the heat up zone and the radiant transfer downstream into the exhaust plume was neglected.

To evaluate the radiant heat fluxes in an absorbing, emitting and scattering media, consider an infinitesimal layer of the media lying between the distances x and $x + dx$ from a cavity radiating at T_o. This media will be assumed to be a homogeneous, gray media with isotropic coefficients of scattering s, emission ν and absorption k.

The radiant energy transfer balance can be obtained from a beam of energy I of solid angle $d\omega$ as it passes through the layer of the media at some angle θ from the normal direction, Fig 27. The energy within the solid angle was changed by a differential dI as it passed through the distance $dx/\cos\theta$. The change was due to the amount of energy in I absorbed in the layer of the media, kI; the amount of energy in I scattered out of the solid angle $d\omega$, sI; the energy from all other energy beams scattered into the solid angle, $s\int_{4\pi} I\,d\omega/4\pi$; and the energy emitted from the layer of media along the solid angle, $\nu\sigma \frac{T^4}{\pi}$. This energy change can be written

$$\cos\theta \frac{dI}{dx} = -kI - sI + \frac{\nu\sigma}{\pi}T^4 + \frac{s}{4\pi}\int_{4\pi} I\,d\omega$$

$$= -JI + \frac{\nu\sigma}{\pi}T^4 + \frac{s}{4\pi}\int_{4\pi} I\,d\omega \qquad \text{(E-1)}$$

Where $J \equiv k + s$ and is called the extinction coefficient.

Equation E-1 can be rearranged to

$$\cos\theta \frac{dI}{J\,dx} + I = \frac{\nu\sigma}{J\pi}T^4 + \frac{s}{J4\pi}\int_{4\pi} I\,d\omega \qquad \text{(E-2)}$$

Changing the independent variable to the optical length τ where

$$d\tau = J\,dx$$

and

$$\tau = \int_o^x J\,dx \qquad \text{(E-3)}$$
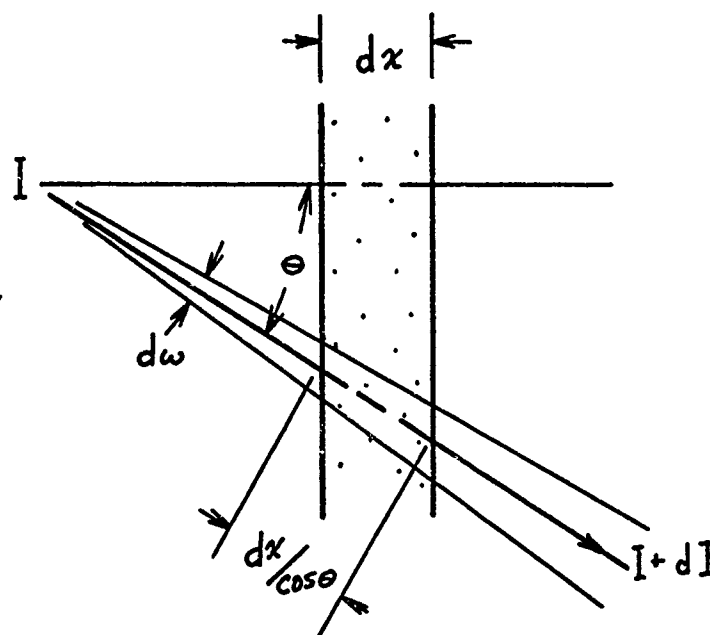
Figure 27.   Radiant Energy Transfer Through
                 an Attenuating Medium

Multiplying Eq E-2 by the integrating factor $e^{\tau/\cos\theta}$, one can obtain

$$e^{\tau/\cos\theta}\left[\frac{dI}{d\tau} + \frac{I}{\cos\theta}\right] = \frac{d}{d\tau}\left[I\,e^{\tau/\cos\theta}\right]$$

$$= \left[\frac{\nu\sigma}{J\pi}T^4 + \frac{s}{4\pi J}\int_{4\pi}I\,d\omega\right]\frac{e^{\tau/\cos\theta}}{\cos\theta} \qquad \text{(E-4)}$$

The energy transferred along beam θ can go both ways. To differentiate which way along the beam the intensity was going, the convention I^+ denotes energy moving in a positive x direction and I^- for the negative direction. Thus, for the solid angle $d\omega = \sin\theta\,d\theta\,d\varsigma$, I^+ integrated over $0 < \theta < \pi/2$ was the total positive direction flux and I^- integrated from $\frac{\pi}{2} < \theta < \pi$ was the flux in the negative direction.

Integrating I^+ from x = 0 to x yields

$$I^+ = I_o\,e^{-\tau/\cos\theta} + \frac{1}{\pi}\int_0^\tau\left[\frac{\nu\sigma}{J}T^4 + \frac{s}{4J}\int_{4\pi}I\,d\omega\right]\frac{e^{-(\tau-y)/\cos\theta}}{\cos\theta}\,dy \qquad \text{(E-5a)}$$

and I^- from x_F to x

$$I^- = I_F\,e^{(\tau_F-\tau)/\cos\theta} - \frac{1}{\pi}\int_\tau^{\tau_F}\left[\frac{\nu\sigma}{J}T^4 + \frac{s}{4J}\int_{4\pi}I\,d\omega\right]\frac{e^{-(\tau-y)/\cos\theta}}{\cos\theta}\,dy \qquad \text{(E-5b)}$$

The total longitudinal flux of radiant energy can be obtained from Eqs E-5a and E-5b by summing the components of the radiant intensities over the appropriate solid angle hemispheres. Since the media was assumed to be homogeneous, there was no dependence on ς , the radiant energy flux q_r in the x direction can be written

$$q_r(\tau) = \int_0^{2\pi}\int_0^{\pi/2} I^+ \cos\theta \sin\theta \, d\theta \, d\zeta + \int_0^{2\pi}\int_{\pi/2}^{\pi} I^- \cos\theta \sin\theta \, d\theta \, d\zeta$$

$$= 2\pi \int_0^{\pi/2} I_o e^{-\tau/\cos\theta} \cos\theta \sin\theta \, d\theta + 2\int_0^{\tau}\left[\frac{\nu\sigma}{J}T^4 + \frac{s}{4J}\int_{4\pi}I \, d\omega\right]\int_0^{\pi/2} e^{-(\tau-y)/\cos\theta} \sin\theta \, d\theta \, dy \quad \text{(E-6)}$$

$$+ 2\pi\int_{\pi/2}^{\pi} I_F e^{(\tau_F-\tau)/\cos\theta} \cos\theta \sin\theta \, d\theta - 2\int_{\tau}^{\tau_F}\left[\frac{\nu\sigma}{J}T^4 + \frac{s}{4J}\int_{4\pi}I \, d\omega\right]\int_{\pi/2}^{\pi} e^{-(\tau-y)/\cos\theta} \sin\theta \, d\theta \, dy$$

Differentiating Eq E-6, one obtains

$$-\frac{dq_r}{d\tau} = 2\pi\int_0^{\pi/2} I_o e^{-\tau/\cos\theta}\sin\theta \, d\theta + 2\pi\int_{\pi/2}^{\pi} I_F e^{(\tau_F-\tau)/\cos\theta}\sin\theta \, d\theta - 4\frac{\nu}{J}\sigma T^4$$

$$-\frac{s}{J}\int_{4\pi}I \, d\omega + 2\int_0^{\tau}\left[\frac{\nu\sigma}{J}T^4 + \frac{s}{4J}\int_{4\pi}I \, d\omega\right]\int_0^{\pi/2}\frac{e^{-(\tau-y)/\cos\theta}}{\cos\theta}\sin\theta \, d\theta \, dy$$

$$\quad \text{(E-7)}$$

$$-2\int_{\tau}^{\tau_F}\left[\frac{\nu\sigma}{J}T^4 + \frac{s}{4J}\int_{4\pi}I \, d\omega\right]\int_{\pi/2}^{\pi}\frac{e^{-(\tau-y)/\cos\theta}}{\cos\theta}\sin\theta \, d\theta \, dy$$

The value for the energy scattered into the solid angle can also be obtained from Eqs E-5a and E-5b

$$\int_{4\pi}I \, d\omega = 2\pi\int_0^{\pi/2} I_o e^{-\tau/\cos\theta}\sin\theta \, d\theta + 2\int_0^{\tau}\left[\frac{\nu\sigma}{J}T^4 + \frac{s}{4J}\int_{4\pi}I \, d\omega\right]\int_0^{\pi/2}\frac{e^{-(\tau-y)/\cos\theta}}{\cos\theta}\sin\theta \, d\theta \, dy$$

$$\quad \text{(E-8)}$$

$$+ 2\pi\int_{\pi/2}^{\pi} I_F e^{(\tau_F-\tau)/\cos\theta}\sin\theta \, d\theta - 2\int_{\tau}^{\tau_F}\left[\frac{\nu\sigma}{J}T^4 + \frac{s}{4J}\int_{4\pi}I \, d\omega\right]\int_{\pi/2}^{\pi}\frac{e^{-(\tau-y)/\cos\theta}}{\cos\theta}\sin\theta \, d\theta \, dy$$

For an optically thin media, that is for $\tau_F, \tau \ll 1$, and noting that I_o and I_F eminate from nonreflecting cavities $I_o = \sigma T_o^4/\pi$ and $I_F = \sigma T_F^4/\pi$, Eqs E-6, E-7 and E-8 can be written

$$q_r(\tau) = q_r(x) \cong \sigma T_o^4 - \sigma T_F^4 \qquad \text{(E-6a)}$$

$$-\frac{dq_r}{d\tau} = 2\sigma T_o^4 + 2\sigma T_F^4 - \frac{4\nu}{J}\sigma T^4 - \frac{z}{J}\int_{4\pi} I\,d\omega \qquad \text{(E-7a)}$$

and

$$\int_{4\pi} I\,d\omega \cong 2\sigma T_o^4 + 2\sigma T_F^4 \qquad \text{(E-8a)}$$

Substituting Eq E-8a into E-7a and using the definitions from Eqs E-1 and E-3, Eq E-7a can be written as the longitudinal component of the radiant energy divergence

$$-\frac{dq_r}{dx} = 2k\sigma T_o^4 + 2k\sigma T_F^4 - 4\nu\sigma T^4 \qquad \text{(E-9)}$$

The resulting formulations for the radiant flux and divergence are seen no longer to depend on the scattering coefficient or the integral equation. This simplified the energy equation significantly. Also, the emittance and absorption coefficients which are dependent on the temperature of radiation for a nongray media are dependent only on the temperature of the differential layer $T(x)$ for a gray media, $k(T_o) = k(T_F) = k(T)$ and by Kirchhoff's law $k(T) = \nu(T)$. The absorption coefficient was assumed to be

dependent on the temperature of the media and not a constant
by the formulation of the definition of the optical distance
τ in Eq E-3

$$\tau = \int_0^x k\, dx \neq kx$$

APPENDIX F

VELOCITY AND TEMPERATURE RELATIONSHIPS

FOR THE GAS-PARTICLE MIXTURE

To determine the degree of error introduced in neglecting the Mach number effect on the velocity-temperature relationship in the gas-particle mixture, the relation for the velocity as a function of Mach number and temperature was derived assuming identical velocity and temperature for all species and phase states. The conservation equations, the equation-of-state and the definition for the Mach number are used.

The Continuity Equation

The continuity equation for the gas-particle mixture is given in Eq C-9 as

$$ u \sum_m \sum_f \rho_{mf} = (1 + F/A) \rho_{air} \, u \tag{C-9} $$

Differentiating Eq C-9, one obtains

$$ \frac{1}{u} \frac{du}{dx} = - \frac{1}{\rho_{air}} \frac{d\rho_{air}}{dx} \tag{F-1} $$

The Momentum Equation

Substituting Eq C-9 into Eq C-13 and expanding, the momentum of the mixture can be written as

$$ u \sum_m \sum_f \rho_{mf} \frac{du}{dx} = (1 + F/A) \rho_{air} \, u \frac{du}{dx} = - \sum_m \sum_{f=g} \frac{dP_{mf}}{dx} \tag{F-2} $$

The Gas Equation-of-State for Air

The pressure term in Eq F-2 includes only the gas phase and from Eq B-7 it was concluded that the pressure was approximated by that of air

$$\sum_m P_{mg} \cong \rho_{air} \underline{R} T = P_{air} \qquad \text{(F-3)}$$

or

$$\frac{1}{P_{air}} \frac{dP_{air}}{dx} = \frac{1}{\rho_{air}} \frac{d\rho_{air}}{dx} + \frac{1}{T} \frac{dT}{dx} \qquad \text{(F-4)}$$

The definition for the Mach number M_N

$$M_N^2 = u^2 / \gamma \underline{R} T \qquad \text{(F-5)}$$

or

$$\frac{1}{\gamma M_N^2} \frac{d(\gamma M_N^2)}{dx} = \frac{2}{u} \frac{du}{dx} - \frac{1}{T} \frac{dT}{dx} \qquad \text{(F-6)}$$

Substituting the continuity and momentum equations F-1 and F-2 into the differential equation-of-state, Eq F-4, and utilizing the equation-of-state, F-3, a relation involving only velocity and temperature is obtained

$$\left[1 - (1 + F/A) u^2 / \underline{R} T \right] \frac{1}{u} \frac{du}{dx} = \frac{1}{T} \frac{dT}{dx} \qquad \text{(F-7)}$$

The variables in Eq F-7 cannot be separated; however, the bracket on the left hand side may be expressed in terms of the Mach number. Thus, substituting Eq F-7 into Eq F-6, relations involving Mach number and velocity and Mach number

and temperature are obtained.

$$\frac{1}{u}\frac{du}{dx} = \frac{d(\gamma M_N^2)/dx}{\left[1+(1+F/A)\gamma M_N^2\right]\gamma M_N^2} = \left[\frac{1}{\gamma M_N^2} - \frac{1+F/A}{1+(1+F/A)\gamma M_N^2}\right]\frac{d(\gamma M_N^2)}{dx} \qquad \text{(F-8)}$$

and

$$\frac{1}{T}\frac{dT}{dx} = \left[\frac{1-(1+F/A)\gamma M_N^2}{1+(1+F/A)\gamma M_N^2}\right]\frac{d(\gamma M_N^2)/dx}{\gamma M_N^2} = \left[\frac{1}{\gamma M_N^2} - \frac{2(1+F/A)}{1+(1+F/A)\gamma M_N^2}\right]\frac{d(\gamma M_N^2)}{dx} \text{ (F-9)}$$

Expressed in logrithm form, Eqs F-8 and F-9 are

$$\frac{d}{dx}\left\{\ln\left[\frac{\gamma M_N^2}{\left[1+(1+F/A)\gamma M_N^2\right]u}\right]\right\} = 0$$

and

$$\frac{d}{dx}\left\{\ln\left[\frac{\gamma M_N^2}{\left[1+(1+F/A)\gamma M_N^2\right]^2 T}\right]\right\} = 0$$

Thus,

$$\frac{\gamma M_N^2}{\left[1+(1+F/A)\gamma M_N^2\right]u} = \text{constant} \qquad \text{(F-10)}$$

$$\frac{\gamma M_N^2}{\left[1+(1+F/A)\gamma M_N^2\right]^2 T} = \text{constant} \qquad \text{(F-11)}$$

Dividing Eq F-11 by Eq F-10, one can obtain the temperature-velocity relationship.

$$\frac{u}{\left[1+(1+F/A)\gamma M_N^2\right]T} = \text{constant}$$

or

$$\frac{u}{u_0} = \left[\frac{1+(1+F/A)\gamma M_N^2}{1+(1+F/A)(\gamma M_N^2)_0}\right]\frac{T}{T_0} \qquad \text{(F-12)}$$

128

Evaluating Eq F-11 at the initial conditions, one obtains

$$\frac{\gamma M_N^2}{(\gamma M_N^2)_o} = \left[\frac{1 + (1+F/A)\gamma M_N^2}{1 + (1+F/A)(\gamma M_N^2)_o}\right]^2 \frac{T}{T_o} \qquad \text{(F-11a)}$$

Equation F-11a can be rearranged as a quadratic equation in $(1 + F/A)\, \gamma\, M_N^2$

$$\left[(1+F/A)\gamma M_N^2\right]^2 + \left\{2 - \frac{\left[1 + (1+F/A)(\gamma M_N^2)_o\right]^2}{(1+F/A)(\gamma M_N^2)_o} \frac{T_o}{T}\right\}(1+F/A)\gamma M_N^2 + 1 = 0 \qquad \text{(F-13)}$$

The variation of $(1 + F/A)\, \gamma\, M_N^2$ with temperature can now be evaluated using the initial conditions $M_{N_0} \simeq 0.1$, $T_o = 300^\circ K$, $\gamma_{air} = 1.4$, $F/A = 0.115\,\phi$ for $\phi = 1$ and 2 and $T_{max} = 3000^\circ K$. Solving Eq F-13

T	300	1000	2000	3000
$(1+F/A)\gamma M_N^2$	0.017	0.05	0.115	0.16
$\left[\dfrac{1 + (1+F/A)\gamma M_N^2}{1 + (1+F/A)(\gamma M_N^2)_o}\right]$	1	1.03	1.095	1.14

Thus, it was seen that little error was introduced for exit flame temperatures below $2000^\circ K$; however, for higher entry Mach numbers and higher temperatures, the error would be significant but still within the uncertainty of the flow measurements.

APPENDIX G

TEMPERATURE MEASUREMENT

The measurement of temperature using the absorption-emission technique is a noninterference method for luminous flames (Refs 27 and 28). The technique requires a monochromatic measurement of the emissive power of the flame $I_{F\lambda}$; the attenuation of a calibrated power source viewed through the flame (absorption) $I_{T\lambda}$; and a measurement of the emissive power of the calibrated source $I_{cs\lambda}$. From these measurements, the absorption coefficient of the flame gases $\alpha_{F\lambda}$ is

$$\alpha_{F\lambda} = 1 - (I_{T\lambda} - I_{F\lambda})/I_{cs\lambda} \qquad \text{(G-1)}$$

Assuming that the flame system is in radiative equilibrium, the spectral emissivity would be equal to the spectral absorptivity. Then the measured emissive powers $I_{F\lambda}$ and $I_{cs\lambda}$ may be described by Kirchhoff's and Planck's radiation laws,

$$I_{F\lambda} = \frac{P_\lambda \, \epsilon_F(\lambda, T_F) C_1}{\lambda^5 (Exp[C_2/\lambda T_F] - 1)} \qquad \text{(G-2)}$$

$$I_{cs\lambda} = \frac{P_\lambda \, \epsilon_{cs}(\lambda, T_{cs}) C_1}{\lambda^5 (Exp[C_2/\lambda T_{cs}] - 1)} \qquad \text{(G-3)}$$

Where P_λ is the spectral constant for the monochrometer.

For wave lengths less than 1μ and temperatures less than 3000°K, $e^{C_2/\lambda T} \gg 1$. And by using the ratio of

measured emissive powers, the calculation of the spectral constant is not necessary. The absolute temperature of the flame may be calculated by the ratio of Eqs G-2 and G-3,

$$T_F = \cfrac{T_{cs}}{1 - \cfrac{\lambda T_{cs}}{c_2} \ln\left[\cfrac{I_{F\lambda}\ \epsilon_{cs}(\lambda, T_{cs})}{I_{cs\lambda}\ \epsilon_F(\lambda, T_F)}\right]} \qquad (G-4)$$

Calibrated Source

A tungsten ribbon filament lamp, General Electric Company type 30A/6V/T24 calibrated by the National Bureau of Standards for brightness temperature at 0.665μ as a function of lamp current was used as the calibrated source. The power supply for the lamp consisted of two heavy duty batteries connected in series to produce a twelve volt output. The current regulation was accomplished by dropping the potential across a one ohm reostat to obtain a constant current through the lamp. The lamp current was monitored by measuring the current across a 50 mv, 50 ohm shunt. The current was displayed on a digital electronic potentiometer calibrated with the shunt. The current was measured in 0.02 ampere digits to within 0.025%.

The brightness temperature S_λ was converted to true temperature by

$$T_{cs} = \cfrac{S_\lambda}{1 + \cfrac{\lambda S_\lambda}{c_2} \ln\left[\epsilon_{cs}(\lambda, T_{cs})\right]} \qquad (G-5)$$

Where the emissivity of tungsten for the wave length range from 0.45μ to 0.68μ was described by Larrabee (Ref 29) as

$$\epsilon(\lambda, T) = 0.4655 - 0.1558\lambda + 0.2675 \times 10^{-4}T - 0.7305 \times 10^{5}\lambda T \quad \text{(G-6)}$$

Calibration of Spectrum

The Warner-Swasey 501 Scanning Spectrometer, with entrance and exit slits set at 0.1 mm, was used to monitor the spectral range from 0.4 to 0.65μ . The detector was a type 4473 photomultiplier set at 994 volts. The spectrum, as displayed on the oscilloscope, was calibrated using a mercury arc lamp to obtain the mercury lines. The spectrometer was then monochromatically set to the maximum signal of the 0.518μ emission peak of the flame spectrum.

Measurements

The flame temperature was measured at the 0.518μ wave length. The lamp emission signal was chopped at one second intervals to obtain the $I_{F\lambda}$ and $I_{T\lambda}$ measurements. The lamp measurement $I_{cs\lambda}$ was taken just prior to the test run with the tungsten lamp current and oscilloscope signal voltage maintained constant throughout the test. Schematic representations of the signals obtained are depicted in Figs 28 and 29.
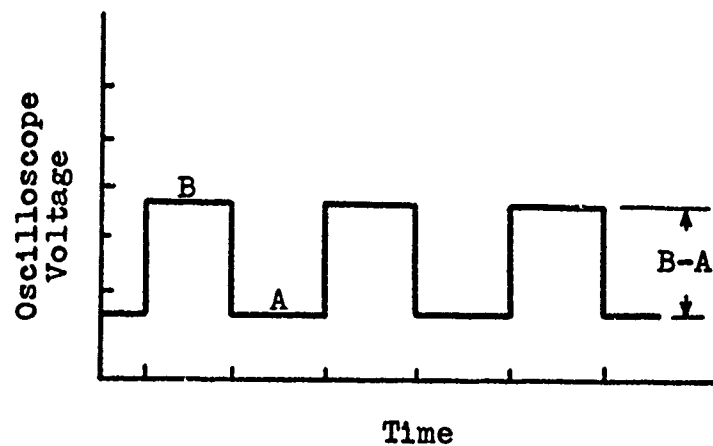
A Zero Emission Reference Line
B Emissive Power of the
   Calibrated source
B-A = I_{cs}

Figure 28. Calibrated Source Lamp Emission Signal
Chopped to Obtain Reference Data
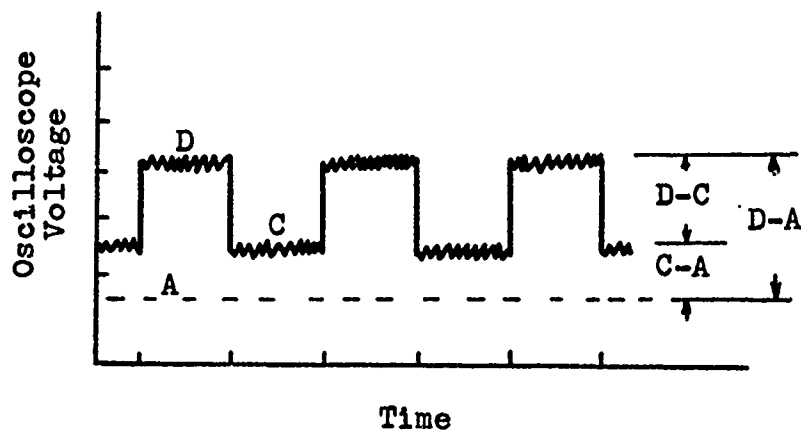
C Emissive Power of the Flame
D Emissive Power of the Flame plus
   the Calibrated Source
D-A = I_T, C-A = I_F

Figure 29. Absorption-Emission Data Signal
of Test Flame

133

APPENDIX H

FORTRAN PROGRAM THEORETICAL COMPUTATIONS

FOR SOLUTION OF EQUATIONS 33 THROUGH 38

(RUN ON CDC 6600)

```
      PROGRAM ORMAND(INPUT,OUTPUT)
      DIMENSION Y(2),YDOT(2)
      COMMON TO,TF,PHI
      READ 1000,TO,TIMEF,DTIME
      PHI=0.
      DO 100 I=1,2
      PRINT 2000
      PHI=PHI+1.
      TF=2900.
      IF(PHI.GT.1.)  TF=2400.
      TIME=0.
      Y(1)=300.
      Y(2)=0.
   10 CONTINUE
      CALL F(TIME,Y,YDOT)
      PRINT 2010,TIME,Y(1),YDOT(1),Y(2),YDOT(2)
      CALL RKDF(TIME,Y,2,DTIME)
      IF(TIME.LE.TIMEF) GO TO 10
  100 CONTINUE
      STOP
 1000 FORMAT(4E10.0)
 2000 FORMAT(1H1,15X,4HTIME,19X,1HT,12X,8HDT/DTIME,17X,
     13HPSI,10X,10HDPSI/DTIME)
 2010 FORMAT(5E20.5)
      END
      SUBROUTINE F(TIME,Y,YDOT)
      DIMENSION Y(2),YDOT(2)
      COMMON TO,TF,PHI
      T=Y(1)
      PSI=Y(2)
      THETA=1.+.31*PHI
      F1=2.33*PHI*(TF/1000.)**4*
     1(1.+(TO/TF)**4-2*(T/TF)**4)/(THETA*T/1000.)
      F4=28.5*(1.+.58*(PHI-1.))*(3.-T/1000.)+2.33*PHI*
     1(1.-PSI/PHI)**.666
      IF(T.GE.2100.)  F1=-F4*(T/1000.)**3/THETA
      F2=.014*PHI
      IF(T.GE.2000.)  F2=0.
      F3=(5650.-1850.*EXP(19.-44000./T))/THETA
      IF(T.GE.2320.)  F3=3800./THETA
      IF(PSI.GE..8)  F1=0.
      G1=427.*PHI*(1.-PSI)*(1.-PSI/PHI)**.33333
      G2=EXP(8.62-20000./T)/T
      YDOT(1)=F1+F3*(F2+G1*G2)
      YDOT(2)=F2+G1*G2
      RETURN
      END
```

134

APPENDIX I

EVALUATION OF THE CONSTANTS A AND β

The reaction rate constant β and the Arrhenius pre-exponential constant A are characteristics of the reaction proces and must be evaluated from experimental data. The reaction rate constant β is defined for a spherical particle reaction process at constant temperature and un-limited oxygen so that the concentration of oxygen C_{O_2} remains constant throughout the combustion process. The empirical law for this reaction process states that the rate of consumption of a fuel particle is proportional to the exposed surface of the particle and the concentration of oxygen surrounding the particle. This law, for a first order reaction rate (Ref 30), is described as

$$- \frac{d m_f}{d t} = n \pi r^2 C_{O_2} M_f \frac{K(T)}{r^a} \tag{I-1}$$

Where n is the number of particles per unit volume and $K(T)$ is a constant of proportionality that is dependent upon temperature. The value of a is equal to zero for chemical limited reaction and equal to one for diffusion limited reaction. The temperature dependence of $K(T)$ has been defined in exponential form by Eq 25 as

$$K(T) = A e^{-E_a/RT} \tag{25}$$

Where E_a and A are defined as the Arrhenius activation energy

135

and pre-exponential constant, respectively, and Eq 25 as the Arrhenius equation.

The mass per unit volume of the fuel particles was expressed in terms of the particle volume, its liquid or solid density δ_f and the number of particles per unit volume in Eq 7

$$m_f = n \, \delta_f \, \frac{\pi d^3}{6} \qquad (7)$$

Substituting Eq 7 into Eq I-1 and expressing the relation as a function of diameter, one obtains

$$-\frac{d}{dt}\left(n \delta_f \frac{\pi d^3}{6}\right) = 2^a \, n \pi \, d^{2-a} \, C_{O_2} \, M_f \, K(T) \qquad (I-2)$$

Integrating Eq I-2 yields

$$d_o^{a+1} - d^{a+1} = \beta \, (t - t_o) \qquad (I-3)$$

Where $\beta = (a+1) \, 2^{a+1} \, C_{O_2} \, M_f \, K(T) / \delta_f \triangleq \mu^{a+1}/sec$

A similar analysis of Eq I-1 can be obtained for a finite source of oxygen and a temperature dependent reaction process. Dividing Eq I-2 by the initial mass per unit volume of fuel $(m_f)_o$, the initial concentration of oxygen $(C_{O_2})_o$ and $K(T)$ evaluated at some reference temperature T_k, one obtains

$$-\frac{d}{dt}\left[\left(\frac{d}{d_o}\right)^3\right] = A'\left(\frac{d}{d_o}\right)^{2-a}\frac{C_{O_2}}{(C_{O_2})_o}\frac{K(T)}{K(T_k)} \qquad (I\text{-}4)$$

Where

$$A' = 3\left[(a+1)2^{a+1}(C_{O_2})_o M_f K(T_k)/\delta_f\right]\Big/(a+1)d_o^{a+1}$$

$$= \frac{3\beta}{(a+1)d^{a+1}} \qquad (I\text{-}5)$$

The Arrhenius pre-exponential constant A may be obtained from Eq I-5 by expressing $K(T_k)$ in the exponential form

$$A = \frac{A'\delta_f d_o^{a+1}e^{E_a/RT_k}}{3(2^{a+1})(C_{O_2})_o M_f} \qquad (I\text{-}6)$$

The experimental value of A' was determined from Eq 37 by a graphical analysis of the data in conjunction with a correlation of the data using the solution of the Fortran Program listed in Appendix H. The value of A' that agreed best with the experimental results was 1423 sec^{-1} for T_k equal to 2320°K. Evaluating the rate constants using this value and an initial particle diameter of one micron, one obtains

$$\beta_{diff} = \tfrac{2}{3}A'd_o^2 = 949 \ \mu^2/sec \qquad (I\text{-}7)$$

and

$$\beta_{chem} = \tfrac{1}{3}A'd_o = 474 \ \mu/sec \qquad (I\text{-}8)$$

137

The pre-exponential constant A can be evaluated using the following values:

$$\text{Exp}\left[E_a/R2320\right] = 5.55 \times 10^3; \qquad \delta_B = 2.34 \; gm_B/cm^3;$$

$$(C_{O_2})_o = 0.21 \; N_{O_2}/N_{air}; \qquad M_B = 10.81 \; gm/mole;$$

$$E_a/R = 20{,}000 ^\circ K; \qquad d_o = 10^{-4} \; cm.$$

$$A_{diff} = 6.78 \times 10^{-3} \left(\frac{N_B}{N_{O_2}}\right) \; N_{air}/cm\text{-}sec$$

Noting from Appendix A that for the boron reaction in which B_2O_3 is the only product, the ratio $N_B/N_{O_2} = 4/3$, then

$$A_{diff} = 9.04 \times 10^{-3} \; N_{air}/cm\text{-}sec \qquad \text{(I-9)}$$

and

$$A_{chem} = 181 \; N_{air}/cm^2\text{-}sec \qquad \text{(I-10)}$$

APPENDIX J

TABLES OF PHYSICAL PROPERTIES FOR METAL FUELS

AND EXPERIMENTAL RESULTS

TABLE I

HEAT CONTENT FROM METAL COMBUSTION

Element	At. No.	Density (gm/cc)	Principle Oxide	Kcal/Mole of Oxide	Kcal/gm of Element	Kcal/cc of Element
Al	13	2.7	Al_2O_3	400	7.4	20.0
B	5	2.34	B_2O_3	300	13.9	31.15
Be	4	1.816	BeO	143	15.75	28.6
Li	3	0.535	Li_2O	143	10 4	5.56
Mg	12	1.74	MgO	143	5.95	10.38
Zr	40	6.44	ZrO_2	261	2.85	18.35
C	6	-----	CO_2	94	7.85	-----
H_2	1	-----	H_2O	58	26.0	-----

References:

JANAF (Ref 22)

Density Information from Uda (Ref 13)

TABLE II

MELTING AND BOILING POINTS OF ELEMENTS AND OXIDES

Element	T_M °K	T_B °K	Oxide	T_M °K	T_B °K
Al	933	2767	Al_2O_3	2315	3250 - 3800
B	2450	3931	B_2O_3	723	2320
Be	1556	2557	BeO	2720	3000 - 4170
Li	453	1620	Li_2O	1843	2836
Mg	922	1378	MgO	3098	3533
Si	1680.	2630	SiO_2	1996	2500 - 3000
Zr	2125	4776	ZrO_2	2900	4548 - 5200
Fe	1809	3145	Fe_2O_3	1650	3687*

Reference:

JANAF (Ref 22)

*Decomposes but does not boil.

TABLE III

CHEMICAL ANALYSIS ᴏᴏ TRONA AMORPHOUS BORON

Element	Percentage	
	(1)*	(2)*
Boron	90.00 - 92.0	- - - - - - -
Mg	3.00 - 5.0	1.7 - 3.3
Fe	0.20	0.7 - 0.33
N	0.10	- - - - - - -
Mn	0.08	0.02 - 0.04
Ca	0.04	0.07 - 0.13
Si	0.04	0.1 - 0.3
Na	0.04	- - - - - - -
Al	0.01	0.007 - 0.013
Pb	0.01	0.02 - 0.04
Ni	0.01	- - - - - - -
Zn	- - - - - - -	0.06 - 0.1
Cu	- - - - - - -	0.004 - 0.006
Zr	- - - - - - -	0.001

Absolute density 2.38 - 2.4
(gm/cc)

Average Particle Size 1.0 - 1.75 (3)*
(μ)

References:

(1)* Hand Book of Metal Powders, Edited by A. R. Poster,
Reinhold Pub. Corp., N. Y., 1966.

(2)* Spectrographic Analysis, by L. Roush, Miami Univ.,
April 22, 1970.

(3)* Stokes Flotation Analysis, by G. Menninger, ARL,
Wright-Patterson AFB, Ohio.

TABLE IV

EXPERIMENTAL DATA AT $\phi = 1.0$

ID (cm)	L (cm)	$(\rho u)_{air}$ (gm/cm^2-sec)	ξ (ms)	ψ	T ($^\circ$K)	$\epsilon_{F\lambda}$	k_λ (cm^{-1})
1.9	22.8	3.20	8.62	0.1	2100	0.1	0.055
1.9	22.8	3.20	8.62	0.246	----	-----	------
1.9	35.6	3.20	13.4	0.3	2300	0.44	0.304
1.9	35.6	3.20	13.4	0.28	2400	0.39	0.26
1.9	35.6	3.20	13.4	0.625	2530	0.4	0.268
2.54	40.6	1.80	27.25	0.9915	2940	0.13	0.055
2.54	50.8	1.80	34.1	-------	2950	0.166	0.0715
2.54	50.8	1.80	34.1	-------	3090	0.073	0.0294
2.54	50.8	1.80	34.1	-------	2880	0.153	0.0655
2.54	50.8	1.80	34.1	-------	3070	0.077	0.0315
2.54	33.0	1.80	22.15	0.94	-----	-----	------
2.54	56.0	2.70	25.0	0.845	-----	-----	------
2.54	56.0	3.60	18.73	0.89	-----	-----	------
2.54	61.0	2.70	29.25	0.99	-----	-----	------

($\rho u < 1.5$ gm/cm^2-sec Graphite Combustor)

ID (cm)	L (cm)	$(\rho u)_{air}$ (gm/cm^2-sec)	ξ (ms)	ψ	T ($^\circ$K)	$\epsilon_{F\lambda}$	k_λ (cm^{-1})
2.54	15.2	0.99	18.6	0.12	-----	-----	------
2.54	25.4	0.99	31.0	0.23	-----	-----	------
2.54	61.0	0.99	74.5	0.688	-----	-----	------

($\rho u < 1.5$ gm/cm^2-sec Zirconia Combustor)

ID (cm)	L (cm)	$(\rho u)_{air}$ (gm/cm^2-sec)	ξ (ms)	ψ	T ($^\circ$K)	$\epsilon_{F\lambda}$	k_λ (cm^{-1})
2.54	30.5	0.99	37.2	0.916	-----	-----	------
2.54	76.2	0.90	94.3	1.0	-----	-----	------
2.54	33.0	1.34	29.5	0.49	-----	-----	------
2.54	40.6	0.90	54.5	0.715	-----	-----	------
2.54	40.6	1.25	39.0	0.372	-----	-----	------
2.54	40.6	1.44	34.1	0.424	-----	-----	------

(2.54 cm Square Zirconia Combustor)

ID (cm)	L (cm)	$(\rho u)_{air}$ (gm/cm^2-sec)	ξ (ms)	ψ	T ($^\circ$K)	$\epsilon_{F\lambda}$	k_λ (cm^{-1})
2.54	20.3	1.41	14.4	1.0	-----	-----	------

TABLE V

EXPERIMENTAL DATA AT $\phi = 1.5$

ID (cm)	L (cm)	$(\rho u)_{air}$ (gm/cm^2-sec)	ξ (ms)	ψ	T ($^\circ$K)	$\epsilon_{F\lambda}$	k_λ (cm^{-1})
1.9	22.8	3.20	8.62	0.572	2160	0.333	0.212
1.9	22.8	3.20	8.62	-----	2200	0.1	0.055
1.9	22.8	4.82	5.75	0.4	----	-----	-----
1.9	22.8	3.20	8.62	0.52	2190	0.35	0.226
1.9	35.6	4.82	8.93	0.423	2200	0.49	0.354
2.54	40.6	3.60	13.6	0.55	----	-----	-----
1.9	35.6	3.20	13.4	-----	2470	0.35	0.226
1.9	35.6	3.20	13.4	-----	2400	0.33	0.21
1.9	35.6	3.20	13.4	-----	2230	0.467	0.33
1.9	35.6	3.20	13.4	0.525	2500	0.36	0.234
2.54	40.6	2.70	18.15	0.405	----	-----	-----
1.9	56.0	3.20	21.1	0.92	2500	0.16	0.092
1.9	56.0	3.20	21.1	-----	2540	0.32	0.202
1.9	56.0	3.20	21.1	-----	2500	0.3	0.187
2.54	40.6	1.80	27.25	0.73	----	-----	-----
2.54	61.0	2.70	27.2	0.995	----	-----	-----
2.54	50.8	1.80	34.1	-----	2600	0.2	0.088
2.54	50.8	1.80	34.1	-----	2570	0.32	0.152
1.9	56.0	1.60	42.2	0.903	2770	0.1	0.041
2.54	30.5	1.22	30.2	0.7	2210	0.6	0.36
2.54	33.0	1.18	33.8	0.744	----	-----	-----

TABLE VI

EXPERIMENTAL DATA at $\phi = 2.0$

ID (cm)	L (cm)	$(\rho u)_{air}$ (gm/cm^2-sec)	ξ (ms)	ψ	T (°K)	$\epsilon_{F\lambda}$	k_λ (cm^{-1})
1.9	22.8	3.20	8.62	0.4	2250	0.25	0.151
1.9	22.8	3.20	8.62	-----	2220	0.25	0.151
1.9	22.8	3.20	8.62	0.488	2140	0.52	0.386
1.9	22.8	3.20	8.62	-----	2250	0.58	0.455
1.9	22.8	3.20	8.62	-----	2240	0.425	0.29
1.9	35.6	3.20	13.4	-----	2300	0.465	0.329
1.9	35.6	3.20	13.4	-----	2320	0.265	0.162
1.9	35.6	3.20	13.4	-----	2320	0.48	0.343
1.9	35.6	3.20	13.4	0.722	2300	0.46	0.324
1.9	35.6	3.20	13.4	0.77	2250	0.38	0.25
1.9	-35.6	3.20	13.4	-----	2330	0.21	0.124
1.9	35.6	3.20	13.4	-----	2370	0.36	0.234
1.9	35.6	3.20	13.4	-----	2330	0.36	0.234
2.54*	20.3	1.38	20.8	0.96	2600	0.2	0.117
1.9	56.0	3.20	21.1	0.895	2600	0.28	0.129
1.9	56.0	3.20	21.1	0.973	2500	0.165	0.095
1.9	56.0	1.60	42.2	0.99	2780	0.1	0.055
1.9	56.0	3.20	21.1	0.905	2500	0.27	0.165
1.9	56.0	3.20	21.1	0.89	2570	0.29	0.18
1.9	56.0	3.20	21.1	0.977	2570	0.24	0.144
1.9	56.0	3.20	21.1	-----	2550	0.22	0.1305
2.54	50.8	1.80	34.1	-----	2630	0.24	0.108
2.54	50.8	1.80	34.1	-----	2600	0.32	0.152
2.54	50.8	1.80	34.1	-----	2640	0.22	0.098
2.54	50.8	1.80	34.1	-----	2490	0.22	0.098
2.54	50.8	1.80	34.1	-----	2545	0.21	0.093

* 2.54-cm Square Zirconia Combustor

TABLE VI

(Continued)

ID (cm)	L (cm)	$(\rho u)_{air}$ (gm/cm²-sec)	ξ (ms)	ψ	T (°K)	$\epsilon_{F\lambda}$	k_λ (cm⁻¹)
2.54	30.5	1.80	20.5	0.585	-----	-----	-----
2.54	61.0	1.80	41.0	0.995	-----	-----	-----
1.9	56.0	3.20	21.1	0.985	-----	-----	-----

($\rho u < 1.5$ gm/cm²-sec Graphite Combustor)

ID (cm)	L (cm)	$(\rho u)_{air}$	ξ	ψ	T	$\epsilon_{F\lambda}$	k_λ
2.54	15.2	0.99	18.6	0.415	-----	-----	-----
2.54	25.4	0.99	31.0	0.865	-----	-----	-----
2.54	61.0	0.99	74.5	0.936	-----	-----	-----

($\rho u < 1.5$ gm/cm²-sec Zirconia Combustor)

ID (cm)	L (cm)	$(\rho u)_{air}$	ξ	ψ	T	$\epsilon_{F\lambda}$	k_λ
2.54	30.5	1.22	30.2	0.945	-----	-----	-----
2.54	30.5	0.99	37.2	1.0	-----	-----	-----
2.54	30.5	0.99	37.2	0.9165	-----	-----	-----
2.54	30.5	1.18	31.2	0.939	-----	-----	-----
2.54	30.5	0.88	41.8	0.993	-----	-----	-----
2.54	30.5	1.18	31.2	0.953	-----	-----	-----

TABLE VII

TYPICAL N_2/O_2 AND $N_2/$ARGON DATA*

L (cm)	ϕ	N_2/O_2	$N_2/$Argon	ψ
15.2	1.0	4.245	83.644	0.12
15.2	2.0	6.205	84.778	0.415
25.4	1.0	4.845	85.841	0.23
25.4	2.0	27.581	83.57	0.865
61.0	1.0	11.988	83.966	0.688
61.0	2.0	58.681	84.470	0.936
Std. Air	---	3.728	83.602	-----

*Data from 2.54-cm ID Graphite Combustor

VITA

Lowell W. Ormand was born on 2 April 1932 near Butler in Custer County, Oklahoma. He graduated from Amphitheater High School, Tucson, Arizona, in May, 1950. In May, 1955, he received a Bachelor of Mechanical Engineering from the University of Arizona and received a commission as a second lieutenant in the USAF Reserve. He was employed by the Shell Chemical Company as a plant maintenance engineer until called to active duty in July, 1955. His Air Force assignments before coming to the Air Force Institute of Technology were as a combat crew member in the 303rd Bomb Wing, SAC; student with the AFIT Civilian Institutions Program at the University of Arizona where he received a Master of Mechanical Engineering in May, 1965; project engineer in the 6511th Parachute Test Group and with the 7th Air Force in Vietnam as a forward air controller. He was assigned to the Air Force Aero Propulsion Laboratory where he accomplished the present investigation and is currently assigned to the Air Force Flight Test Center. He attended pilot training in 1955, Squadron Officers School in 1959 and accepted a commission in the Regular Air Force in 1962.

Colonel Ormand is married to the former Barbara Welch of Tucson, Arizona and they have four children, David, Katherine, Michael and Rebecca.

Permanent Address: 2227 E. Drachman
                    Tucson, Arizona 85719

This dissertation was typed by Barbara Ormand.